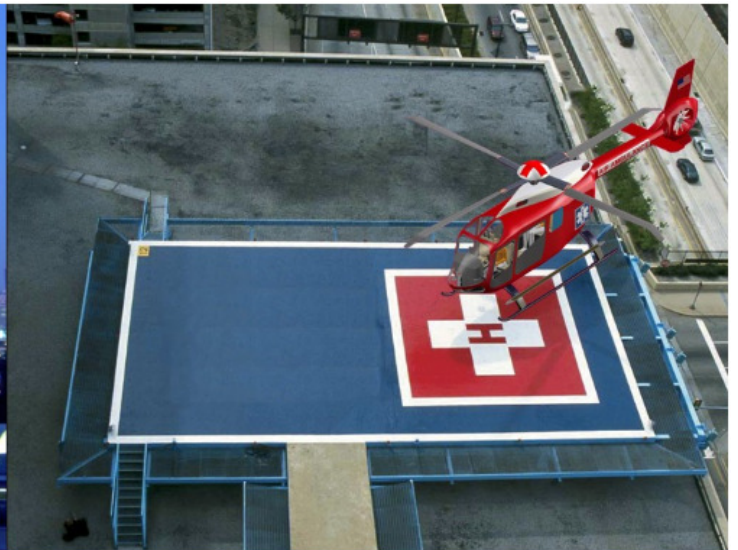




25th Annual Student Design Competition
Graduate Category



Daniel Guggenheim School of Aerospace Engineering
Georgia Institute of Technology
Atlanta, Georgia 30332

Acknowledgements


We would like to recognize and thank the following individuals for their special assistance in the completion of this design project:

Dr. Daniel Schrage
Dr. Lakshmi Sankar
Dr. Byung-Ho Ahn
Dr. Suresh Kannan
Dr. Jieun Ku Pervine
CPT Joseph Davis
Mr. Emre Gündüz
Mr. Kyle Collins
Mr. Tom Hanson
Mr. Apinut Sirojvisuth

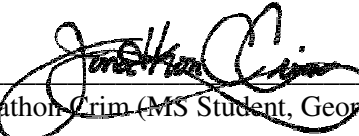
Dr. Robert Loewy
Dr. Mark Costello
Dr. Jae-Woo Lee
Dr. Patrick Biltgen
Dr. Haiying Liu
Mr. Jeremy Bain
Mr. Ho-Jung Kang
Mr. Jongki Moon
Mr. Kshitij Shrotri
Mr. Bernard Laurendeau

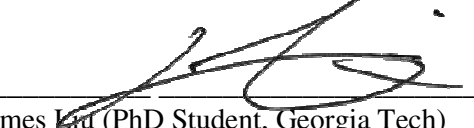
Dr. JVR Prasad
Dr. Han Gil Chae
Dr. Yung Yu
Dr. Sandeep Agarwal
MAJ Stephen Suhr
Mr. Shai Birmaher
Mr. Jeonghwan Lee
Mr. Pete Hart
Mr. Bill Sung
Ms. Ashlie Brown

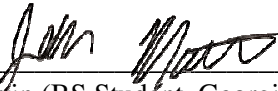
2008 Georgia Tech Graduate Design Team



Jacquelyn Banas (BS Student, Georgia Tech)

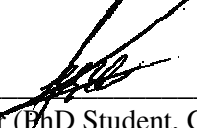

Thomas Cooper (MS Student, Georgia Tech)

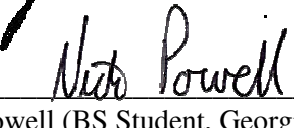

Jonathon Crim (MS Student, Georgia Tech)


James Liu (PhD Student, Georgia Tech)



John Martin (BS Student, Georgia Tech)



CPT Joe Minor (MS Student, Georgia Tech)

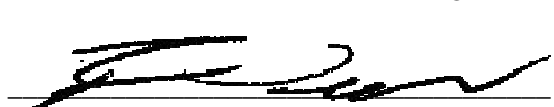

F. Ersel Olcef (PhD Student, Georgia Tech)


Nick Powell (BS Student, Georgia Tech)


Alexander Robledo (BS Student, Georgia Tech)


Roosevelt Samuel (MS Student, Georgia Tech)


Ngoc Anh Vu (MS Student, Konkuk University)


CPT Brian Wade (MS Student, Georgia Tech)

For participating in the 2008 AHS design competition, graduate students received academic credit for AE6334: Rotorcraft Design and undergraduate students received academic credit for AE4351: Rotorcraft Design.

Executive Summary

For a new helicopter to succeed in today's and future markets, it must be capable of performing multiple missions for a variety of customers. This aircraft must be able to complete every mission efficiently and inexpensively, while also meeting or exceeding all emissions and noise regulations. This new helicopter must also be environmentally friendly. In order to meet this requirement, new technologies must be implemented and closely integrated to create an optimized robust design. The Athena Helicopter detailed in this report is an example of such a helicopter. The Athena incorporates a number of innovative and modern technologies and combines them to safely and effectively take full advantage of their benefits, while minimizing their cost and environmental impacts. It is a truly a "SMART-COPTER" that exhibits the characteristics necessary for success through its entire lifecycle.

Throughout the design an Integrated Product and Process Development (IPPD) methodology was used for conducting tradeoffs to find optimal solutions. This approach focused on the heart or "core" of the helicopter – the main rotor system, the power generation system, and the control system. Based on its simplicity and unique control characteristics, the Hanson elastic articulated (EA) hub was selected for use. The EA's flex beam design and near 1/rev feathering frequency allow the use of rotating electromechanical actuators (EMAs) for primary (cyclic and collective) and Higher Harmonic Control (HHC) through Individual Blade Control (IBC). The HHC provides the Athena with numerous benefits in the form of power reduction, vibration reduction, and noise reduction. The redundant fly-by-wire design provides flexibility in flight control augmentation and allows for advanced control implementation, including envelope protection and trajectory optimization.

A new combustor designed for the optimized turboshaft engine reduces emissions and provides fuel flexibility for transition to lower emission biofuels. The engine's distributed FADEC increases safety and reliability while also optimizing fuel consumption based on fuel type and mission profile. Between the engine and transmission, a dual speed unit provides the ability to lower the rotor speed 8% to reduce noise and power requirements, or to maintain 100% RPM for increased maneuvering ability and/or high speed flight.

At the center of the Athena design is an open control platform (OCP) that provides an open system architecture and a common interface for the flight management computer, FADEC engine controls, helicopter sensors, Health Usage and Monitoring System (HUMS), RPM variation, flight controls and pilot interfaces. This distributed integration allows for all of the Athena's advanced technologies to be managed and optimized to achieve the best possible performance based on mission requirements. This "Smartness" makes the Athena a truly robust design, capable of minimizing energy consumed while adapting to multiple missions without the loss of performance or safety.

Table of Contents

ACKNOWLEDGEMENTS	I
EXECUTIVE SUMMARY	II
TABLE OF CONTENTS	III
LIST OF FIGURES	VII
LIST OF TABLES	X
LIST OF SYMBOLS AND ABBREVIATIONS	XII
PROPOSAL REQUIREMENTS MATRIX	XVI
TABLE OF PHYSICAL DATA	1
DIAGRAM SHEET 1 - THREE-VIEW.....	2
DIAGRAM SHEET 2 - AIRCRAFT PROFILE	3
DIAGRAM SHEET 3 – ENGINE CENTERLINE SCHEMATIC.....	4
DIAGRAM SHEET 4 – DRIVE TRAIN SCHEMATIC	5
1 INTRODUCTION	6
2 REQUIREMENTS ANALYSIS	7
2.1 HELICOPTER MISSION ANALYSIS	8
2.2 OVERALL DESIGN TRADE STUDY APPROACH.....	9
2.2.1 Quality Function Deployment Matrix	9
2.3 OVERALL EVALUATION CRITERION	11
2.3.1 Mission Capability Index	12
2.3.2 Safety Evaluation Criterion.....	12
2.3.3 Noise Evaluation Criterion.....	13
2.3.4 Fuel Consumption Evaluation Criterion	13
2.3.5 Emission Index Evaluation Criterion	14
2.3.6 IQ Index Evaluation Criterion.....	15
2.3.7 Life Cycle Cost Evaluation Criterion.....	15
3 PRELIMINARY SIZING AND PERFORMANCE.....	15
3.1 VEHICLE SIZING METHOD	15
3.2 CIRADS: CONCEPT-INDEPENDENT ROTORCRAFT ANALYSIS AND DESIGN SOFTWARE.....	16
3.2.1 Validation of CIRADS’ Predictions.....	17
3.2.2 Athena Vehicle Sizing Mission.....	18
3.2.3 Configuration Selection: Initial RF Analysis	18
3.2.4 Selection of Major Design Parameters: RF Sensitivity Analysis.....	19
3.3 ROTOR MORPHING TRADE STUDY	19
3.3.1 Dual Speed Optimization	20
4 MAIN ROTOR BLADE AND HUB DESIGN.....	21
4.1 ROTOR BLADE DESIGN	21
4.1.1 Airfoil Selection	21
4.1.2 Twist Selection.....	22
4.1.3 Blade Planform Design	22
4.1.4 Selection of Tip Speed and Disc Loading.....	23

4.1.5	Selection of Blade Number and Solidity	24
4.1.6	Acoustic Analysis.....	24
4.2	HANSON “IDEAL ROTOR” HUB	25
4.3	ADVANCED ROTOR-CONTROL.....	26
4.3.1	Individual Blade Control (IBC).....	26
4.3.2	Higher Harmonic Control (HHC)	27
4.3.3	Roll-Ring Power/Data Transfer Unit	29
4.4	ROTOR DYNAMICS.....	29
4.4.1	Flexure Design	30
4.4.2	Static Droop Analysis	31
4.4.3	Ground Resonance	32
4.4.4	Air Resonance	33
4.5	FINAL DESIGN PARAMETERS.....	33
5	ANTI-TORQUE SELECTION AND DESIGN	34
5.1	ANTI-TORQUE CONFIGURATION SELECTION	34
5.2	FENESTRON DESIGN	35
5.2.1	Selection of Tip Speed and Disc Loading.....	35
5.2.2	Number of Blades and Solidity	35
5.2.3	Blade Spacing.....	36
5.2.4	Airfoil Selection and Blade Twist.....	36
5.2.5	Number of Stator Vanes.....	36
5.2.6	Duct Design.....	37
6	PROPULSION AND TRANSMISSION.....	37
6.1	SUMMARY OF ENGINE SYSTEM DESIGN	37
6.2	REQUIREMENTS AND APPROACH.....	38
6.3	POWER SYSTEM SELECTION	38
6.4	ELECTRIC HYBRID TRADE STUDY	39
6.5	PARAMETRIC CYCLE ANALYSIS	40
6.6	PERFORMANCE CYCLE ANALYSIS	42
6.7	COMPRESSOR.....	43
6.8	FUELS.....	45
6.8.1	Fuels Selection	45
6.8.2	Overall Life Cycle Emissions: Coal Derivative Fuels and Biomass Fuels	46
6.9	COMBUSTOR	47
6.9.1	Pollutant Formation in Turbine Engine Combustors	47
6.9.2	Ultra-low NOx Combustors	48
6.9.3	The Athena Combustor: A Two Stage LPP Combustor.....	48
6.9.4	Emissions from Two Stage LPP Combustors	50
6.9.5	Designing the Two Stage LPP Combustor – overcoming LLP disadvantages	50
6.10	TOTAL EMISSION CHAIN.....	52
6.10.1	JP8 Lifecycle Emissions.....	53
6.10.2	Biomass Synjet Lifecycle Emissions	53
6.11	TURBINE.....	54
6.11.1	Axial vs. Centrifugal Turbines.....	54
6.11.2	Component Design and Materials Selection	54
6.11.3	Turbine Performance and analysis	55
6.12	WEIGHT ANALYSIS	57
6.13	MANUFACTURING.....	57
6.14	FEDERAL AVIATION REGULATIONS (FAR) REQUIREMENTS	58

6.15	TRANSMISSION DESIGN	59
6.15.1	Hanson Transmission Design.....	59
6.15.2	Variable Speed Module (VSM) Selection and Operation	60
6.15.3	Variable Speed Module (VSM) Design	62
7	INTELLIGENT CONTROL SYSTEM ARCHITECTURE	63
7.1	OPEN CONTROL PLATFORM.....	63
7.1.1	Levels of Autonomy.....	64
7.2	FADEC ENGINE CONTROL SYSTEM.....	64
7.2.1	Distributed FADEC.....	65
7.2.2	Engine Controller Architecture	65
7.2.3	Flight/Propulsion Control System.....	66
7.3	MISSION PLANNER.....	67
7.3.1	Envelope Protection	68
7.3.2	Control Reconfiguration & Safety	69
7.4	EXAMPLE MISSION & GUST MODELING	70
7.4.1	Example: Police Surveillance Mission.....	70
7.4.2	GUST Modeling.....	71
7.5	COCKPIT DISPLAY AND INTERFACE SYSTEM	72
7.5.1	Cyclic, Collective, Pedal System	74
8	PERFORMANCE, STABILITY AND HANDLING QUALITIES	75
8.1	ATHENA'S PERFORMANCE.....	75
8.1.1	Performance Comparison.....	77
8.2	FLIGHTLAB MODEL.....	77
8.3	FLIGHTLAB ANALYSIS AND RESULTS	78
8.3.1	Trim Variables	78
8.3.2	High-g Maneuvers.....	81
8.3.3	Flight Loads and Moments.....	81
8.3.4	Dynamic Stability and Handling Qualities.....	83
9	STRUCTURAL DESIGN	84
9.1	VEHICLE WEIGHT AND BALANCE.....	84
9.1.1	Weight and Balance Requirements	84
9.1.2	Weight Analysis	84
9.1.3	Center of Gravity Analysis.....	85
9.2	STRUCTURAL DESIGN CRITERIA.....	85
9.3	FUSELAGE DESIGN.....	86
9.3.1	Configuration Selection.....	86
9.3.2	Composite Structure.....	86
9.3.3	Fuselage Analysis.....	87
9.3.4	Fatigue Monitoring.....	87
9.3.5	Manufacturing	88
9.4	LANDING GEAR	88
9.4.1	Configuration	88
9.4.2	Dimensions and Materials	88
9.4.3	Limit Drop Test.....	89
9.5	CABIN CONFIGURATION AND LAYOUT.....	89
10	COST ANALYSIS.....	90
10.1	OVERVIEW OF LIFE CYCLE COST.....	90

10.2	ENGINE COST MODEL	91
10.3	ATHENA COST MODEL.....	91
10.3.1	Research, Testing, Development and Evaluation.....	91
10.3.2	Recurring Production Cost.....	92
10.3.3	Direct Operating Cost (DOC)	92
10.4	ECONOMIC UNCERTAINTY ANALYSIS	93
11	SAFETY AND CERTIFICATION.....	93
11.1	SAFETY ANALYSIS	93
11.1.1	Functional Analysis.....	94
11.1.2	Functional Hazard Assessment	94
11.1.3	Preliminary System Safety Assessment (PSSA).....	95
11.1.4	Athena Safety Features.....	95
11.2	CERTIFICATION PLAN	96
11.2.1	Certification schedule.....	96
12	CONCLUSION.....	96
	APPENDIX A – GROUP WEIGHT STATEMENT.....	98
	APPENDIX B – RECURRING COST BREAKDOWN.....	99

List of Figures

FIGURE 1-1: GEORGIA TECH PRELIMINARY DESIGN PRODUCT AND PROCESS DEVELOPMENT	6
FIGURE 1-2: PROJECT TIMELINE	7
FIGURE 2-1: MILITARY CONVOY SECURITY MISSION	8
FIGURE 2-2: PARA-MILITARY SURVEILLANCE MISSION	8
FIGURE 2-3: PUBLIC MULTI-PURPOSE VFR TRAINING MISSION	9
FIGURE 2-4: QFD SHOWN WITH ALL SIX “ROOMS”	10
FIGURE 3-1: SCHEMATIC ILLUSTRATION OF THE RF METHOD	16
FIGURE 3-2: CIRADS VALIDATION USING LYNX DATA	17
FIGURE 3-3: SIZING MISSION	18
FIGURE 3-4: FUEL CONSUMPTION OF DUAL-SPEED ROTOR	21
FIGURE 3-5: AIRSPEED-ALTITUDE LIMITS TO AVOID RETREATING BLADE STALL.....	21
FIGURE 4-1: SPECIFIC RANGE WITH DIFFERENT AIRFOILS	22
FIGURE 4-2: POWER REQUIRED WITH DIFFERENT AIRFOILS	22
FIGURE 4-3: BLADE TWIST.....	22
FIGURE 4-4: ROTOR BLADE SPECIFICATIONS	23
FIGURE 4-5: VALIDATION OF DESIGN TWIST.....	23
FIGURE 4-6: POWER REQUIRED VS. VT AND DL	23
FIGURE 4-7: VARIATION OF FUEL AND POWER REQUIRED WITH SOLIDITY	24
FIGURE 4-8: NOISE BREAKDOWN WITH ATHENA FLYING	24
FIGURE 4-9: ACOUSTIC FOOTPRINTS AT MAX GROSS WEIGHT ¹⁶	24
FIGURE 4-10: HANSON HUB ¹⁷	25
FIGURE 4-11: BLADE PITCH TORQUE - RATE ENVELOPE FOR ZF TEST HELICOPTER CH-53G ¹⁹	26
FIGURE 4-12: ZF EMA LAYOUT ¹⁹	26
FIGURE 4-13: IBC VIBRATION REDUCTION ²⁴	27
FIGURE 4-14: BVI WITHOUT IBC.....	28
FIGURE 4-15: BVI WITH IBC.....	28
FIGURE 4-16: POWER IMPROVEMENTS.....	28
FIGURE 4-17: ROLL RING CUT AWAY.....	29
FIGURE 4-18: ROLL RING UNIT ON ATHENA HUB	29
FIGURE 4-19: ATHENA MAIN ROTOR NATURAL FREQUENCIES.....	30
FIGURE 4-20: HANSON FLEXURE CROSS SECTION.....	31
FIGURE 4-21: HANSON FLEXURE DIMENSIONS.....	31
FIGURE 4-22: ANSYS MODEL OF BLADE CROSS SECTION	31
FIGURE 4-23: STATIC DROOP	31
FIGURE 4-24: LEAD-LAG AND BODY MODES	32
FIGURE 4-25: TIME RESPONSE OF ROTOR CG LOCATION.....	32
FIGURE 4-26: ROTOR CG CONTOUR IN XY PLANE.....	32
FIGURE 4-27: EA AND AIR RESONANCE	33
FIGURE 5-1: FENESTRON DESIGN.....	35
FIGURE 5-2: FAN POWER VS. DIAMETER	35
FIGURE 5-3: FENESTRON AIRFOIL SELECTION.....	36
FIGURE 6-1: ENGINE DESIGN AND SIZING PROCESS	38
FIGURE 6-2: TOPSIS PLOT COMPARING PROPULSION SYSTEMS	39
FIGURE 6-3: PARAMETRIC CYCLE ANALYSIS IN GASTURB 10	41
FIGURE 6-4: OFF DESIGN PERFORMANCE ANALYSIS.....	42
FIGURE 6-5: ATHENA ENGINE MODELED USING NPSS.....	42
FIGURE 6-6: ATHENA ENGINE PERFORMANCE PLOT- MCP.....	43
FIGURE 6-7: ATHENA ENGINE PERFORMANCE PLOT 5-MINUTE TO POWER WITH EMISSIONS TRENDS	43

FIGURE 6-8: CENTRIFUGAL COMPRESSOR PERFORMANCE MAP	44
FIGURE 6-9: PARTICULATE EMISSIONS FROM F-T BLENDS WITH JP8	46
FIGURE 6-10: LIFECYCLE SYNJET CO2 EMISSIONS	47
FIGURE 6-11: ATHENA REVERSE FLOW, TWO STAGE LEAN-LEAN LPP COMBUSTOR (LL)	49
FIGURE 6-12: CO AND UHC EMISSIONS FROM A TWO STAGE LPP COMBUSTOR OVER VARIOUS OVERALL EQUIVALENCY RATIOS.	50
FIGURE 6-13: NOX EMISSIONS FROM A TWO STAGE COMBUSTOR OVER VARIOUS EQUIVALENCY RATIOS.	50
FIGURE 6-14: THERMO-ACOUSTIC PRESSURE FLUCTUATION IN EXPERIMENTAL LPP COMBUSTOR WITH STR CONTROLLER.	51
FIGURE 6-15: LIFECYCLE PROCESSES FOR JP8 AND BIOMASS SYNJET.....	52
FIGURE 6-16: TURBINE COOLING TECHNOLOGY PROJECTIONS.....	55
FIGURE 6-17: ALLOWABLE TURBINE TEMPRITURES AND COOLING METHODS.	55
FIGURE 6-18: POWER TURBINE OFF-DESIGN PERFORMANCE MAP.	55
FIGURE 6-19: HIGH PRESSURE TURBINE OFF-DESIGN PERFORMANCE MAP.	55
FIGURE 6-20: TURBINE MATERIAL SELECTION PLOT.	56
FIGURE 6-21: BLADE STRESS VS SPECIFIC STRENGTH.....	56
FIGURE 6-22: ATHENA’S HANSON TRANSMISSION	59
FIGURE 6-23: ACTUAL HANSON TRANSMISSION	59
FIGURE 6-24: VARIABLE SPEED MODULE (VSM) CONCEPT	62
FIGURE 6-25: MOUNTED VARIABLE SPEED MODULE (VSM).....	62
FIGURE 7-1: OVERALL CONTROL SYSTEM ARCHITECTURE.....	63
FIGURE 7-2: DISTRIBUTED FADEC ARCHITECTURE USING THE OCP	65
FIGURE 7-3: ENGINE CONTROLLER ARCHITECTURE.....	65
FIGURE 7-4: BLOCK DIAGRAM OF FLIGHT/PROPULSION CONTROL.....	66
FIGURE 7-5: FLIGHT CONTROL SYSTEM.	67
FIGURE 7-6: NOTIONAL ILLUSTRATION OF RECEDING-HORIZON OPTIMIZATION	67
FIGURE 7-7: ILLUSTRATION OF ENVELOPE PROTECTION	69
FIGURE 7-8: EXAMPLES OF IBC ACTUATOR FAILURE/DEGRADATION SCENARIOS	69
FIGURE 7-9: TRANSLATIONAL AND ANGULAR VEHICLE ACCELERATIONS AFTER FAILURE AT ONE ROTOR BLADE ACTUATOR WITHOUT AND WITH CONTROL RECONFIGURATION	70
FIGURE 7-10: POLICE SURVEILLANCE MISSION PROFILE	70
FIGURE 7-11: FLIGHT TRAJECTORY FOR POLICE SURVEILLANCE IN A NOISE-SENSITIVE ENVIRONMENT. 71	71
FIGURE 7-12: TRAJECTORY SIMULATION IN GUST	71
FIGURE 7-13: ATHENA CONSOLE LAYOUT	72
FIGURE 7-14: ATHENA RETRACTABLE HEADS-UP DISPLAY (HUD)	73
FIGURE 7-15: ATHENA UP FRONT DISPLAY (UFD)	74
FIGURE 8-1: POWER REQUIRED AND RATE OF CLIMB VS. AIRSPEED	75
FIGURE 8-2: SPECIFIC RANGE VS. AIRSPEED	76
FIGURE 8-3: SPECIFIC ENDURANCE VS. AIRSPEED.....	76
FIGURE 8-4: HOGE ALTITUDE VS. WEIGHT	76
FIGURE 8-5: PAYLOAD VS. RANGE.....	76
FIGURE 8-6: ENDURANCE VS. PAYLOAD	76
FIGURE 8-7: HEIGHT-VELOCITY DIAGRAM	76
FIGURE 8-8: POWER VS. AIRSPEED	77
FIGURE 8-9: HOURLY FUEL CONSUMPTION VS. ALTITUDE	77
FIGURE 8-10: FLIGHTLAB SCHEMATIC THROUGH DESIGN PROCESS	78
FIGURE 8-11: ATHENA MR COLLECTIVE POSITION.....	79
FIGURE 8-12: BO-105MR COLLECTIVE POSITION.....	79
FIGURE 8-13: ATHENA MR LATERAL CYCLIC.....	79
FIGURE 8-14: BO-105 MR LATERAL CYCLIC.....	79

FIGURE 8-15: ATHENA MR LONGITUDINAL CYCLIC	79
FIGURE 8-16: BO-105 MR LONGITUDINAL CYCLIC	79
FIGURE 8-17: TR COLLECTIVE POSITION.....	80
FIGURE 8-18: BO-105 TR COLLECTIVE POSITION	80
FIGURE 8-19: ATHENA BODY PITCH ATTITUDE.....	80
FIGURE 8-20: BO-105 BODY PITCH ATTITUDE.....	80
FIGURE 8-21: ATHENA BODY ROLL ATTITUDE	80
FIGURE 8-22: BO-105 BODY ROLL ATTITUDE.....	80
FIGURE 8-23: STEADY TURN LOAD FACTOR	81
FIGURE 8-24: HUB FORCES AND MOMENTS, HIGH-G MANEUVER.....	81
FIGURE 8-25: MR HUB HORIZONTAL FORCE.....	82
FIGURE 8-26: MR HUB ROLLING MOMENT	82
FIGURE 8-27: MR HUB SIDE FORCE.....	82
FIGURE 8-28: MR HUB PITCHING MOMENT	82
FIGURE 8-29: MR HUB NORMAL FORCE.....	82
FIGURE 8-30: MR HUB TORQUE	82
FIGURE 8-31: ROOT LOCUS AT A HOVER	83
FIGURE 8-32: ROOT LOCUS AT 100 KNOTS FORWARD FLIGHT	83
FIGURE 8-33: HANDLING QUALITIES IN FORWARD FLIGHT – DUTCH ROLL MODE	83
FIGURE 8-34: HANDLING QUALITIES IN HOVER	83
FIGURE 9-1: CENTER OF GRAVITY ENVELOPE.....	85
FIGURE 9-2: MAXIMUM LOAD FACTOR ENVELOPE	86
FIGURE 9-3: 3.5G LOADING CONDITIONS.....	86
FIGURE 9-4: CRASHWORTHY SUBFLOOR DESIGN	87
FIGURE 9-5: STATIC FUSELAGE ANALYSIS	87
FIGURE 9-6: DELMIA ASSEMBLY	88
FIGURE 9-7: LANDING GEAR VISUALIZATION MODEL	89
FIGURE 9-8: LEVEL RESERVE DROP TEST ANALYSIS	89
FIGURE 9-9: CABIN LAYOUT.....	90
FIGURE 9-10: FUSELAGE CONFIGURATION CONCEPT.....	90
FIGURE 10-1: VALIDATION OF PC BELL COST MODEL.....	90
FIGURE 10-2: ATHENA PRODUCTION COST BREAKDOWN	92
FIGURE 10-3: ATHENA OPERATING COST DIRECT PIE CHART	92
FIGURE 10-4: @ RISK OUTPUT REPORT (\$2008)	93
FIGURE 11-1: FUNCTIONAL DECOMPOSITION BLOCK DIAGRAM.....	94
FIGURE 11-2: FIVE PHASES OF CERTIFICATION	96
FIGURE 11-3: ATHENA CERTIFICATION SCHEDULE	96

List of Tables

TABLE 2-1: OEC COEFFICIENT BREAKDOWN.....	11
TABLE 3-1: VALIDATION OF PERFORMANCE ESTIMATES (MD-500E)	17
TABLE 3-2: VALIDATION OF PERFORMANCE ESTIMATES (EC-120)	17
TABLE 3-3: A PRIORI DATA	18
TABLE 3-4: RF SIZING RESULTS	19
TABLE 3-5 ROTOR-MORPHING CONCEPTS INVESTIGATED”	19
TABLE 3-6: RANGE MISSION COMPARISON OF ONE-SPEED AND DUAL-SPEED ROTOR	20
TABLE 4-1: TRANSFER REQUIREMENTS ²⁶	29
TABLE 4-2: SPANWISE FLEXURE STIFFNESS DATA.....	31
TABLE 4-3 FINAL DESIGN PARAMETERS	33
TABLE 5-1: ANTI TORQUE SELECTION MATRIX	34
TABLE 5-2: FENESTRON CONFIGURATION	37
TABLE 6-1: ATHENA ENGINE SPECIFICATIONS.....	37
TABLE 6-2: SUMMARY OF ENGINE TECHNOLOGIES.....	37
TABLE 6-3: ENGINE TYPES CONSIDERED SUMMARY.....	38
TABLE 6-4: HYBRID VS TURBOSHAFT TRADE STUDY RESULTS.	40
TABLE 6-5: COMPONENT EFFICIENCY ASSUMPTIONS FOR TECH. LEVEL	41
TABLE 6-6: FUEL COMPARISON BY ENERGY DENSITY	45
TABLE 6-7: FUELS WITH ENERGY DENSITY, EMISSIONS, AND AVAILABILITY RELATIVE TO JP8	46
TABLE 6-8: POLLUTANT FORMATION METHODS	47
TABLE 6-9: SUMMARY OF COMBUSTOR TRADE STUDY RESULTS	48
TABLE 6-10: SUMMARY OF LPP COMBUSTOR ISSUES AND ATHENA'S SOLUTION	50
TABLE 6-11: FOREIGN AND DOMESTIC CRUDE OIL TRANSPORTATION BY METHOD AND PADD	53
TABLE 6-12: LIFECYCLE EMISSIONS FROM JP8.....	53
TABLE 6-13: SOYBEAN PRODUCTION BY STATE.....	53
TABLE 6-14: LIFECYCLE EMISSIONS FROM BIOMASS SYNJET.....	54
TABLE 6-15: ATHENA TURBINE DESIGN PARAMETERS	56
TABLE 6-16: ATHENA ENGINE COMPONENT WEIGHT BREAKDOWN.....	57
TABLE 6-17: FAR PART 27 ENGINE REQUIREMENTS AND ATHENA’S SOLUTIONS	58
TABLE 6-18: FAR PART 33 ENGINE REQUIREMENTS AND ATHENA’S SOLUTIONS	58
TABLE 6-19: TRANSMISSION GEAR STRESS (TO POWER), VSM HIGH (680 FT/S ROTOR TIP SPEED).....	60
TABLE 6-20: TRANSMISSION GEAR STRESS (TO POWER), VSM LOW (630 FT/S ROTOR TIP SPEED).....	60
TABLE 6-21: TRANSMISSION GEAR DIMENSIONS	60
TABLE 6-22: VARIABLE SPEED MODULE (VSM) OPERATING METHODS.....	61
TABLE 6-23: VARIABLE SPEED MODULE (VSM) GEAR DESIGN	62
TABLE 6-24: VARIABLE SPEED MODULE (VSM) STRESSES	62
TABLE 7-1: SENSOR SUITE	66
TABLE 7-2: MULTIPURPOSE DISPLAY (MPD) ARCHITECTURE.....	73
TABLE 8-1: ATTAINED PERFORMANCE AND WEIGHT SPECIFICATIONS.....	75
TABLE 8-2: COMPARISON OF ATHENA PERFORMANCE WITH MD 500 AND EC 120.....	77
TABLE 9-1: COMPONENT WEIGHT BREAKDOWN	84
TABLE 9-2: DROP TEST RESULTS.....	89
TABLE 9-3 ATHENA EQUIVALENT FLAT PLATE AREA.....	90
TABLE 10-1: ENGINE COST SUMMARY 2008 DOLLARS / EUROS (BASED ON €1=\$1.57)	91
TABLE 10-2: COMPARISON OF TOTAL DEVELOPMENT COST 2008 DOLLARS / EUROS (BASED ON €1=\$1.57).....	91
TABLE 10-3: COMPARISON OF ATHENA VS EC 120 AND MD 500 – 2008 DOLLARS/ EUROS (BASED ON €1=\$1.57).....	92

TABLE 10-4: DOC COMPARISON OF EC 120, MD500 AND ATHENA – 2008 DOLLARS/EUROS (BASED ON €1=\$1.57).....	92
TABLE 11-1: ATHENA’S FHA (CATASTROPHIC).....	94
TABLE 11-2: ATHENA SAFETY FEATURES	95

List of Symbols and Abbreviations

Symbols:

b	Number of Blades
c	Chord
C_d	Drag Coefficient
C_l	Lift Coefficient
f	Flat Plate Drag Area
L_v	Dihedral Effect
L_p	Damping in Roll
$L_{\delta a}$	Roll Control Power
M_u	Speed Stability
M_w	Angle of Attack Stability
M_q	Pitch Damping
$M_{\delta c, \delta e}$	Cyclic Pitch control Effectiveness
N_v	Directional Stability
N_r	Yaw Damping
$N_{\delta p}$	Yaw Control Power
R	Radius
T_{04}	Turbine Inlet Temperature
V_{DL}	Design Limit Flight Speed
V_H	Design Maximum Level Flight Speed
V_{NE}	Never Exceed Flight Speed
V_T	Blade Tip Speed
X_u	Drag Damping
X_w	Drag due to Angle of Attack
X_q	Drag due to Pitch Rate
$X_{\delta c, \delta e}$	Drag due to Collective and Cyclic Control Displacements
Y_v	Sideward Damping
$Y_{\delta a}$	Side Force due to Cyclic Control
Z_u	Lift due to Velocity
Z_w	Heave Damping
α	Angle of Attack
δ_a	Lateral Cyclic Control
δ_c	Collective Cyclic Control
δ_e	Longitudinal Cyclic Control
δ_p	Pedal Control
η_{pc}	Compressor Efficiency
η_{pb}	Burner Polytrophic Efficiency
η_{pt}	Turbine Polytrophic Efficiency

θ	Body Pitch Attitude
θ_o	Collective Pitch
θ_{tro}	Tail Rotor Collective Pitch
θ_{ls}	Longitudinal Pitch
θ_{lc}	Lateral Pitch
π_b	Burner Pressure Ratio
π_c	Compressor Pressure Ratio
π_d	Diffuser Pressure Ratio
σ	Compressor Exit Slip Factor
σ	Solidity
ω	Disk Loading

Abbreviations:

AGL	Above Ground Level
AHS	American Helicopter Society
AI	Autorotation Index
AR	Aspect Ratio
BL	Butt Line
BVI	Blade Vortex Interaction
CAD	Computer Aided Design
CAE	Computer Aided Engineering
CAM	Computer Aided Manufacturing
CAS	Command Augmentation System
CFD	Computational Fluid Dynamics
CG	Center of Gravity
CIRADS	Concept Independent Rotorcraft Analysis and Design Software
DOC	Direct Operating Cost
EA	Elastic Articulated
ECS	Environmental Control System
EMA	Electro-Mechanical Actuators
FAA	Federal Aviation Administration
FADEC	Full-Authority Digital Engine Control
FAR	Federal Aviation Regulation
FEA	Finite Element Analysis
FFBD	Functional Flow Block Diagram
FHA	Functional Hazard Assessment
FM	Figure of Merit
FOD	Foreign Object Damage/Debris
FTA	Fault Tree Analysis
F-T	Fischer-Tropsch
FTD	Flight Test Data

GSP	GasTurb Engine Program
GT	Georgia Tech
GTPDP	Georgia Tech Preliminary Design Program
GUST	Georgia Tech Unified Simulation Tool
HHC	Higher Harmonic Control
HOGE	Hover Out of Ground Effect
HPT	High Pressure Turbine
HUD	Heads-Up Display
HUMS	Health Usage and Monitoring System
IBC	Individual Blade Control
IFR	Instrument Flight Rules
IPPD	Integrated Product and Process Development
ISA	International Standard Atmosphere
LCC	Life Cycle Cost
LPP	Lean Premixed, Prevaporized
LTO	Landing-Take Off
MA	Markov Analysis
MCP	Maximum Continuous Power
MPD	Multi Purpose Display Unit
MSL	Mean Sea Level
MTBF	Mean Time Between Failure
MTTR	Mean Time to Repair
NACA	National Advisory Committee on Aeronautics
NASA	National Aeronautics and Space Administration
NPSS	NASA Numerical Propulsion System Simulation
NLR	National Aerospace Laboratory, Netherlands
NM	Nautical Mile
NOE	Nap-of-the-Earth
NPV	Net Present Value
OCP	Open Control Platform
OEC	Overall Evaluation Criterion
PADD	Petroleum Administration for Defense District
PDM	Product Data Management
PLM	Product Lifecycle Management
PSSA	Preliminary System Safety Assessment
PT	Power Turbine
QFD	Quality Functional Deployment
RBD	Reliability Block Diagrams
RF	Ratio of Fuel
RFP	Request For Proposal
RPM	Revolutions per Minute
ROC	Rate of Climb
RQL	Rich-burn/Quick-Quench/Lean-Burn

RTDE	Research, Development, Testing and Evaluation
SCAS	Stability and Control Augmentation System
SFC	Specific Fuel Consumption
SHP	Shaft Horsepower
SLS	Sea-Level Standard
SN	Smoke Number
SPN	Stochastic Petri Nets
STA	Station Line
STP	Standard Temperature and Pressure
TOPSIS	Technique for Ordered Preference by Similarity to Ideal Solution
TR	Tail Rotor
TRL	Technology Readiness Level
TURBN	Turbine Preliminary Design Program
UBC	Unburned Hydrocarbons
UFD	Up Front Display
UHF	Ultra High Frequency (Radio)
VAB	Variable Action Button
VFR	Visual Flight Rules
VHF	Very High Frequency (Radio)
VLCC	Very Large Crude Carrier
VROC	Vertical Rate of Climb
VSM	Variable Speed Module
VTOL	Vertical Take-off and Landing
WL	Water Line

Proposal Requirements Matrix

	Status	Section
General Vehicle Requirements		
Design “SMART-COPTER” capable of vertical takeoff and landing (VTOL) from unprepared area in less than 10 minutes from being positioned on heli-surface.	✓	3.2 7.4
Address benefits of advanced energy reducing technology including: - Rotor Morphing - Higher Harmonic Control - Anti-Torque System - Drag Reduction - Advanced Engine Design and/or Alternative Fuels.	✓	3.3 4.3 5.0 9.5 6.1/6.8
Initial Operational Capability in year 2020	✓	11.2
Utilize advanced technologies in order to enhance safety and reduce noise and vibrations	✓	4.1 4.3 7.3 7.5 9.3 11.1.4
Aircraft must be “low maintenance” with a design focus on reliability and maintainability including lifecycle support, modularity and LEAN implementation.	✓	10.0
Mission Profile Requirements		
Aircraft must be capable of lifting the following payload: - 1 pilot and 4 passengers plus luggage or - 1 pilot and 500kg of freight	✓	8.1 9.5
Must perform multiple military, para-military and commercial missions in addition to those specified in the RFP	✓	2.1 7.3 7.5
Comfort of passengers must equal that of equivalent helicopter with focus on ECS, Seats, Internal Noise, Sun Protection and Vibration.	✓	4.3 9.5
Minimum internal volume: height 1.1 m, length 1.4 m, width 1.0 m	✓	9.5
Performance Capability Requirements		
Aircraft must have sufficient power to hover for 15 minutes at 1500m and ISA +20C	✓	8.1
Minimum recommended cruise speed of 100 knots and range of 300NM	✓	8.1
Use of advanced techniques to enhance mission survivability	✓	7.3 9.3 9.4
A semi-automatic take-off and landing system to allow normal use of aircraft by non professional pilots	✓	7.1 7.3 7.5
Aircraft crashworthiness should meet federal standards to improve overall vehicle safety	✓	9.3
Cost Requirements		
Lifecycle cost reduction that addresses recurring costs, non recurring costs, operating costs and provides comparison with similar sized helicopters.	✓	10.0
Local and complete pollution analyses of the vehicles consumption of energy on the ground and in flight over the entire lifecycle of the vehicle.	✓	6.8.2 6.10

Table of Physical Data

VEHICLE DATA:

Design Gross
 Weight 3262 lb / 1480 kg
 Maximum Gross
 Weight 3450 lb / 1565 kg
 Empty Weight 1545 lb / 700 kg
 Fuel:
 -Tank Capacity · 60 gal / 227 liter
 -Weight 397 lb / 180 kg
 Useful Load 1717 lb / 778 kg
 Number of Seats··· 5
 Cabin Size:
 - Height·· 3.6 ft / 1.1 m
 - Length·· 4.6 ft / 1.4 m
 - Width··· 3.3 ft / 1.0 m

MAIN ROTOR DATA:

Radius 14.75 ft / 4.5 m
 Chord 0.88 ft / 0.268 m
 Number of Blades ·· 4
 Solidity 0.075
 Disc Loading 4.77 lb/ft²
 23.26 kg/m²
 Twist -18/25 deg
 Twist Change Point· 0.50R
 Tip Speed 630/680 ft/sec
 192/207 m/sec
 Shaft Speed 408/440 RPM
 Mast Tilt:
 - Forward · 3 deg
 - Left···· 1 deg
 Airfoil SC1094/SC1095
 Airfoil Transition ·· 0.85R-0.90R
 Tip Sweep Angle··· 20 deg
 Tip Anhedral Angl· 20 deg

PERFORMANCE SUMMARY 100% RPM @ DESIGN GROSS WEIGHT:

<u>Characteristic</u>	<u>Sea Level Standard</u>	<u>1500m/ISA+20</u>
Maximum Forward Airspeed	158 kts / 293 km/hr	146 kts / 270 km/hr
Maximum Range	329 NM / 609 km	346 NM / 641 km
Maximum Range Airspeed	119 kts / 220 km/hr	119 kts / 220 km/hr
Maximum Endurance	4.10 hr	5.45 hr
Maximum Endurance - R/C Airspeed	59 kts / 109 km/hr	66 kts / 122 km/hr
Maximum Vertical Rate of Climb	1,329 ft/min / 6.75 m/sec	824 ft/min / 4.19 m/sec

PERFORMANCE SUMMARY 92% RPM @ DESIGN GROSS WEIGHT:

<u>Characteristic</u>	<u>Sea Level Standard</u>	<u>1500m/ISA+20</u>
Maximum Forward Airspeed	138 kts / 256 km/hr	126 kts / 233 km/hr
Maximum Range	368.6 NM / 683 km	379.7 NM / 703 km
Maximum Range Airspeed	112 kts / 207 km/hr	117 kts / 217 km/hr
Maximum Endurance	5.27 hr	5.63 hr
Maximum Endurance – R/C Airspeed	60 kts / 111 km/hr	67 kts / 124 km/hr
Maximum Vertical Rate of Climb	2,038 ft/min / 10.35 m/sec	1,998 ft/min / 10.15 m/sec

TRANSMISSION DATA:

<u>Rating</u>	<u>SHP</u>
Type Split Torque Hanson Transmission	
Takeoff Power (5 min) 514 HP / 383 kW	
Maximum Continuous Power ·· 414 HP / 308 kW	

FENESTRON DATA:

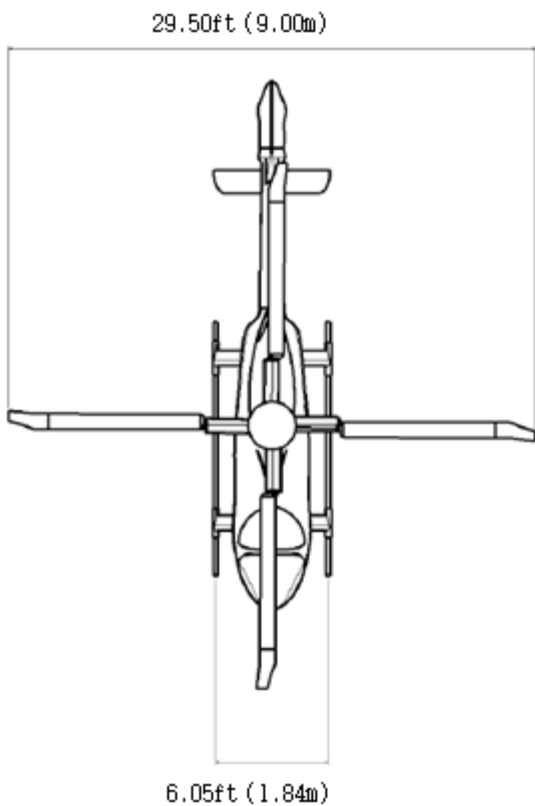
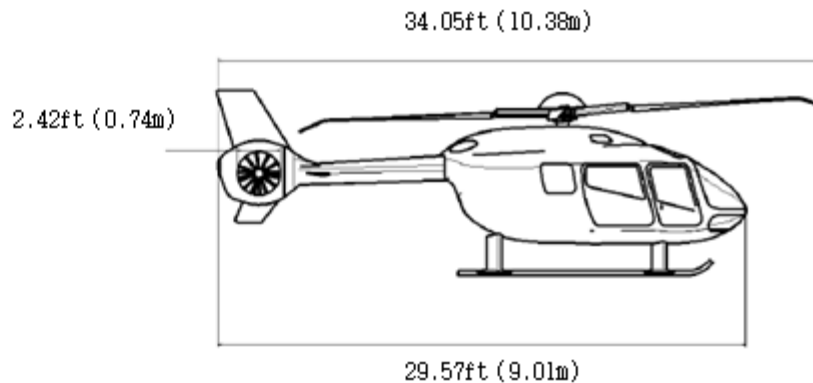
Diameter 2.4 ft / 0.731 m
Chord 0.21 ft / 0.064 m
Number of Blade ··· 10 (unequal spacing)
Number of Stators··· 11 (equal spacing)
Solidity 0.56
Tip Speed······· 575ft/sec 175 m/sec
Shaft Speed 4576 RPM
Blade Airfoil····· VR7
Stator Airfoil····· NACA 65 Type

ENGINE DATA:

<u>Rating</u>	<u>SLS</u>	<u>SFC</u>
Takeoff Power (5 min)	467 HP 348 kW	0.4462 lb/Hp/hr 0.2710 kg/kW/hr
Max Continuous Power	376 HP 280 kW	0.4489 lb/Hp/hr 0.2730 kg/kW/hr

	<u>SLS</u>	<u>Burn Rate</u>
Cruise: (100% RPM)		
Max Range	250 HP 186 kW	123.7 lb/hr 55.99 kg/hr
Max Endurance	162 HP 121 kW	98.61 lb/hr 44.77 kg/hr
Cruise: (92% RPM)		
Max Range	235 HP 175 kW	116.3 lb/hr 52.75 kg/hr
Max Endurance	169 HP 126 kW	94.88 lb/hr 43.04 kg/hr

Diagram Sheet 1 - Three-View



Scale: 1:25

Diagram Sheet 2 - Aircraft Profile

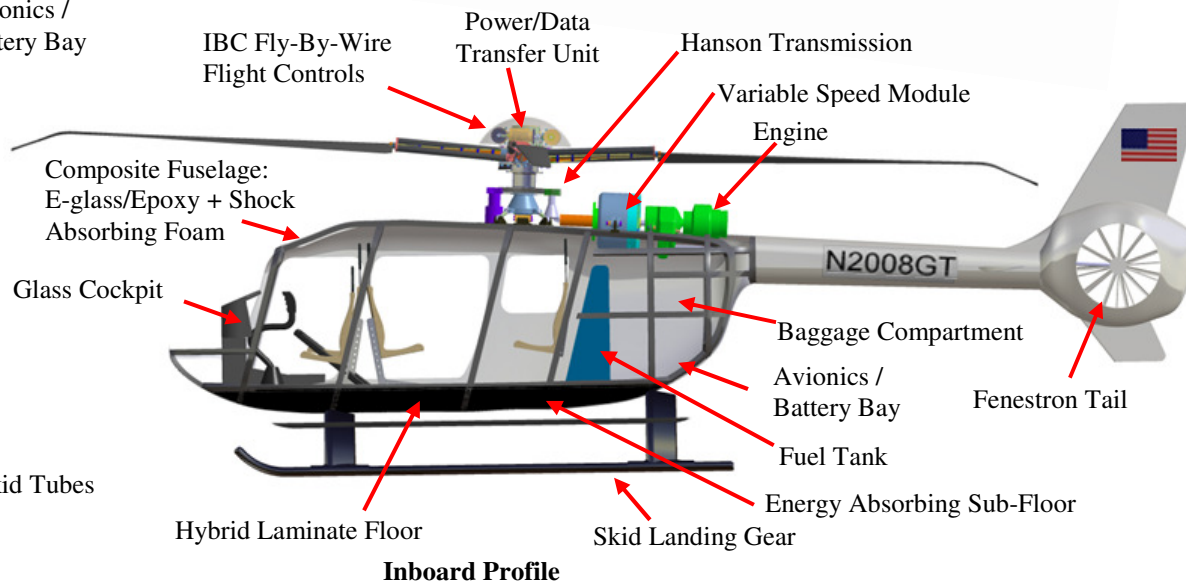
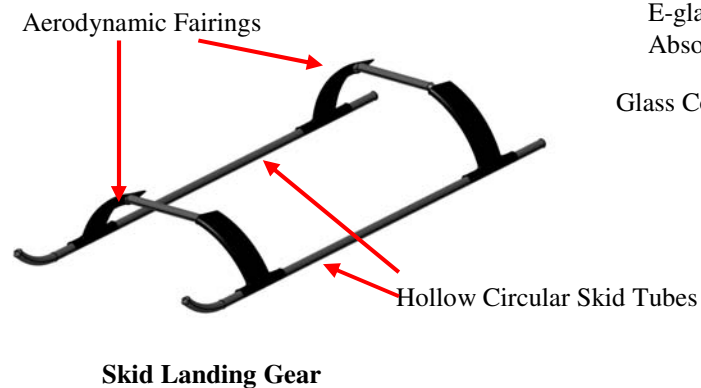
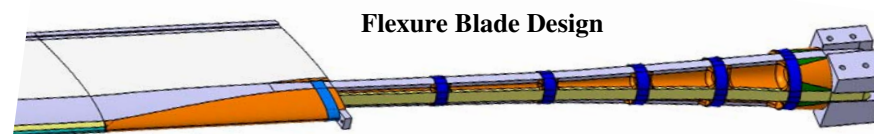
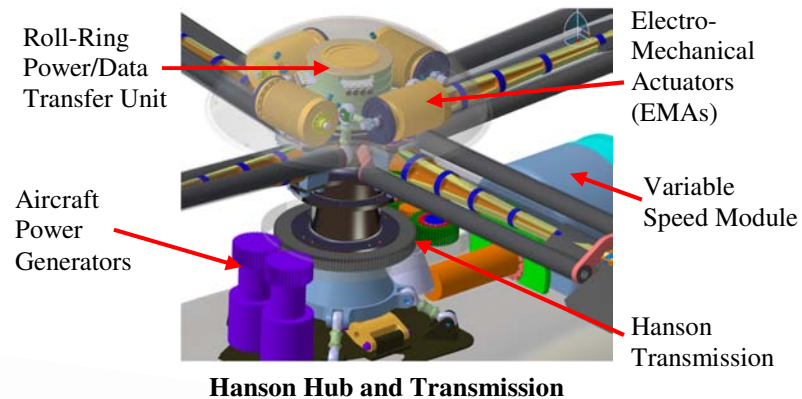
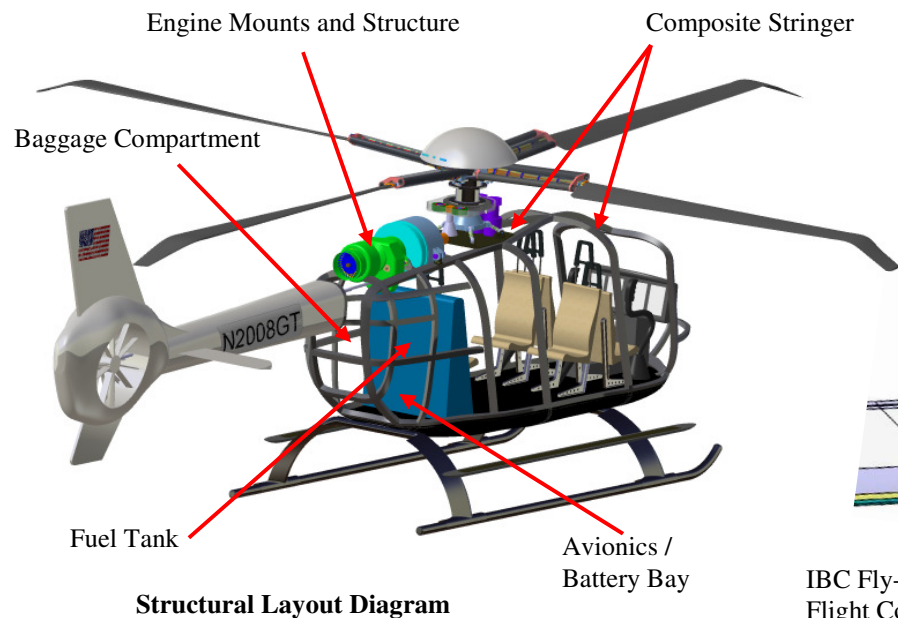


Diagram Sheet 3 – Engine Centerline Schematic

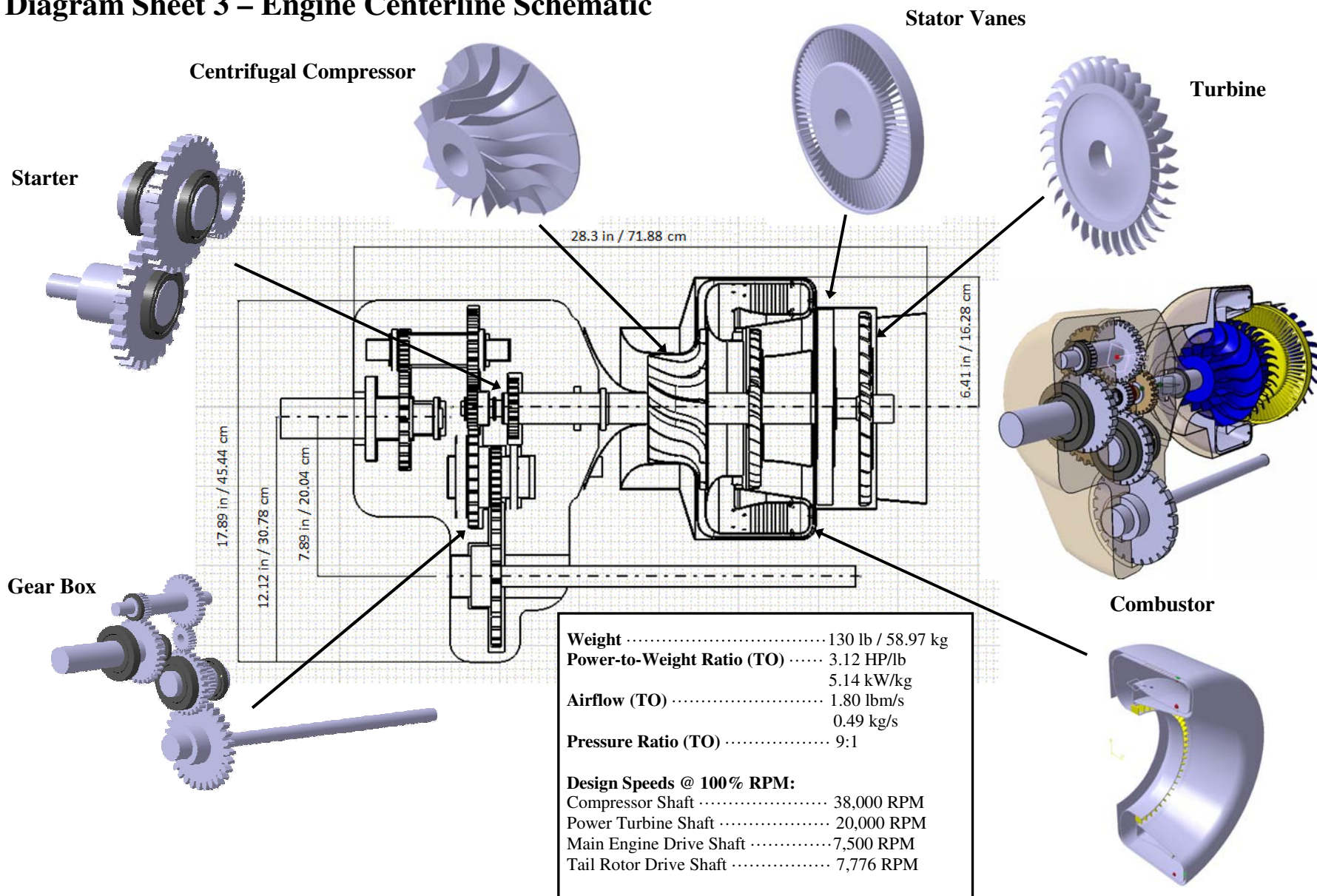
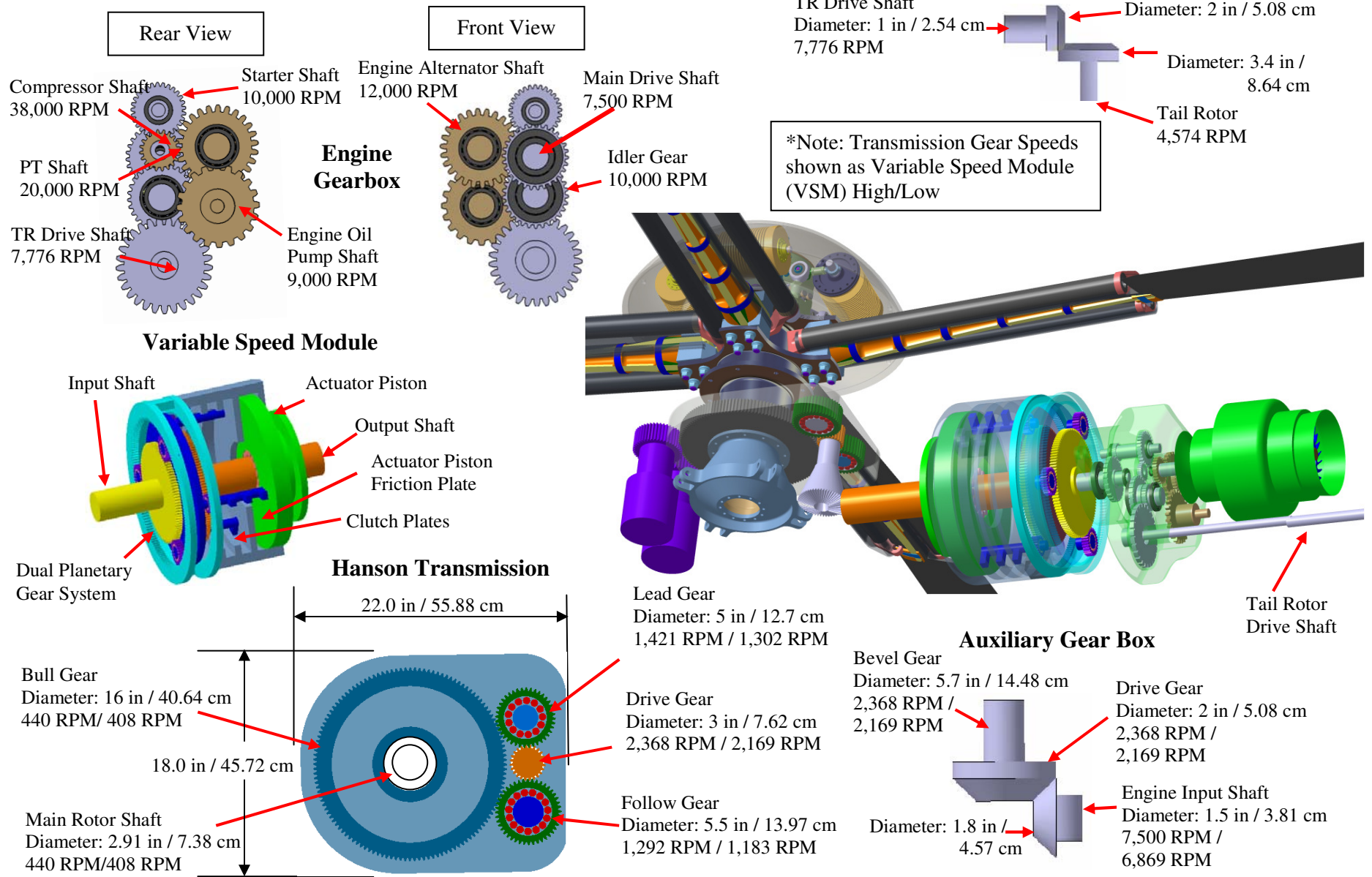


Diagram Sheet 4 – Drive Train Schematic



1 INTRODUCTION

In response to the 25th Annual Student Design Competition sponsored by the American Helicopter Society (AHS) International and Eurocopter, this graduate student team report describes the preliminary design of a short range, medium speed, five seat “SMART-COPTER,” with a focus on minimizing energy consumption. In order to take into account the full life cycle of the design from manufacturing to operation and maintenance, an integrated product and process development (IPPD) methodology was used to conduct parallel analysis to achieve effective synthesis of numerous product and process design disciplines. Figure 1-1 depicts graphically the IPPD process consisting of three design loops: Conceptual Design, Preliminary Design, and Process Design. An initial Product Data Management (PDM) loop is identified, as well. This methodology is particularly well suited to this design competition because the IPPD process includes both product and process development and allows for the integration of computer aided design (CAD), computer aided Engineering (CAE), computer aided manufacturing (CAM), and for supporting Product Lifecycle Management (PLM) and Life Cycle Cost (LCC).

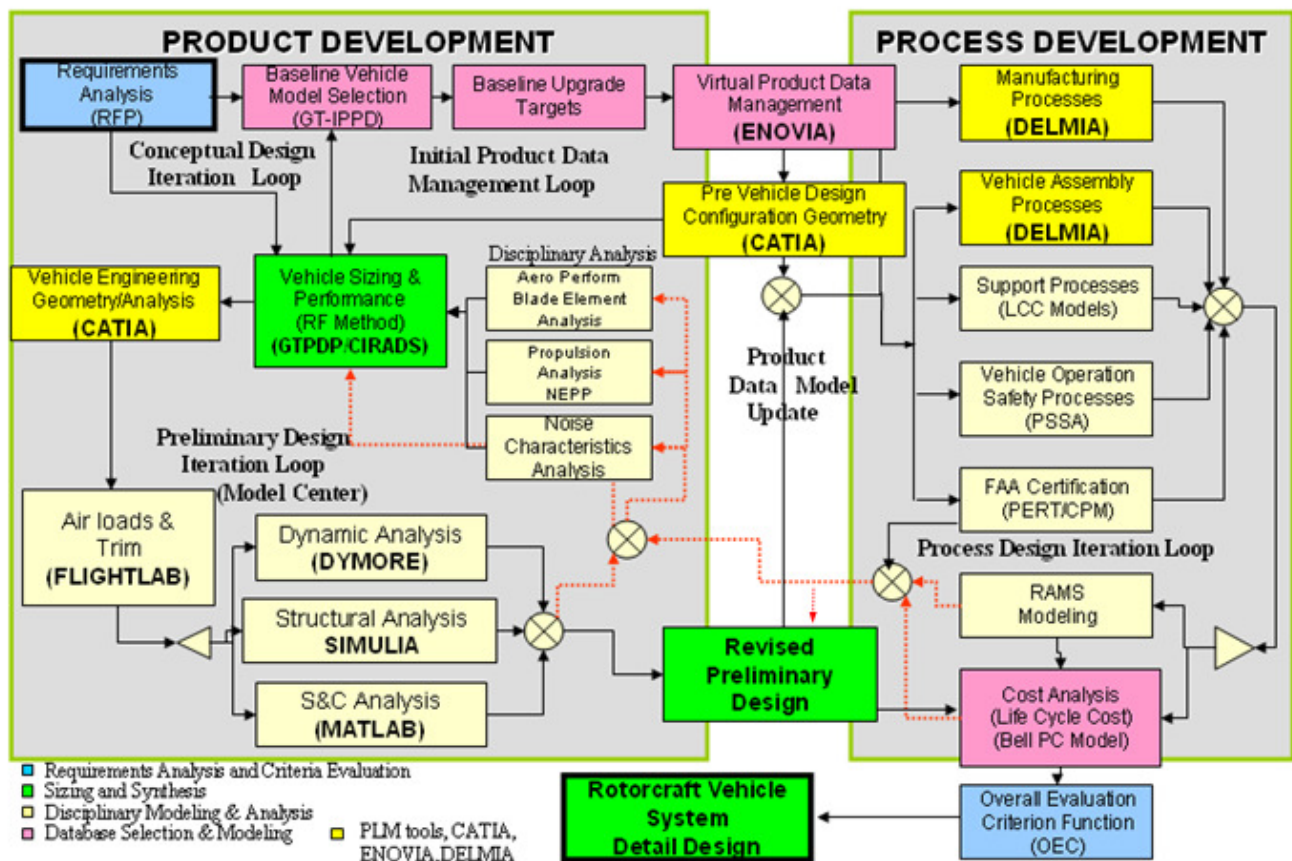


Figure 1-1: Georgia Tech Preliminary Design Product and Process Development

The design process began with analysis of the requirements outlined in the 25th Annual AHS Student Design Competition Request for Proposals (RFP) for a “SMART-COPTER.” These requirements served as the foundation for the initial design. Once the RFP requirements were analyzed, the team developed a conceptual design baseline vehicle using the Georgia Tech Concept Independent Rotorcraft Analysis and Design Software (CIRADS) and the Georgia Tech Preliminary Design Program (GTPDP) synthesis tools. Once the baseline vehicle was established, an initial CATIA model was developed in order to start both the product and process design loops.

The baseline development was followed by preliminary design where a more detailed analysis identified the necessary modifications to refine the baseline concept. This analysis included aerodynamic performance optimization, structural design, structural analysis, material selection, refined CAD modeling, helicopter stability and control analysis, dynamic analysis, propulsion system design, manufacturing assessment, safety analysis, and life cycle cost analysis. The team has also addressed the influence of the manufacturing processes required for the design. To address the manufacturability of the design, DELMIA, a state-of-the-art CAM tool, was used in conjunction with CATIA V5, for integrated design and manufacturing. It was through the delicate balance of product and process demands that the team effectively arrived at a design solution that best met the RFP requirements. The timeline followed during this process is shown in Figure 1-2 concurrent with the supporting rotorcraft course offered at GT.

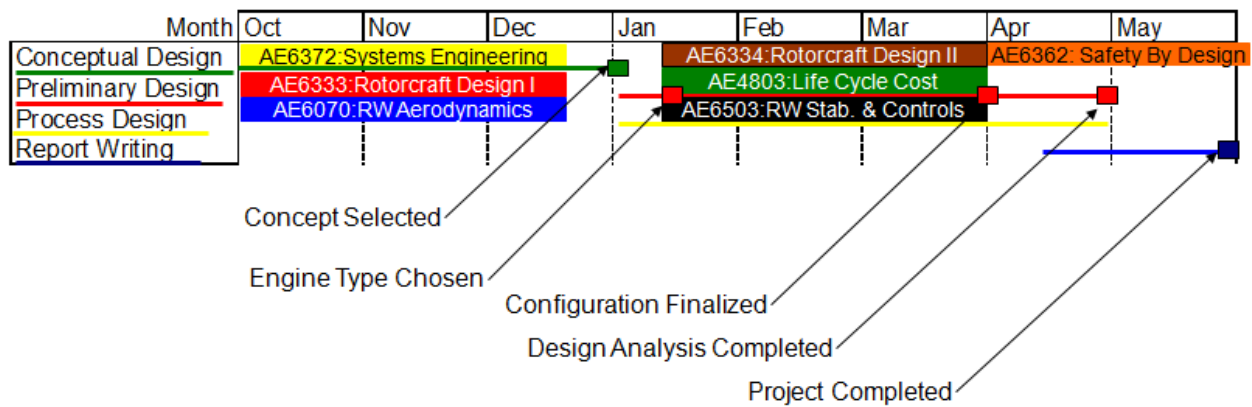


Figure 1-2: Project Timeline

2 REQUIREMENTS ANALYSIS

The RFP outlines that the design must be able to perform all conceivable military, para-military, and public multi-purpose transport missions. It specifies that the vehicle should be designed for minimizing fuel consumption for a one-hour flight at 120 knots, and have a range of 300 nautical miles. Based on this information, an airspeed of 120 knots and a range of 300 nautical miles were used as the cruise segment of the mission analysis.

The RFP presents a requirement for hover out of ground effect (HOGE) for 15 minutes at maximum takeoff weight and environmental conditions of 1500 meters (4921ft) and ISA +20°C. This hover requirement determined the engine sizing and installed power requirements.

The payload and crew requirements were clearly specified as a crew member of 100kg (220lbs) and maximum cargo weight of 500kg (1102lbs). The RFP also dictated a minimum internal volume and weight configuration for passengers, and that the vehicle minimizes energy consumption throughout its lifecycle.

2.1 Helicopter Mission Analysis

The functions for the proposed rotorcraft were separated into three categories: military, para-military, and multi-purpose public-air-vehicle. The three categories have many functions in common but the composition and duration of mission segments can be quite varied. In order to evaluate the mission “robustness” of the vehicle, three typical missions were developed. These missions represent a cross section of possible missions and were used to evaluate the design and ensure its multi-mission capability.

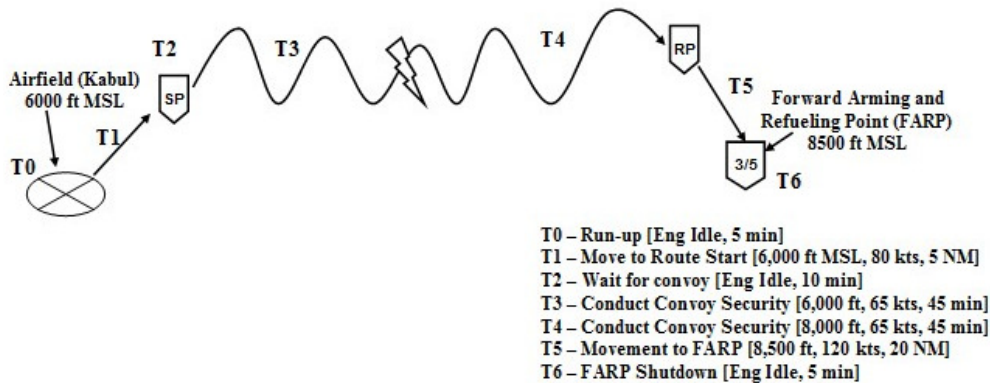


Figure 2-1: Military Convoy Security Mission

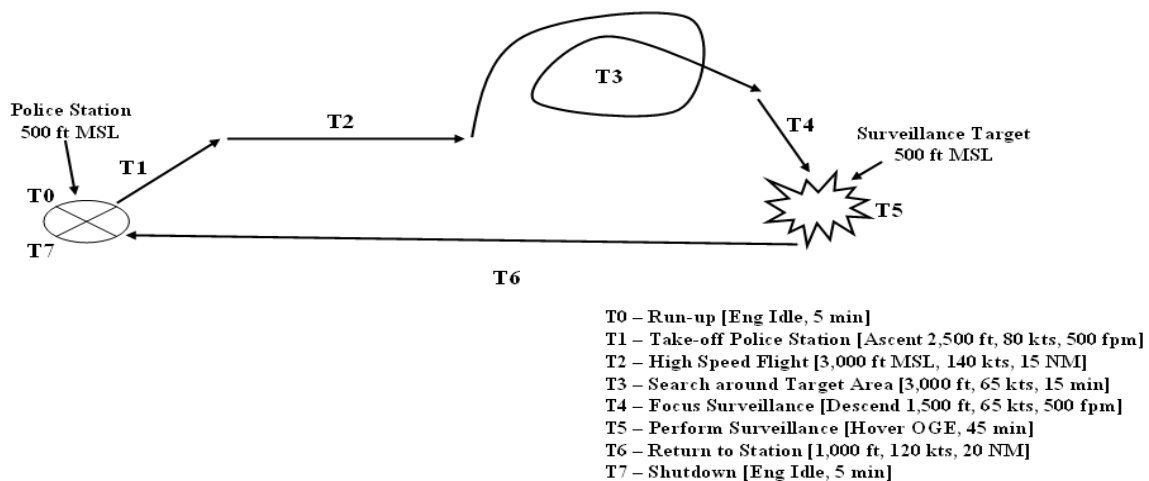


Figure 2-2: Para-Military Surveillance Mission

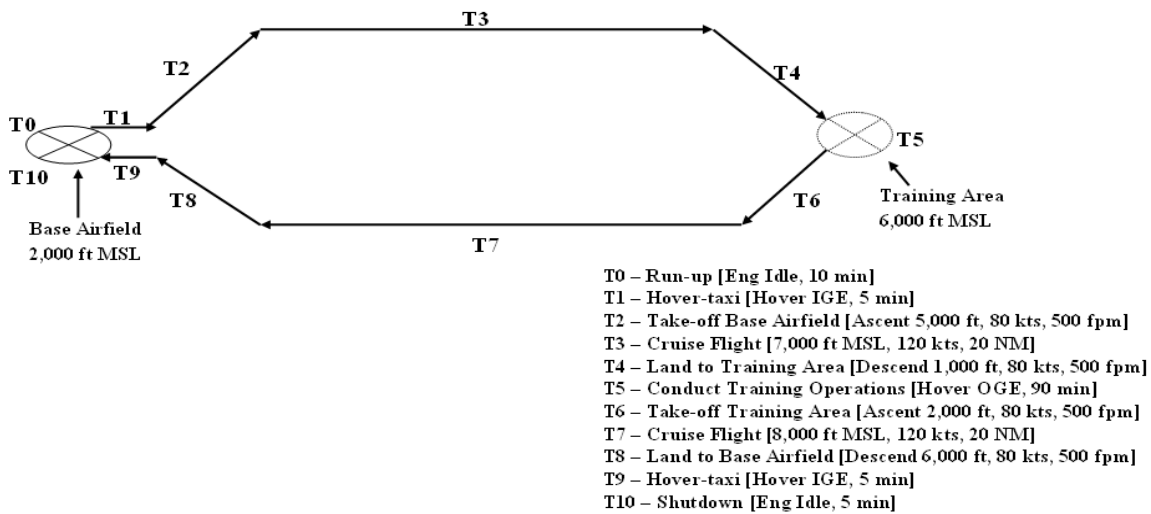


Figure 2-3: Public Multi-Purpose VFR Training Mission

The overall result of the mission analysis was the determination that the vehicle must satisfy a number of different customers and therefore be robust in nature. The mission analysis also assisted in determining customer requirements to be incorporated in the Quality Functional Deployment (QFD) planning matrix.

2.2 Overall Design Trade Study Approach

To properly capture the customer requirements and lay the foundation for a successful design, several common management and planning tools were used, including: affinity diagrams, tree diagrams, pareto charts, and a Quality Function Deployment (QFD) matrix. These tools helped define and prioritize the customer requirements. Clearly defining typical missions and capturing the customer requirements at the beginning of the design process reduced the number of design changes required, and reduced the overall cost of the project.

2.2.1 Quality Function Deployment Matrix

A QFD matrix was used to determine relationships between the customer requirements defined in the RFP, or determined through mission analysis, with their corresponding engineering characteristics. A QFD matrix, sometimes called the “House of Quality,” has several sections that represent different ways of valuing both customer requirements and engineering characteristics. The QFD developed for the 2008 AHS competition consists of six “rooms” and is shown in Figure 2-4. In addition to defining the most important requirements, the QFD matrix also provided the team with an initial set of engineering targets and performance goals.

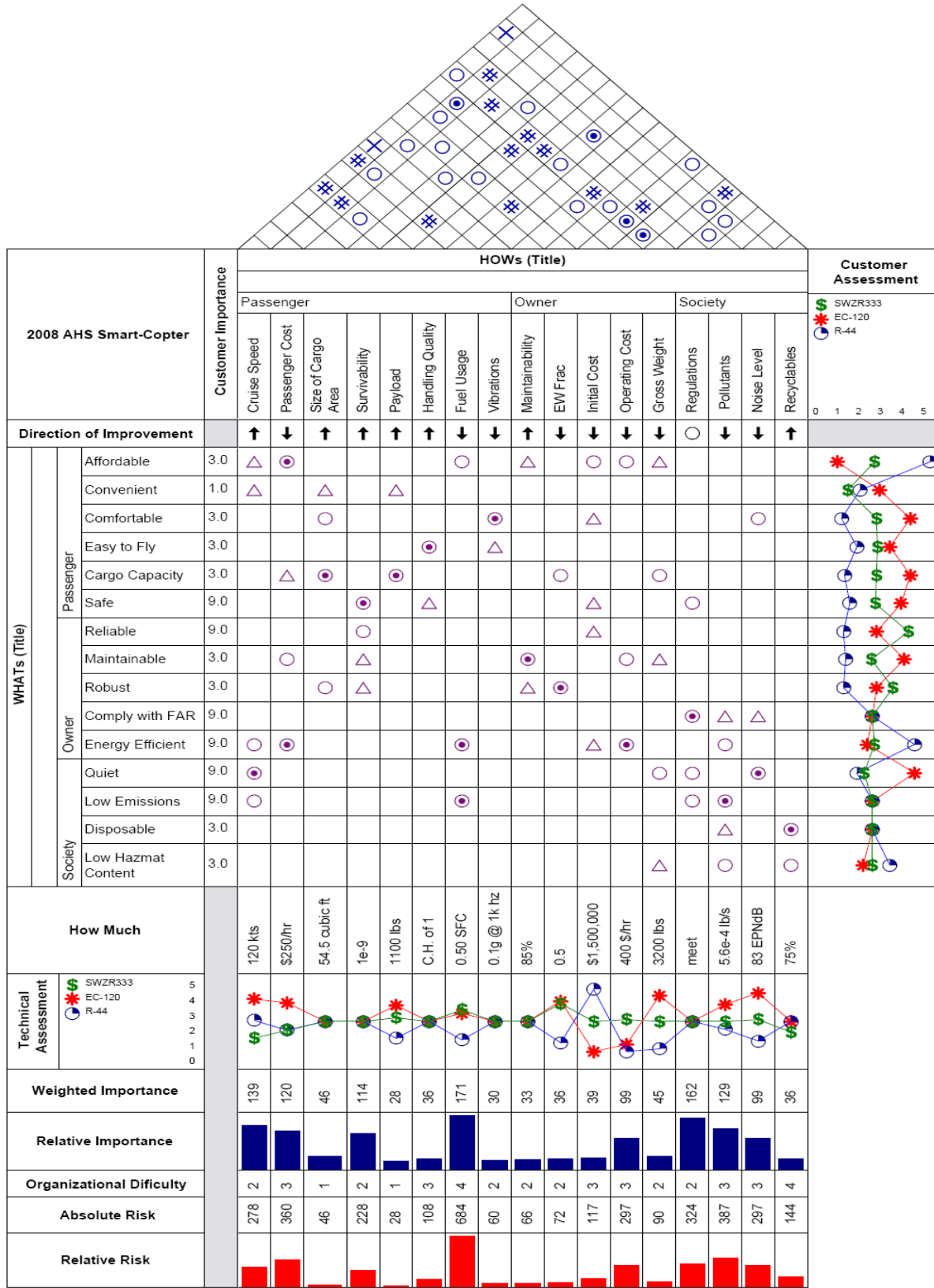


Figure 2-4: QFD Shown With All Six "Rooms"

2.3 Overall Evaluation Criterion

The QFD matrix quantified the engineering characteristics most important to meeting the customer's requirements. From this analysis of critical requirements an Overall Evaluation Criterion (OEC) was developed to provide a single scalar measure, from zero to one (with one being best), that defined the total value of a design configuration. It encapsulated all pertinent design considerations and was the single meter against which conceptual design trades were weighed and measured. During the preliminary design phase it was used to ensure a robust design capable of meeting and exceeding all customer requirements. For the 2008 AHS Student Design Competition seven key metrics were determined to be critical; Mission Capability, Safety, Noise, Fuel Consumption, Emissions, Intelligence and Life Cycle Cost.

$$OEC = \frac{(0.18MCI + 0.12SI + 0.10NI + 0.21FCI + 0.13EI + .07IQI) \cdot 5}{4 + LCC}$$

All indices are values of 0 to 1 where:

MCI = Mission Capability Index

SI = Safety Index

NI = Noise Index

FCI = Fuel Consumption Index

EI = Emissions Index

IQI = Intelligence Index

LCC = Life Cycle Cost Index

The coefficients in front of each index set the weighing of the index. They were derived from the weighted importance values in the QFD matrix for the engineering characteristics that influenced each index. These relative importance values were converted to percent importance and transformed into coefficients that result in a value between 0 and 1 for the overall evaluation criterion. The engineering characteristics and weighted importance values and resulting percentage importance are contained in Table 2-1.

Table 2-1: OEC Coefficient Breakdown

<u>Evaluation Criterion</u>	<u>Engineering Requirements from QFD</u>	<u>Weighted Importance</u>		<u>Relative Importance</u>
MCI = Mission Capability Index	Cruise Speed	139		
	Maintainability	33		
	MCI Total		172	17.90%
SI = Safety Index	Survivability	114		
	SI Total		114	11.86%
NI = Noise Index	Noise	99		
	NI Total		99	10.30%
FCI = Fuel Consumption Index	Fuel Usage	171		
	EW Ratio	36		
	FCI Total		207	21.54%
EI = Emissions Index	Pollutants	129		
	EI Total		129	13.42%
IQI = Intelligence Index	Handling Quality	36		
	Vibrations	30		
			66	6.87%
LCC = Life Cycle Cost Index	Initial Cost	39		
	Operating Cost	99		
	Recyclables	36		
	LCC Total		174	18.11%
Total			961	100.00%

2.3.1 Mission Capability Index

$$MCI = Availability \cdot \left[0.5 \cdot \frac{Endurance}{4} \cdot \left[0.8 \frac{V_{br}}{120} + 0.2 \cdot \frac{V_D}{140} \right] + 0.3 \cdot \frac{PL}{10} + 0.2 \cdot \frac{V_Y}{45} \right]$$

Where:

Availability = $\frac{MTBF}{MTBF + MTTR}$, Subjective value based on overall design (baseline=85%)

Endurance= Endurance at 5000/95 Max Endurance with no reserve (TGT= maximum value = 4 hr)

V_{br}= Best Range Speed (TGT= maximum value= 120 kts / 222 km/hr)

V_D= Dash Speed (TGT= maximum value= 140 kts / 259 km/hr)

PL= Power Loading (TGT=10.0 lbs/hp / 6.08 kg/kW)

V_Y= Sideward Flight Speed (TGT=45 kts / 83 km/hr)

The first term in this index measures the availability of the aircraft (available time/total time), this value was based on analysis of current aircraft, and then adjusted with design changes that would increase or decrease the estimated availability of the aircraft. The availability was then multiplied by a number of weighted performance parameters. The first term weighted at 50% importance was the endurance of the aircraft over a specified mission divided by 4 hours, multiplied by 80% of the maximum best range airspeed divided by 120 knots and 20% of the dash speed divided by 140 knots. The final two terms were weighted 30% and 20% respectively and consisted of the power loading of the aircraft divided by 10 lbs/hp and the maximum sideward flight speed divided by 45 knots.

2.3.2 Safety Evaluation Criterion

$$SI = 0.4 \cdot \left[\frac{D \& R}{100} \right] + 0.2 \cdot \left[\frac{AI_{Sikorsky}}{25} \right] + 0.2 \cdot \left[\frac{Survivability}{100} \right] + 0.2 \cdot [Q_{safety}]$$

Where:

D&R = Dependability and Reliability, sum of improvements above traditional baseline aircraft (0-100)
(FADEC=+20, HUMS=+30, Carefree Maneuvering=+20)

AI= Autorotative Index using Sikorsky Method (TGT= 25)

Survivability= Sum of improvements above traditional baseline aircraft (0-100)
(Crashworthy Subfloor=+20, Assisted Flight Control System=+20, Trajectory Optimization=+10)

Q_{safety}= AntiTorque Safety factor based strictly on effect of tail-ground contact
(Tail Rotor = 0.2, Fenestron = 0.7, NOTAR = 1.0)

In creating a safety criterion, it was necessary to take into account the safety of individuals flying in the aircraft as well as the ground crew and those near the aircraft when not in flight. Improvements to the air crew's safety were measured by three terms. The first measured relative improvement to the reliability of the aircraft in avoiding critical failures. The second was the ability of the aircraft to autorotate safely to the ground following a complete loss of engine power to the rotor. The third term was

a relative measure of the vehicles ability to avoid a crash or survive a crash if unavoidable. The anti-torque term primarily accounts for ground safety, although it was also reflects improvements to the safety the aircraft's occupants during low altitude and terrain flight operations.

2.3.3 Noise Evaluation Criterion

$$NI = 0.4 \cdot \left[1 - \frac{N_{FO} - 70.0}{10} \right] + 0.2 \cdot \left[1 - \frac{N_H - 65.0}{10} \right] + 0.2 \cdot \left[1 - \frac{N_{Interior}}{100} \right] + 0.2 \cdot \left[1 - \frac{N_{Trajectory}}{4} \right]$$

Where:

N_{FO} = Noise level during 500ft AGL fly over at 110 kts from WOPWOP (TGT=70.0 dB)

N_H = Noise level during 500ft AGL hover from WOPWOP (TGT=65.0 dB)

$N_{Interior}$ = Qualitative noise level inside helicopter 0dB (silent) to 100 dB (loudest) (baseline=50 dB)

$N_{Trajectory}$ = Ability of the pilot and aircraft to avoid noise sensitive areas

(1= Standard Aircraft, 2=Avionics show noise sensitive areas, 3= Aircraft provides guidance cues to pilot for best route to minimize noise in sensitive areas, 4= Aircraft auto pilot flies optimal noise reduction trajectory)

Because this aircraft will be operated in and around high population density areas, noise reduction was a driving factor in design. For noise considerations, the program results from WOPWOP¹, at a hover and in forward flight, were used. A subjective upper threshold of 10 additional dB's (twice as loud) would drive the index to a value of zero. In order to take into account the comfort of the passenger the internal noise levels were accounted for using a qualitative measure from 0 to 100. A final segment of the noise index was the level in which the aircraft can assist the pilot avoid noise sensitive ground areas such as city centers and parks. This ability compounds the gains made by reducing the vehicle's external noise.

2.3.4 Fuel Consumption Evaluation Criterion

$$FCI = 0.15 \cdot \left[\left(\frac{5.0}{f} \right) + \left(\frac{0.5}{\phi} \right) + FM + \frac{\left(\frac{L}{D} \right)_{Rotor}}{12} \right] + 0.4 \cdot \left(\frac{0.5}{BSFC} \right)$$

Where:

f = Design Equivalent Flat Plate Area (TGT= 5.0 ft / 1.524 m)

$BSFC$ = Design Brake Specific Fuel Consumption (TGT= 0.5 lb/hp.hr / 0.304 kg/kW.hr)

ϕ = Design Empty Weight Fraction (TGT= 0.50)

FM = Figure of Merit (TGT= 0.85)

$\left(\frac{L}{D} \right)_{Rotor}$ = Lift over Drag of Rotor (TGT= 12)

Although a directly calculated fuel burn over a specific mission would be the best measure of this criterion, this more complex equation, which takes into account five primary factors which effect fuel consumption, was derived to assist in preliminary design. In order to maximize this index, the vehicle had to minimize empty-weight fraction, equivalent flat plate drag area, 'f', and brake specific fuel consumption and maximize Figure of Merit (FM) and Rotor Lift to Drag ratio. The evaluation criterion was formulated to capture the above parameters, with 40% of the value being determined by the BSFC and the remaining four factors accounting for the remaining 60%.

2.3.5 Emission Index Evaluation Criterion

$$EI = 1 - \frac{1}{5} \cdot \left(\frac{EI(NO_x)}{4.722} + \frac{EI(CO)}{1.105} + \frac{EI(UHC)}{1.832} + \frac{EI(CO_2)}{3157} + \frac{SN}{29.7} \right)$$

Where:

EI(NO_x) = Emission Index for Nitrogen (baseline= 4.722 grams nitrogen/kg fuel)

EI(CO) = Emission Index for Carbon monoxide (baseline= 1.105 grams CO/kg fuel)

EI(UHC) = Emission Index for Unburnt Hydrocarbons (baseline= 1.832 grams UHC/kg fuel)

EI(CO₂) = Emission Index for Carbon Dioxide (baseline= 3157 grams carbon dioxide/kg fuel)

SN= Smoke Number: a measure of particulate matter from soot (baseline = 29.7)

This index was baselined against a standard turboshaft engine with the same power output as the Athena engine. This standard engine would have an overall emissions index (EI) of zero while an engine with no pollution effects would score a 1.0. The standard measurement for unburned hydrocarbons, carbon monoxide, carbon dioxide, and oxides of nitrogen is an EI. The EI is the mass of pollutant in grams divided by the mass of fuel used in kilograms, calculated through a landing take-off cycle (LTO) including take-off, climb out, approach, and idle modes of operation. Smoke, or particulate matter, would be measured in the form of a dimensionless smoke number (SN) calculated from the reflectance of a filter paper measured before and after the passage of a known volume of a sample for a fixed time and flow rate of the sample. A SN of 20-40 generally defines the smoke visibility threshold. The standard measurements for emissions indices and smoke number have been modeled in GasTurb 10 (GSP 10), a gas turbine simulation program developed by the National Aerospace Laboratory, Netherlands (NLR), the NASA Numerical Propulsion System Simulation (NPSS) program, and an Excel spreadsheet developed by the team based on combustor research outlined in chapter 6 of this report.

2.3.6 IQ Index Evaluation Criterion

$$IQI = 0.3 \cdot \left[\frac{LoA}{5} \right] + 0.2 \cdot [M_{assist}] + 0.3 \cdot [IBC] + 0.2 \cdot [M_{control}]$$

Where:

LoA = Level of Autonomy (No Assist=1, SCAS/CAS =2, Attitude Command/Control=3, Velocity Commands=4, Full Autopilot=5)

M_{assist}= Maneuverability Assistance (Envelope Protection = +0.4, Trajectory Optimization = +0.3, Obstacle Awareness = +0.1, Obstacle Avoidance = +0.2)

IBC= Individual Blade Control, (Primary Flight Control = +0.4, 2/rev Harmonic Control = +0.3, >2/rev (higher) Harmonic Control = +0.3)

M_{control}= Method of Control (Control Tubes/Mixing Assembly = 0, Fly-by-wire = 0.7, Fly-by-light = 1)

The intelligence criterion was designed to capture the vehicle’s ability to take advantage of recent technological advances that improve overall safety, comfort and maneuverability. These advances also contribute to the other indices (i.e. IBC reduces noise, fly-by-wire reduces weight, etc.), but they were grouped together here to simplify the evaluation criterion and express the “smartness” of the design as compared to traditional helicopters.

2.3.7 Life Cycle Cost Evaluation Criterion

$$LCC = 0.2 \cdot \left(\frac{RDTE}{40,000,000} \right) + 0.5 \cdot \left(\frac{PC}{1,500,000} \right) + 0.3 \cdot \left(\frac{DOC}{400} \right)$$

Where:

(All figures in 2008 dollars derived from Bell PC Cost Model)

RDTE = Research, Development, Tests, Evaluation Costs (Baseline= \$40,000,000)

PC = Production Cost per helicopter (Baseline= \$1,500,000)

DOC = Direct Operating Cost including maintenance and POL (Baseline= \$400/hr)

The life cycle cost criterion takes into account the three major costs associated with rotorcraft: research, development, test and evaluation costs, production costs and direct operating costs. These costs were determined using the Bell PC cost model. These cost segments have been weighted according to the customer requirements from the QFD.

3 PRELIMINARY SIZING AND PERFORMANCE

3.1 Vehicle Sizing Method

Successful rotorcraft vehicle sizing and performance estimation must adeptly integrate aerodynamic and weight analyses.² Such integrated analyses is comprised of: selecting a rotorcraft configuration, sizing the selected configuration, and sizing the engine---all according to the performance

and weight requirements of the Request for Proposal. For this design, preliminary vehicle sizing was done using the RF method,³ an approach that allows the linking of aerodynamic and weight requirements. Figure 3-1 shows a schematic illustration of the RF method.

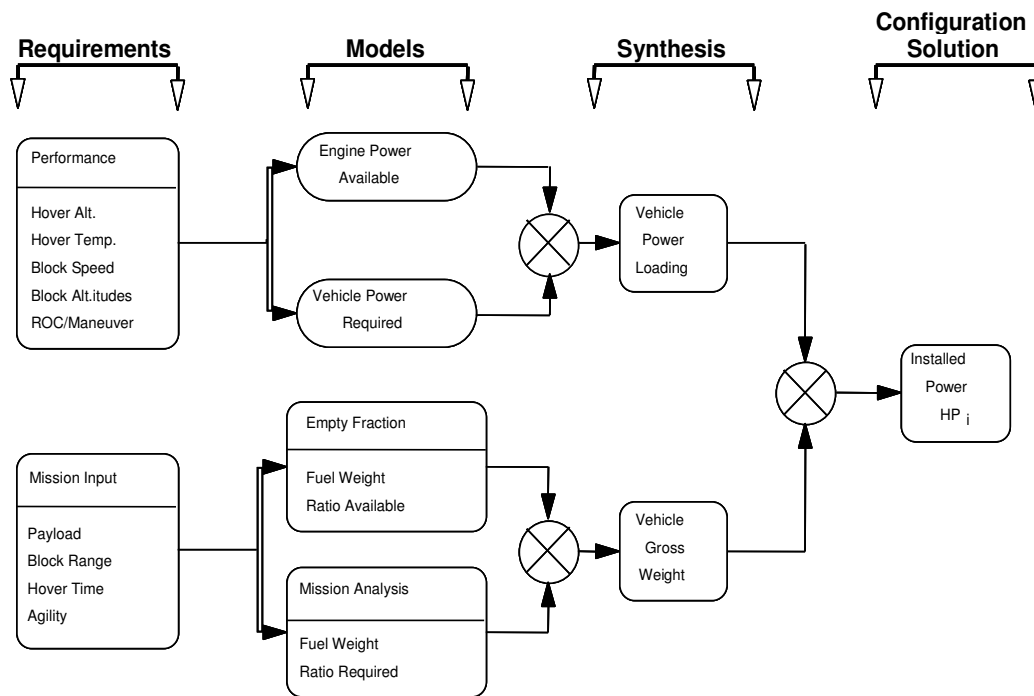


Figure 3-1: Schematic Illustration of the RF Method

The RF method allows the estimation of feasible gross weights of different rotorcraft configurations by balancing, for a specified mission, the fuel weight required and available, and the power required and available. It is thus possible to optimize an objective function (i.e., fuel required) and obtain a corresponding value for a chosen design parameter (i.e., disc loading). A feasible configuration is obtained when the fuel and power available for the mission are respectively equal to the fuel and power required.

3.2 CIRADS: Concept-Independent Rotorcraft Analysis and Design Software

The conceptual-design sizing program employed for initial sizing and performance estimation was CIRADS: Concept-Independent Rotorcraft Analysis and Design Software.⁴ Developed at Georgia Tech to expedite conceptual design, CIRADS can be used to calculate vehicle size and performance for prescribed missions, or to calculate performance for an existing rotorcraft. A specified rotorcraft model is used to calculate required power, and a specified engine model is used to calculate power available. CIRADS can also be used for special performance problems: range, endurance, rate of climb, and to

model rotor and wing stall. It provides the versatility to consider all feasible rotorcraft configurations including tilt rotors, coaxial rotors, tandem rotors, and single main rotors. Additionally, for a single main rotor helicopter it can model Fenestron, NOTAR, and conventional tail rotor configurations. Its usefulness for this RFP is underscored by its capability to model variable rotor configurations---such as tip speed, diameter, and chord length---during a prescribed mission.

3.2.1 Validation of CIRADS' Predictions

To ensure reasonable accuracy, CIRADS' performance predictions were compared with available flight test data from a Lynx XZ170 helicopter.⁵ Figure 3-2 shows the results of the comparison. Each lettered point denotes a different flight condition reported in the compiled data. The results indicate that CIRADS predicts power required with reasonable accuracy.

Performance estimates were made for the MD-500E and the EC-120B, and then compared with manufacturer-advertised performance.^{6,6.7} Tables 3-1 and 3-2 again show that CIRADS estimates vehicle performance with reasonable accuracy.

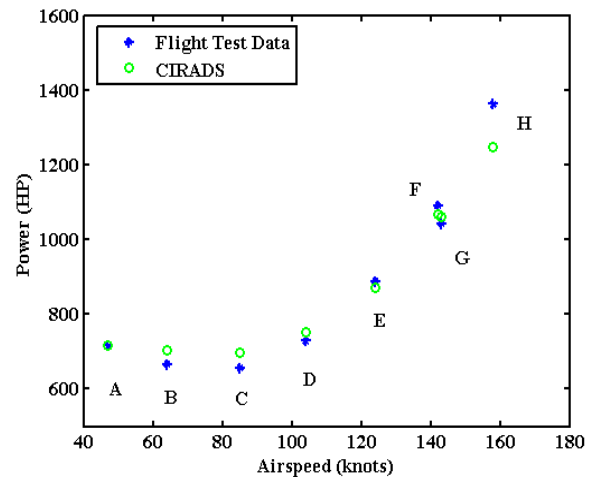


Figure 3-2: CIRADS Validation using Lynx Data



	Manufacturer Value	CIRADS Estimate
V_{MAX} (kts)	135	138
V_{BR} (kts)	120	100
V_{BE} (kts)	50	59
Range (NM)	259	250.8
Endurance (hrs)	2.7	3.08
R/C_{MAX} (ft/min)	1,770	2,603

Table 3-1: Validation of Performance Estimates (MD-500E)



	Manufacturer Value	CIRADS Estimate
V_{MAX} (kts)	150	148
V_{BR} (kts)	115	110
V_{BE} (kts)	65	67
Range (NM)	397	392
Endurance (hrs)	4.5	4.81
R/C_{MAX} (ft/min)	1,350	1,331

Table 3-2: Validation of Performance Estimates (EC-120)

3.2.2 Athena Vehicle Sizing Mission

The RF method was used to assess feasible configurations that met the Request for Proposal requirement of a 300-nautical-mile range capability. A 20-minute fuel reserve was also added to ensure sufficient versatility for all military, para-military, and civilian missions that Athena may encounter. The final sizing mission used is depicted in Figure 3-3.

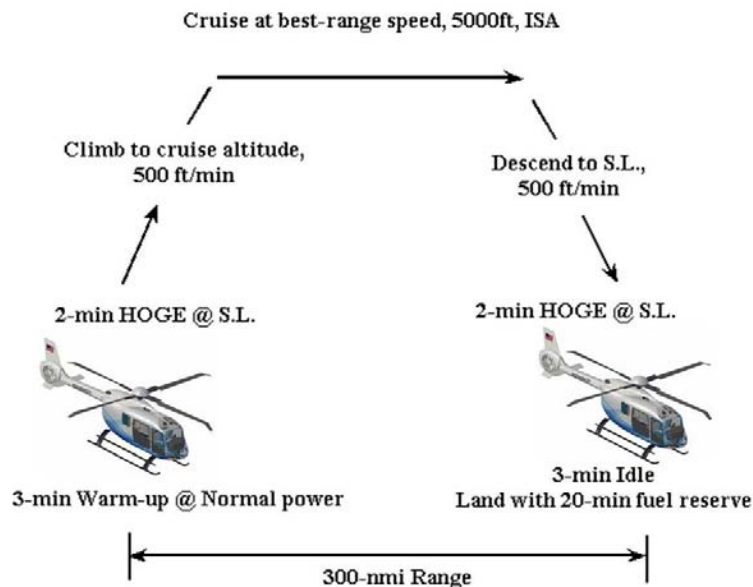


Figure 3-3: Sizing Mission

3.2.3 Configuration Selection: Initial RF Analysis

A survey of historical data was conducted to compare feasible gross weights of the following rotorcraft configurations: single main rotor, coaxial helicopter, and mono-tilt rotor. Table 3-3 summarizes this *a priori* data.³ The RF method was used to determine that the single main rotor configuration was the minimum-weight solution. Table 3-4 summarizes the results of this initial RF analysis. In addition to the lower gross weight, the single main rotor helicopter was also able to meet all customer requirements outlined in Chapter 2.

Table 3-3: A Priori Data

<i>A Priori</i> Design Parameters	Units	Traditional Helicopter	Coaxial Helicopter	Mono-Tilt Rotor
Disk Loading	lb/ft ²	6	9	15
Empty Weight Fraction	ND	0.55	0.6	0.55
Equivalent Flat Plate Drag	ft ²	5	6	5
Rotor Solidity	ND	0.1	0.1	0.1
Tip Speed	ft/sec	650	650	650
Downwash Factor	ND	0.03	0.05	0.08
Aux Prop Percent Thrust	ND	NA	NA	NA
Wing Span	ft	NA	NA	15
Wing Aspect Ratio	ND	NA	NA	6

3.2.4 Selection of Major Design Parameters: RF Sensitivity Analysis

Table 3-4: RF Sizing Results

Performance Parameter	Units	Single Main Rotor Helicopter	Coaxial Helicopter	Tilt Rotor
Minimum Gross Weight	lbs	3,422	4,141	4,352
Hover Power 4,921ft/77F	HP	402	502	621
99% Max Range Airspeed	kts	128	133	143
99% Max Range Airspeed Power	HP	319	498	443
Empty Weight	lbs	1711	2277	2393
Weight of Total Fuel Required	lbs	390	544	638

The sizing of the single main rotor configuration was refined using an RF sensitivity analysis to determine tip speed, disc loading, and solidity. The sensitivity analysis was geared to the RFP requirement to minimize energy consumption during cruise flight. That requirement promoted fuel weight, related to fuel consumption, as the best objective function to minimize during sizing.

At the inception of each sizing iteration, vehicle installed power and engine SFC were assumed. CIRADS then sized the vehicle for a 300 NM range capability at a target speed of 120 knots, where the range capability was calculated as a function of cruise speed, gross weight, and altitude. For this design, the high, hot hover-out-of-ground-effect (HOGE) requirement was used as the engine sizing criterion. After each iteration, the engine was rescaled to the predicted power required. The vehicle’s weight was also recalculated after each iteration with component weight equations that were scaled with a “technology factor” to improve the accuracy of the weight estimation for a future helicopter with initial production in 2020.

3.3 Rotor Morphing Trade Study

Because the RFP specifically address rotor morphing, a thorough trade study of possible technologies was conducted (Table 3-5.).

This investigation took into account the additional weight of the components, the changes in safety and availability, and the potential increase in R&D, production, and operational costs

Table 3-5 Rotor-Morphing Concepts Investigated^{7,8,9,10}

Concept	Description	Pros	Cons
Variable Tip Speed	-Multiple tip speeds -Rotor RPM can be varied for optimum performance	-Reduces power required -Traditional blades improve safety -Reduces noise	-Transmission or variable speed module increases complexity and weight
Variable Diameter	-Rotor diameter can be increased for better hover performance, and decreased in forward flight	-Reduces power required	-Increase rotor complexity and weight -Increases maintenance -Additional R&D Costs and longer certification
Variable Twist	-Rotor blade twist can be changed statically or actively to reduce power requirements	-Reduces power required -Increases lift-to-drag ratio	-Increase rotor complexity and weight -Increases maintenance -Empty weight increase

of the system. As a result of this trade study a variable tip speed design was determined the most realistic given the 2020 operational requirement. A further trade study was conducted between a continuously variable transmission and a dual speed design (see Chapter 6). A dual-tip speed design was chosen for its potential to reduce fuel consumption and reduce noise with minimal impact on cost, safety, and availability.

3.3.1 Dual Speed Optimization

To validate that a dual RPM design will meet the RFP requirements and justify increases in cost and complexity, a sizing iteration was run and compared to the baseline results. Table 3-6 shows the results of this iteration along with the original baseline results. Although, there is a slight increase in empty weight due to the variable speed module, there is an 11 percent reduction in fuel required for the range mission, and a nine-percent reduction in power required for the hover OGE capability. Figure 3-4 shows the hourly fuel consumption rate of the one-speed and dual-speed designs at the vehicle’s best-range speed. It is clear that the dual-speed design has a smaller rate of fuel consumption despite its slightly higher gross weight.

While operating at reduced tip speeds reduces fuel consumption, there are times when operation at 100% tip speed is necessary to avoid blade stall. Airspeed-altitude limits showing retreating blade tip stall are calculated with CIRADS, and shown in Table 3-5. The figure shows that at an arbitrary speed, 120 knots, there is a 7,000 ft ceiling increase in ceiling while operating at 100% PRM as opposed to 90% RPM. Although, these are not the Athena’s maximum operational ceiling, the results show the occasional need for the higher tip speed.

Table 3-6: Range Mission Comparison of One-Speed and Dual-Speed Rotor

Parameter	Units	Baseline	Dual Tip Speed (92% RPM in Cruise)
Empty Weight	lbs	1509	1545
Disk Loading	lbs/sq.ft	4.77	4.77
	kg/m ²	23.26	23.26
Engine Power Required	HP	408	371
	kW	304	277
Fuel Required for Idle	lbs	8	8
	kg	3.6	3.6
Fuel Required for HOGE	lbs	10	10
	kg	4.5	4.5
Fuel Required for Reserve	lbs	34	32
	kg	15.4	14.5
Fuel Required for Climb	lbs	25	23
	kg	11.3	11.3
Fuel Required for Descent	lbs	19	17
	kg	8.6	7.7
Fuel Required for Cruise	lbs	337	307
	kg	152.9	139.3
Total Fuel	lbs	433	397
	kg	196.4	180.1

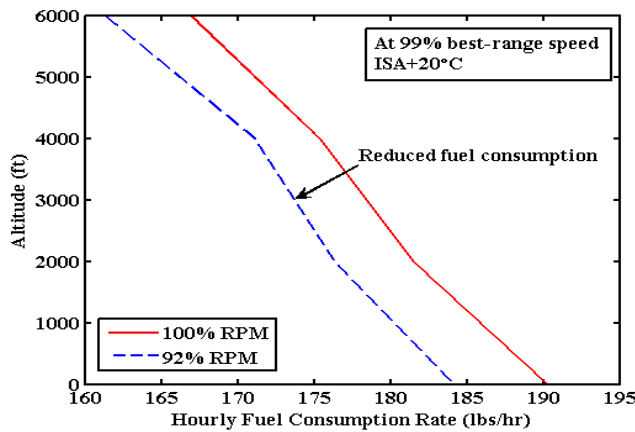


Figure 3-4: Fuel Consumption of Dual-Speed Rotor

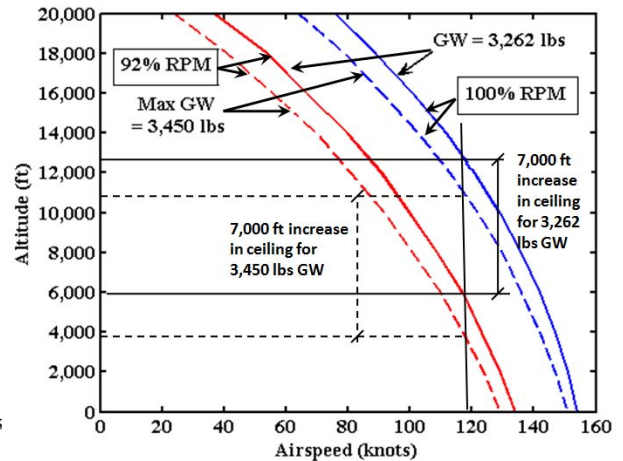


Figure 3-5: Airspeed-Altitude Limits to Avoid Retreating Blade Stall

4 MAIN ROTOR BLADE AND HUB DESIGN

Athena’s main rotor system was designed to be aerodynamically efficient, safe, light-weight and practicable. It is a washplate-less design that employs advanced rotor controls--namely, Individual Blade Control (IBC) and Higher Harmonic Control (HHC)--to achieve reduced vibration and reduced noise throughout its operational envelope. With an emphasis on efficient cruise flight, the Athena’s rotor blades use a combination of non-linear twist distribution and an advanced tip design, which includes taper, sweep, and anhedral to achieve high efficiency in both hover and cruise flight.

4.1 Rotor Blade Design

The main rotor is designed to optimize Athena’s cruise performance and to provide good hover efficiency. It is a low-drag, light-weight design that takes advantage of the Athena’s Higher Harmonic Controls (HHC) to reduce power required and vibrations.

4.1.1 Airfoil Selection

A trade study was conducted to evaluate the effect of airfoil section on power required and cruise performance with specific range as the measure of cruise efficiency. CIRADS was used to compare the specific range values and power required (Figures 4-2 and 4-3). In this trade study only airfoils whose performance data was publicly available were considered. The SC-1094 was chosen as the main lifting airfoil because it required the least power and had the highest specific range. The SC-1095 airfoil was selected for the outer 95% of the rotor blade because of its high drag-divergence Mach number and lower pitching moments.

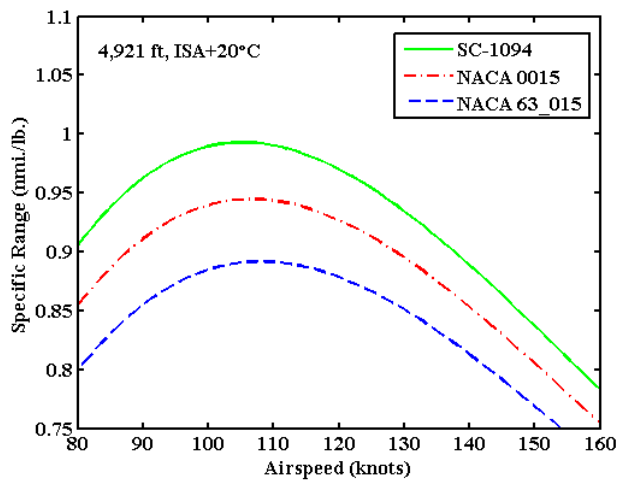


Figure 4-1: Specific Range with Different Airfoils

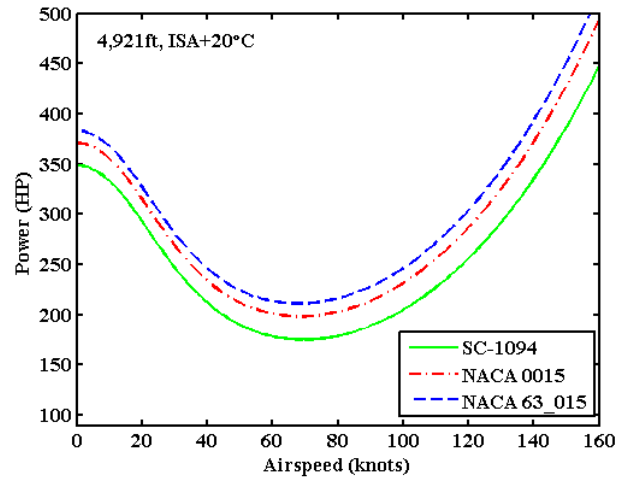


Figure 4-2: Power Required with Different Airfoils

4.1.2 Twist Selection

A double linear-twist design was employed for the Athena’s rotor blades: inboard of 90% radius, the blade is linearly-twisted by -18 deg; outboard it is twisted by 25 deg. The conflicting aerodynamic requirements of hover flight and forward flight usually compel designers to choose linearly-twisted blades between -8 and -14 degrees. For Athena’s rotor blades, a relatively large twist is used to reduce hover power. The blade tips are twisted by 25 degrees to maintain positive angles of attack at the tip and to avoid the production of negative thrust. Figure 4-1 compares Athena’s twist distribution to that of the UH-60’s main rotor¹¹ and a scale model of the RAH-66.¹² Although this high twist may increase vibrations, the Athena’s HHC will reduce them greatly.

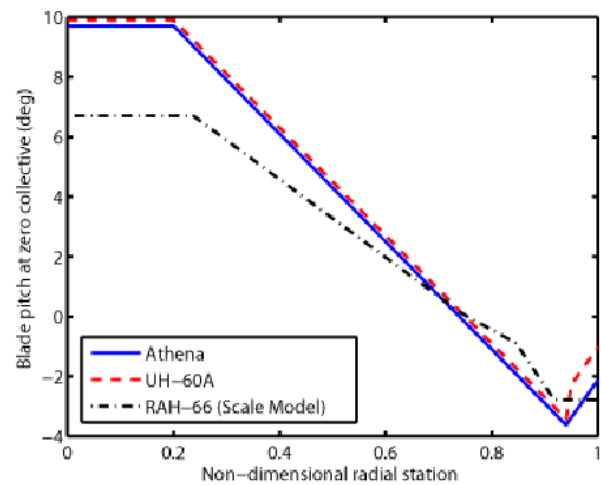


Figure 4-3: Blade Twist

4.1.3 Blade Planform Design

Taper: A 5:8 taper is used to decrease the hover power required. As shown in Figure 4-4, the outboard 90% of the blade is tapered.

Sweep: Sweep is used to delay the onset of compressibility effects at high speeds. Compressibility effects increase power required and noise. The Athena’s rotor blade is swept back 20 degrees to delay the onset of these effects.

Anhedral: Blade anhedral has been shown to reduce both noise and power required.¹³ Collins and Bain¹⁴ have used high fidelity CFD techniques to show these benefits. Based on this research the Athena’s rotor blade tips have a 20 degree anhedral.

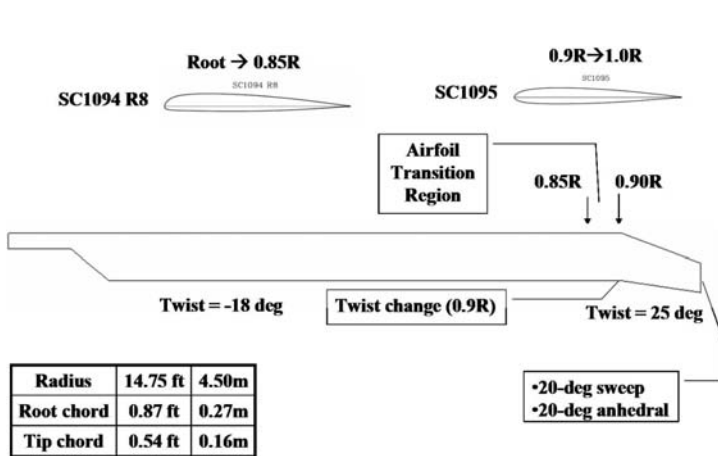


Figure 4-4: Rotor Blade Specifications

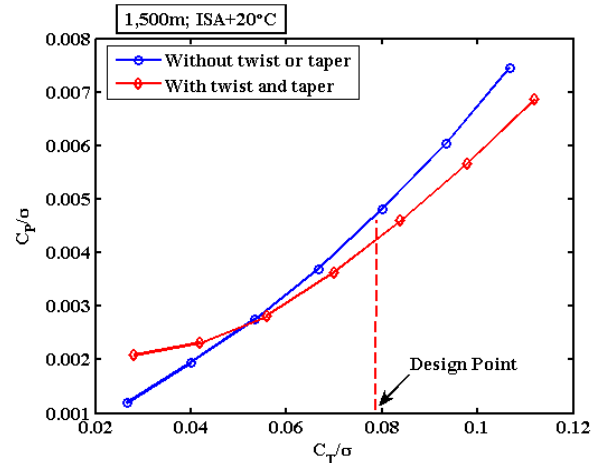


Figure 4-5: Validation of Design Twist

4.1.4 Selection of Tip Speed and Disc Loading

Figure 4-6 shows the variation of power required with disc loading at several tip speeds. The figures indicate that lower tip speeds correspond to lower power required. At each tip speed, the disc loading corresponding to minimum power required is denoted by a marker. The choice of low tip speeds is restricted by; the requirement to cruise at a target speed of 120 knots, maneuverability of the helicopter, and compliance with the FAR 27 provision to be able to withstand gusts of up to 30 ft/s. The CIRADS stall model indicated that for tip speeds less than 650 ft/s, even for solidity ratios as high as 0.08, the retreating rotor blade would encounter stall at cruise speeds of 120 knots or greater. Compliance with FAR Part 27 restricts the selection of extremely low tip speeds because these low tip speeds cannot withstand the 30 ft/s gust without stalling. The Athena’s tip speed and disc loading were chosen such that FAR Part 27 requirements were satisfied with a 10% stall margin.

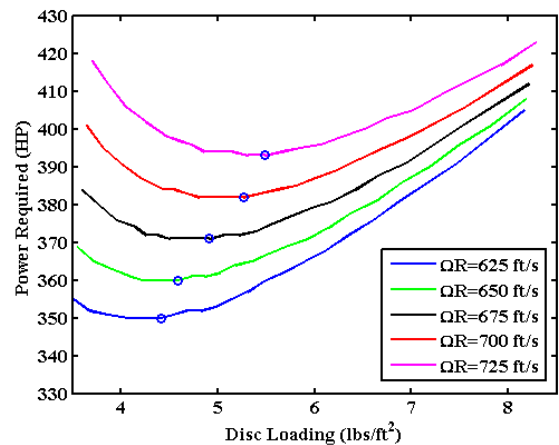


Figure 4-6: Power Required vs. VT and DL

4.1.5 Selection of Blade Number and Solidity

Figure 4-7 shows the variation with solidity of the fuel required for a 300 NM range and the required engine power for the high, hot hover environmental conditions. The figure shows the acceptable choices of solidity for blade aspect ratios (AR) less than or equal to 20. While more blades would be useful for vibration reduction, fewer blades correspond to less required fuel and engine power. The minimum solidity that precludes stall at a 120-knot cruise speed is 0.075; four blades were chosen accordingly.

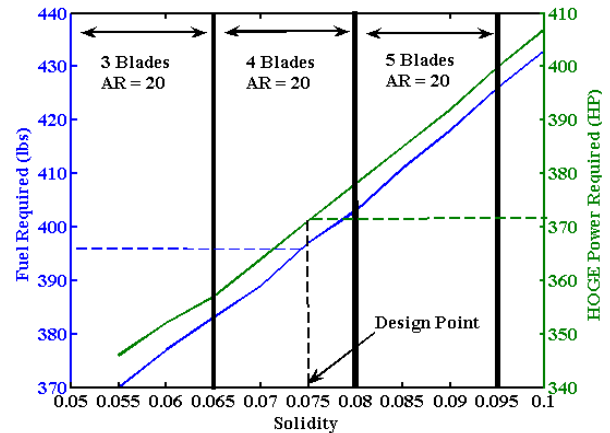


Figure 4-7: Variation of Fuel and Power Required with Solidity

4.1.6 Acoustic Analysis

Athena’s acoustic signature was determined using WOPWOP¹ at each of its operating RPMs. In order to perform this analysis the Athena FLIGHTLAB¹⁵ model was used to generate sectional lift and drag coefficients at 18 radial and 24 azimuthal locations for a 110 knot flight at both tip speeds. This information, along with the rotor dynamics information was used by WOPWOP to produce the perceived decibel level at a given observer position. In order to check the WOPWOP predictions, the two major sources of noise in steady level flight, thickness noise and loading noise, were plotted along with total noise for Athena at 110 knots, 500 ft AGL flying towards an observer. Figure 4-8 depicts the increasing noise as the Athena gets closer to the observer; it also shows which source of noise dominates the total sound. Beyond 1400 feet, thickness noise dominates because it is largest in the plan of the

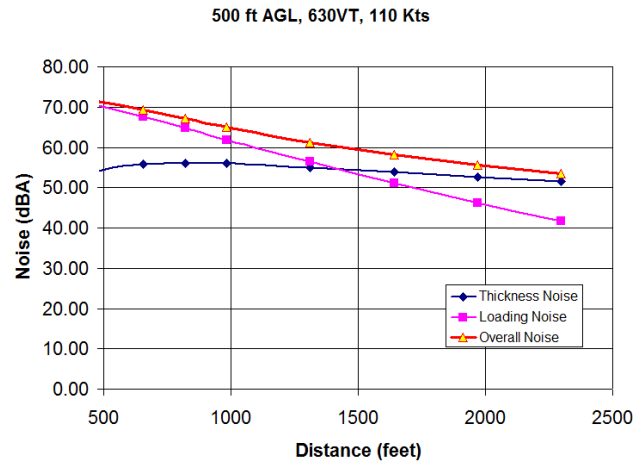


Figure 4-8: Noise Breakdown with Athena Flying Towards Observer

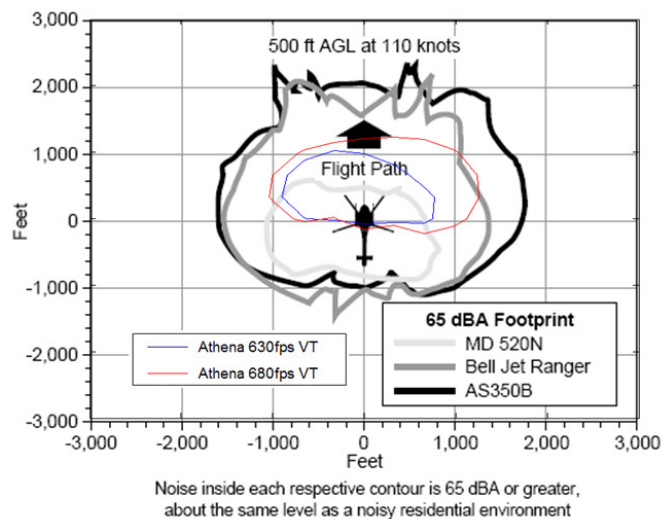


Figure 4-9: Acoustic Footprints at Max Gross Weight¹⁶

rotor disc.¹³ When Athena gets closer than the 1400 feet, the loading noise becomes dominant. Next, in order to put the data in a graphical format and provide comparison to existing aircraft, perceived noise was calculated for a 500ft AGL fly over to observers located in a 1 km grid. A surface plot of this noise was generated in MATLAB, and the 65dBA contour was plotted over a figure found in the MD-520N Technical Description Manual available online.¹⁶ Figure 4-9 shows that the Athena is comparable with the MD-520N and far quieter than either the Bell-206 or the AS350B. The figure also clearly depicts the acoustic advantage of reducing the rotor RPM.

4.2 Hanson “Ideal Rotor” Hub

Athena’s hub is a bearingless, swashplate-less configuration designed to reduce parasite drag, noise and vibrations, and to improve handling qualities.

The Hanson (Bearingless) Hub is a simple, safe, and stable hub design that was successfully flight-tested on an auto-giro by Tom Hanson in 1970,¹⁷ and many of its qualities have been proven in wind tunnel tests at NASA Langley. Over the past year, Georgia Tech and Konkuk University (in Seoul, Korea) have participated in a joint research effort to analyze and prove the unique qualities posited in Mr. Hanson’s design handbook.¹⁷ The team used some of this research data to evaluate the Athena’s hub design.

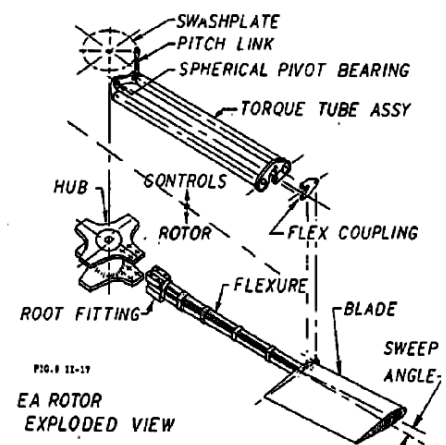


Figure 4-10: Hanson Hub¹⁷

The Hanson (Bearingless) Hub provides all of the essential elements of an “ideal rotor” as described in Tom Hanson’s *Hub Design Handbook*.¹⁷

- Simplification of design
- Multiple load paths
- High ratio of ultimate tensile strength to blade centrifugal force
- Minimum number of structural joints
- Ability to maintain controlled flight after serious damage
- Principal blade natural frequencies below their respective forcing frequencies
- Stability about the feathering axis
- Minimum rotor noise by reducing V_T
- Improved handling qualities

The Hanson hub is based on a flexure design which uses a series of straps integrated into the blade structure to achieve “elastic articulation” – eliminating the need for the usual flapping, feathering, and lead-lag bearings. Control inputs are provided to each blade through a combination of two torque tubes that provide structural redundancy.

4.3 Advanced Rotor-Control

Advanced rotor control schemes are attractive because of their potential to improve performance and reduce noise and vibrations. These advanced control schemes include other benefits: reduction in flight control system weight of 25%, reduction in maintenance cost of approximately 42%, reduction in Mean Time to Repair (MTTR) of approximately 50%, increased aircraft availability by 15% and enhanced ballistic tolerance.¹⁸

4.3.1 Individual Blade Control (IBC)

Individual Blade Control (IBC) is the physical control methodology of applying pitch-control inputs to blades individually rather than through a conventional swashplate control that applies pitch-control inputs to all blades based on azimuth station.

The ZF Luftfahrttechnik Company's InHuS (Innovative Hubschrauber Steuerung = Innovative Helicopter Control) program has conducted extensive research and analysis on the use of electro-mechanical actuators (EMAs) in a production helicopter. ZF determined that a brushless DC motor with an integrated mechanical reduction stage gear box could provide the required forces for an integrated control system providing both primary control inputs and individual blade control (IBC).¹⁹

Figure 4-11 shows the torque-rate envelope used by ZF to set the requirements for EMA testing. In order to show the concept could be applied to large force requirements, the analyses were completed for a large helicopter resembling a CH-53G. A small helicopter, the size of the Athena, using Hanson's auto-trim rotor with its near 1/rev feathering frequency, will require much smaller forces and EMAs than the ZF tests. Using EMAs coupled with a fly-by-wire architecture provides freedom to implement state-of-the-art flight control software able to optimize handling qualities through active control.

Athena's EMAs are mounted on top of the rotor hub for ease of maintenance and proximity to the power/data transfer unit. A cutaway of the ZF EMA and gear box which the Athena EMAs will be based on is shown in Figure 4-12

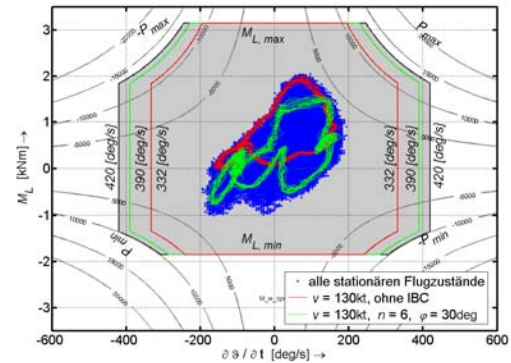


Figure 4-11: Blade Pitch Torque - Rate Envelope for ZF test Helicopter CH-53G¹⁹

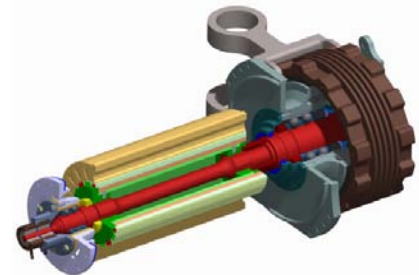


Figure 4-12: ZF EMA Layout¹⁹

4.3.2 Higher Harmonic Control (HHC)

The theory of Higher Harmonic Control (HHC) has been around since the 1950's.²⁰ HHC has shown large benefits in wind tunnel tests,^{21,22,23,20,24,25} but its use on production helicopters has been greatly delayed due to cost, reliability, and safety concerns of the added complexity. HHC essentially makes use of 2/rev to (N+1)/rev (where N is the number of blades) control inputs which demand very significant response times and flexibility. HHC can be applied through either a swashplate or through IBC. In the Athena, HHC will be used to suppress the vibrations and improve performance of the main rotor by adding inputs at multiples of N/rev frequencies.

In the Athena conventional controls (cyclic and collective) and HHC are combined through IBC which provides substantial simplification. This combination requires IBC units with a capability of providing high amplitude angles (~20 degrees, collective controls) for long durations of time, moderate amplitude inputs (~5 degrees, cyclic controls) and small amplitude inputs with higher frequencies but short durations of time (Higher Harmonic Controls). This highly demanding task can be achieved with the Athena's swashplate-less design combining EMA's with the additional benefits of Hanson Rotor. The Hanson Hub design utilizes matched stiffness blades and flap-feathering dynamic coupling through the use of slightly forward swept blades, meaning that feathering inputs are put into the system at 1/rev, resulting in lower required control forces. Aerodynamic effects create damping to the feathering motion of the blade where its resistance to pitch changes is reduced.

4.3.2.1 Vibration Reduction

As mentioned above, using higher harmonic controls from 2/rev through (N+1)/rev and (N-1)/rev can significantly reduce vibrations. Because vibrations occur due to aerodynamic asymmetry of the rotor in forward flight, HHC can alleviate this asymmetry at its source. Example results from the wind tunnel tests are shown in Figure 4-13. In the tests,²⁴ the highest vibration reduction was achieved with 1 degree amplitude HHC. Research has shown that oscillatory components of forces and moments could be reduced by 80%.^{21,22,23,20,24,25}

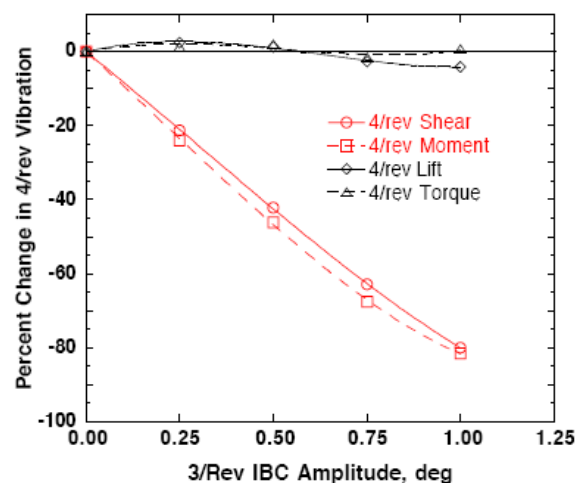


Figure 4-13: IBC Vibration Reduction²⁴

4.3.2.2 BVI-Noise Reduction

The three major sources of main rotor noise are: high speed conditions on the advancing blade during forward flight, high load factors during maneuvers, and blade vortex interaction (BVI) in all flight conditions. It is possible to reduce the intensity of each these interactions using HHC, and reduce noise and vibration. Figure 4-14 and Figure 4-15 show the comparison of sound pressures with and without HHC. The data was recorded during forward flight of the S-76B helicopter at a 450 fpm rate of descent in close proximity of the rotor. This flight condition was selected because of the particularly high amount of BVI that occurs in this condition.

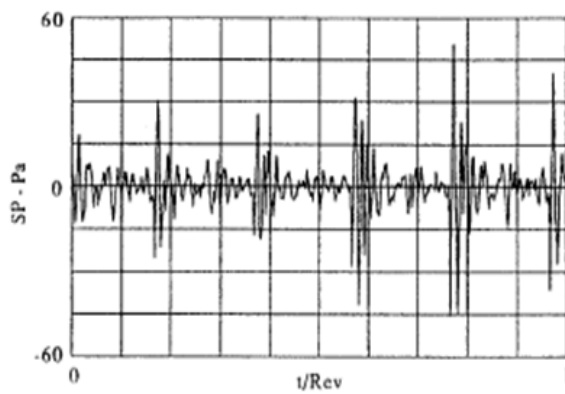


Figure 4-14: BVI without IBC²³

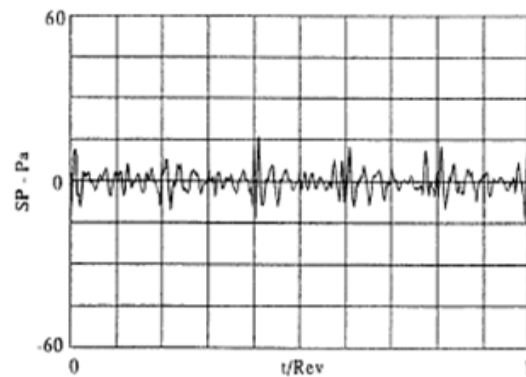


Figure 4-15: BVI with IBC²³

4.3.2.3 Blade Stress Reduction

HHC can also be used to reduce blade stresses from high amplitude oscillatory loads. Straub²² and Shaw²⁵ have shown successful use of HHC to reduce blade bending stresses, increase blade fatigue life and reduce the overall life cycle cost of the helicopter.

4.3.2.4 Power Required Reduction

Using HHC can delay the onset of retreating blade stall and increase performance by about 5%.²³ Swashplate control acts in 1/rev harmonic fashion which is very close to the blade flapping frequency. This causes large responses to inputs. HHC can be used to overcome these problems, and redistribute the blade stall region over the rotor disk. Figure 4-16 shows the reduction in required power of a test helicopter. In forward flight, the Athena will benefit from similar power reductions.

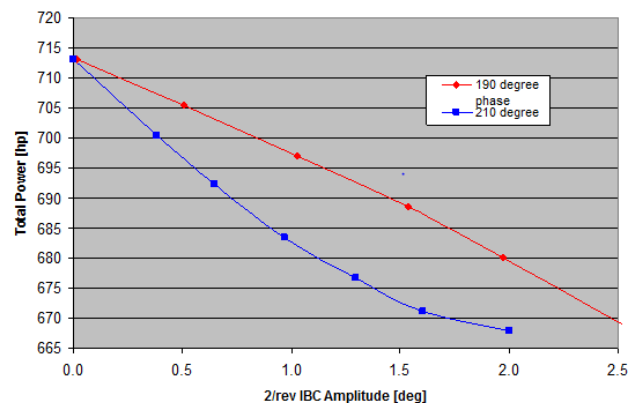


Figure 4-16: Power Improvements²³

4.3.3 Roll-Ring Power/Data Transfer Unit

Athena’s control actuators are in the rotating plane, so there is a need to transfer large amounts of power and data from the aircraft fixed system to the rotating hub. A team at the Boeing Company recently completed a trade study to identify the best technology to accomplish this task.²⁶ The team developed requirements for power and data requirements for the MD-900 and then compared the viability and performance of available technologies, which included RF Wireless, Slip Rings, Roll Rings, and a Rotating Transformer.

Following a comprehensive trade study, including bench testing, the roll ring concept was found to be the best for method for both power and data transfer.²⁶ The roll ring design was bench-tested for an equivalent of 623 hours at 400 RPM with minimal changes in data or power transfer. It was also shown that redundant channels can easily be incorporated to improve safety and reliability.

Based on this trade study, a roll ring transfer unit will be utilized on the top of Athena’s rotor hub to transfer control data and actuator power to the rotating frame. The roll-ring is shown below in Figure 4-17 and Figure 4-18.

Table 4-1: Transfer Requirements²⁶

MD900 - DPT	
Non-contacting transfer with power amplification on rotor:	
data rate from rotor to airframe, Mbps	30
data rate from airframe to rotor, Mbps	30
power available on airframe	115VAC, 400Hz
power required on rotor - data	28VDC, 5A
- actuation	400VDC, 21A
outer diameter, height of unit, in	OD=5, H=10 or OD=15, H=2
inner diameter of unit, in	2.75
stationary wire bundle diameter - max, in	1
Contacting transfer with power amplification in the airframe:	
Data circuits: 5V TTL	14
Power circuits - data: 28VDC	4 at 5A ea
Power circuits - actuation: 1500Vpp	18 at 7.6A ea

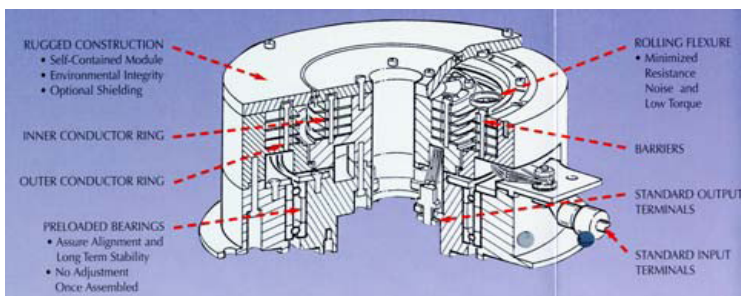


Figure 4-17: Roll Ring Cut Away²⁶

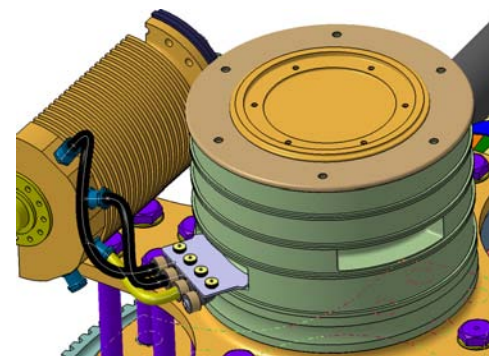


Figure 4-18: Roll Ring Unit on Athena Hub

4.4 Rotor Dynamics

Resonance and instability are dependent on the blade natural frequencies, vehicle frequencies, and rotor rotational speed. For the Athena’s two speed rotor, these instabilities must be checked for both rotor speeds, and the transition between the two. A fanplot of the Athena’s rotor was constructed using dynamic modeling.^{27,28,29} Instabilities will occur when the frequencies of motion in the rotor from flap,

lag, or torsion occur close to a natural frequency of the rotor rotation (1P, 2P, 3P, etc. meaning once per revolution, twice per revolution, etc.). The Athena rotor is designed to avoid instabilities in all but the first flap frequency, which is close to 1P. The Hanson Hub is designed this way because it allows for reduced control input loads because a small load will naturally produce a large deflection since the first flapping frequency is close to 1P. The rotor motion’s frequencies are changed by adjusting the flex beam and blade structural properties or the control system stiffnesses in order to avoid 3/rev, 4/rev and 5/rev harmonics at the two operational rotor speed conditions. The Athena’s two rotational speed conditions are marked with vertical lines in the fanplot shown in Figure 4-19. The rotor rotational frequencies are kept sufficiently far from the rotor’s natural frequencies to avoid any damaging resonance conditions.

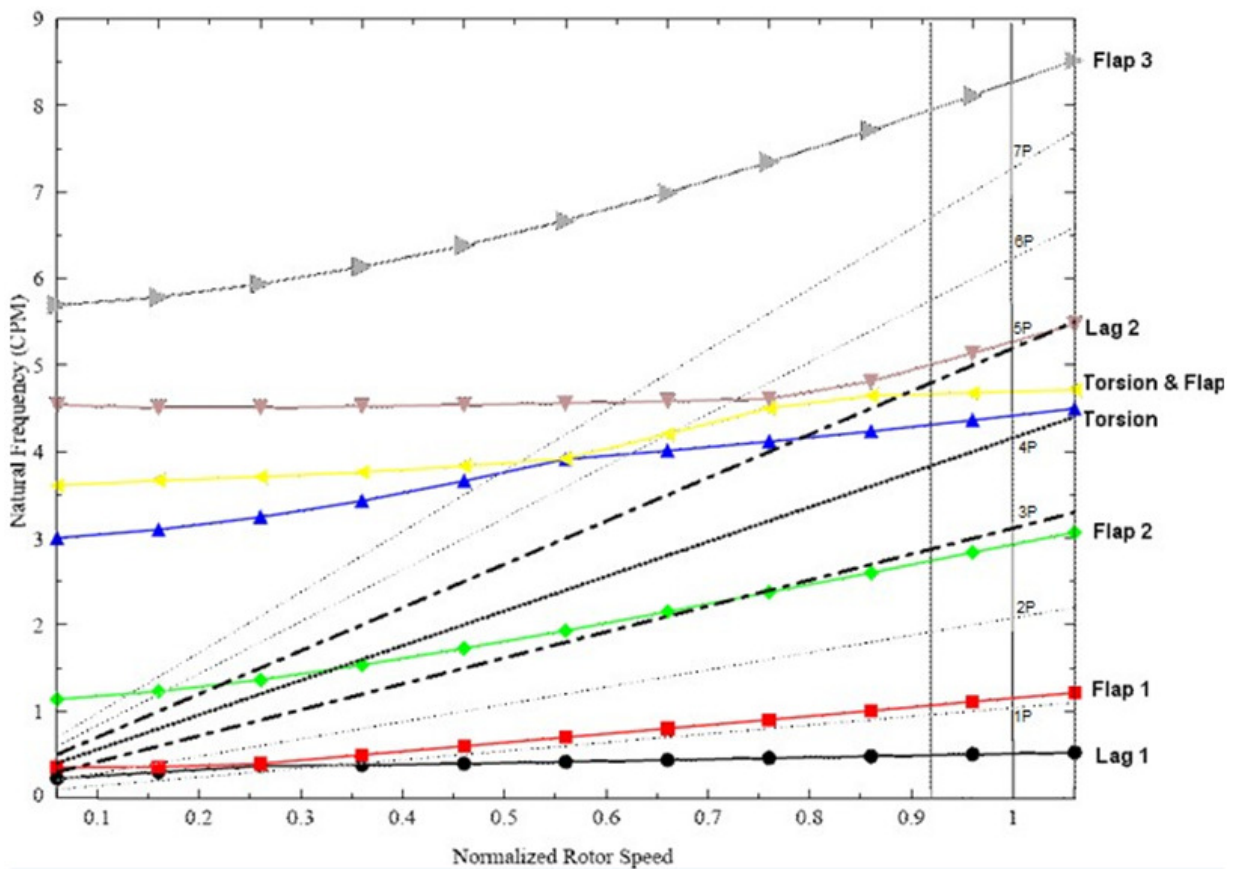


Figure 4-19: Athena Main Rotor Natural Frequencies

4.4.1 Flexure Design

The Hanson hub is based on a flexure design. It uses a series of straps integrated into the blade structure to achieve “elastic articulation.” This structure eliminates the need for the usual flapping, feathering, and lead-lag bearings. The hub is built using composite materials which eliminate flapping and lead/lag hinges thereby reducing weight and complexity. Safety is emphasized by designing the

flexure to be structurally redundant. The flexure is composed of a core and four flex straps that decouple the in-plane and flapping motions. Feathering inputs are achieved through an elastic torque tube. Kevlar 49/Epoxy is used for the straps because of its high stiffness and structural damping characteristics. The flexures are sized according to Hanson’s design handbook.

Figure 4-20 shows the standard Hanson flexure cross section. Figure 4-21 shows the variation of both height and width of the flexure with radial position. The figure shows that the design is free of an overlapping condition, where the spar caps would be overlapping and would represent an impossible design. Table 4-2 lists the material properties as a function of radial location. The stiffness values for the dynamics analysis are obtained using ANSYS and VABS. Figure 4-22 shows the ANSYS model of the airfoil cross section.

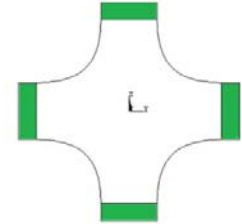


Figure 4-20: Hanson Flexure Cross Section

Table 4-2: Spanwise Flexure Stiffness Data

	Flapwise	Chordwise	Torsion	Axial	Shear
4%	5092033.79	4933414.475	375954.3	4480000	168000
5%	4278722.84	4145438.552	315906.1	4480000	168000
6%	3898588.37	3777145.457	287840.0	4480000	168000
7%	3191361.46	3091949.003	235624.1	4480000	168000
8%	2554857.23	2475272.193	188629.9	4480000	168000
9%	1989075.70	1927115.029	146857.2	4480000	168000
10%	1494016.86	1447477.511	110306.0	4480000	168000
11%	1069680.71	1036359.638	78976.5	4480000	168000
16%	587953.25	587953.2493	44096.5	4480000	168000
	EI (lb*in ²)	EI (lb*in ²)	GJ (lb*in ²)	EA (lb*in ²)	GA (lb*in ²)

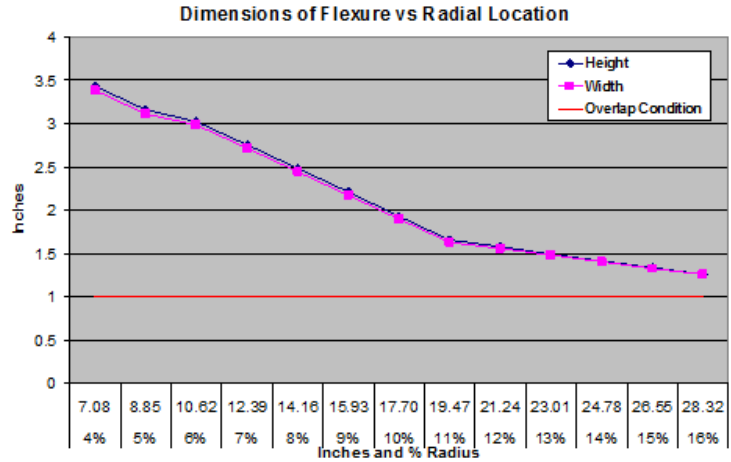


Figure 4-21: Hanson Flexure Dimensions

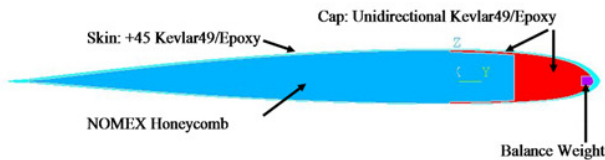


Figure 4-22: ANSYS Model of Blade Cross Section

4.4.2 Static Droop Analysis

An analysis of a stationary blade showed a static droop of 8.76 inches (22.25 cm) and is shown in Figure 4-23. This analysis was completed with no precone angle. Adding 2.5 degrees of precone angle would keep the blade tips at the same level with the rotor hub and reduce the steady loads to a minimum in flight.

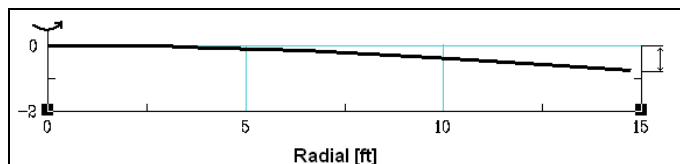


Figure 4-23: Static Droop

4.4.3 Ground Resonance

The current design with a non-dimensional lag frequency at 0.5 is theoretically susceptible to ground resonance. Therefore, a thorough analysis has been carried out to ensure that this condition is not encountered during Athena's operational rotor RPM. Johnson³⁰ has shown that the product of damping terms related with lead-lag degree of freedom and body motion must be greater than zero to avoid instability. As a consequence of this requirement, both sub-systems must have non-zero damping values, if there is any possibility of ground resonance condition.

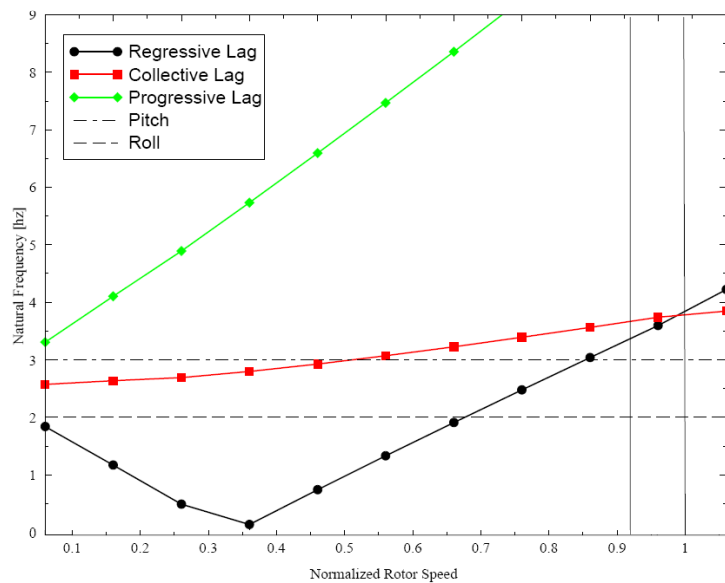


Figure 4-24: Lead-Lag and Body Modes

This Analysis was conducted by plotting the regressive lag mode for the operational rotor speeds. Figure 4-24 shows the uncoupled frequency placement. The highest risk of resonance is found at 87% rotor RPM. The time response to a modal excitation is presented in Figure 4-25 for the 87% RPM condition and shows Athena is ground resonance free even at this most critical frequency. In the absence of damping term default 1% critical damping is provided to the body degree of freedom. Figure 4-26 depicts the same time response in plane such that travel of the rotor cg position can be observed as a converging spiral.

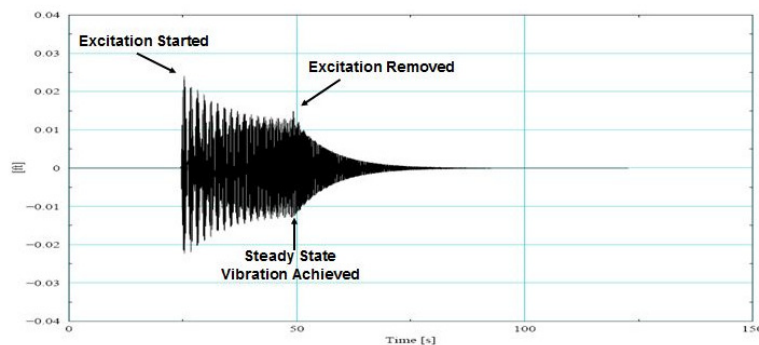


Figure 4-25: Time Response of Rotor CG Location

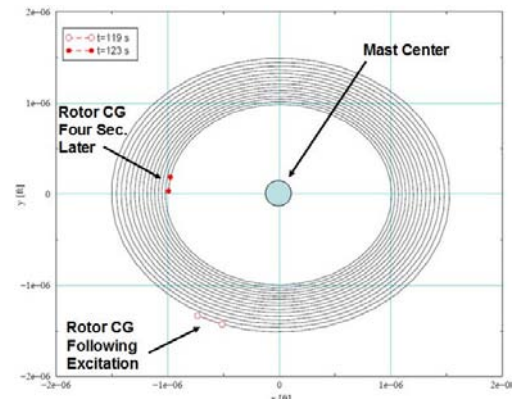


Figure 4-26: Rotor CG Contour in XY Plane

4.4.4 Air Resonance

Tom Hanson has shown that using a matched-stiffness rotor like the Athena's elastically-articulated rotor precludes the occurrence of air resonance. Figure 4-27 illustrates a case of developed air resonance for a BO-105 helicopter with a hingeless rotor. The figure depicts the preclusion of air resonance for a matched-stiffness rotor. The critical point of air resonance would occur far below the flight RPM range, "thus eliminating even the theoretical possibility of air resonance."³¹

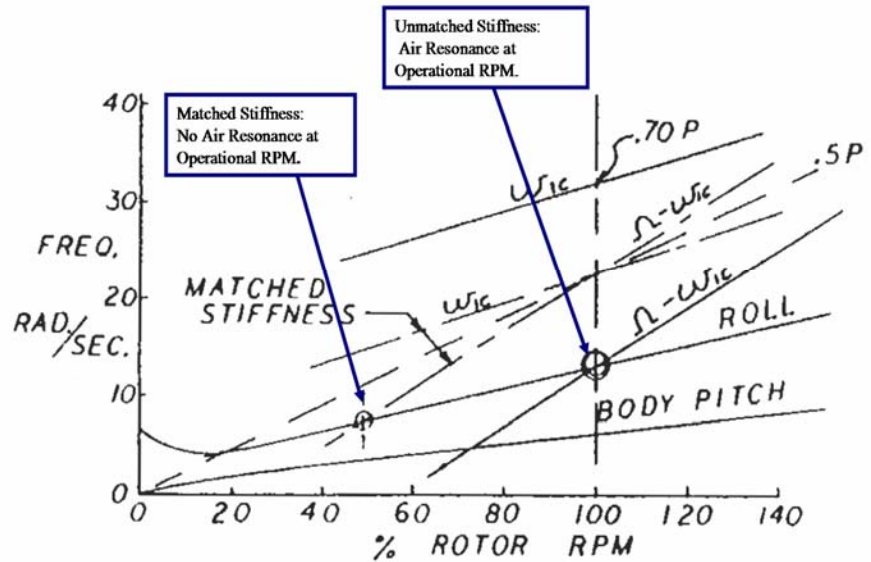


Figure 4-27: EA and Air Resonance³¹

4.5 Final Design Parameters

Table 4-3 identifies Athena's final aerodynamic design parameters

Table 4-3 Final Design Parameters

Parameter	Units	Athena
Gross Weight	lbs	3262
	kg	1480
Fuel Weight	lbs	397
	kg	180
Disc Loading	lbs/sq. ft	4.77
	kg/m ²	23.26
Radius	ft	14.75
	m	4.5
Tip Speed	ft/s	630/680
	m/sec	192/207
Solidity	--	0.075
Twist	deg	-18/ 25
Chord	ft	0.88
	m	0.268
Engine Sizing Power Required	HP	371
	kW	277

5 ANTI-TORQUE SELECTION AND DESIGN

An anti-torque device for a single main rotor helicopter must provide sufficient thrust, without stalling, to counteract main rotor torque, provide yaw acceleration, and overcome tail rotor precession effects.³² The primary drivers of Athena’s anti-torque device design were: efficiency, availability, safety, noise, and cost.

5.1 Anti-torque Configuration Selection

Table 5-1 compares three anti-torque devices for Athena using the four metrics.

Efficiency: Fenestron tail rotors are “found to have lower power requirements than an open tail rotors to produce the same amount of thrust.”³³ In forward flight, the Fenestron can be unloaded to get the best lift-to-drag ratio of the tail surfaces. Unloading the Fenestron reduces the forward-flight power required. The NOTAR requires more power than both the conventional tail rotor and Fenestron; the NOTAR is much less efficient than the Fenestron.

Availability: Protecting the Fenestron with a shroud and unloading it in forward flight can increase the availability of the Fenestron. The NOTAR ranks the lowest in availability, as the moving parts in its nozzle are delicate, and this decreases accessibility.

Safety: The shroud of a Fenestron, and the coverings of the NOTAR, protect the anti-torque system from strikes in low-altitude operation and reduce the risk of injury to ground personnel.

Noise: The Fenestron does not experience the noise due to main rotor-tail rotor interaction effects, as the conventional tail rotor does, although it is less quiet than the NOTAR.

Based on this trade study a Fenestron was selected for the Athena.

Table 5-1: Anti Torque Selection Matrix

	Weighting	Conventional Tail Rotor	Fenestron Tail	NOTAR
Efficiency	9	2	3	1
Availability	5	3	2	1
Safety	3	1	2	3
Noise	2	1	2	3
Cost	1	3	2	1
		41	49	32



5.2 Fenestron Design

The Fenestron tail rotor was designed to meet the stringent criteria recommended by the *Tail Rotor Design Guide*.³⁴ It was sized to provide trim thrust, maneuver thrust (for a 15 deg/sec yaw in 1.5 sec), precession thrust, and a 10% stall margin. A blade element momentum code modified for ducted fans³³ was used with experimental results to size the fan, the stationary rotators (stators), and the duct of the Fenestron. The design criterion requires a total thrust represented by Equation 5-1

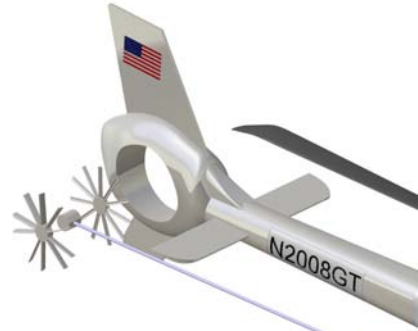


Figure 5-1: Fenestron Design

$$T_{total} = T_{trim} + T_{maneuver} + T_{precess} + T_{stall_margin}$$

Equation 5-1 Total Fenestron Thrust

5.2.1 Selection of Tip Speed and Disc Loading

Higher tip speeds can reduce the fan weight because smaller-chord blades are feasible, while lower tip speeds will reduce Fenestron noise. In order to maximize the noise evaluation criterion, 575 ft/s was selected as the Athena's tip speed.³⁵ This lower speed reduces noise due to compressibility effects.³⁵

Designers have historically selected tail rotor aspect ratios (radius/chord) between five and nine.³⁶ Employing this restriction on aspect ratio, a modified blade element code was used to calculate power required vs Fenestron diameter (Figure 5-2). A fan diameter of 2.4ft (0.732m) was selected to reduce forward-flight parasite drag and reduce weight.

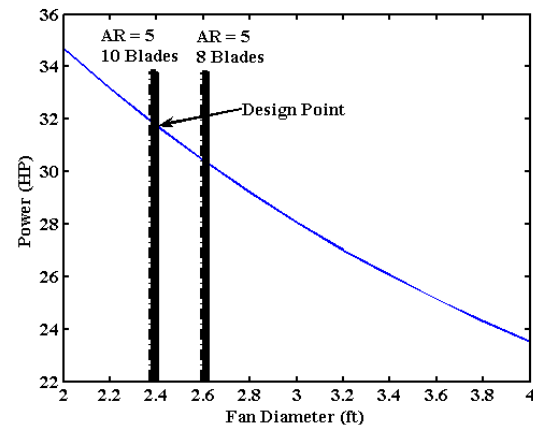


Figure 5-2: Fan Power vs. Diameter

5.2.2 Number of Blades and Solidity

A high number of blades, relative to a conventional tail rotor, was selected to create higher frequencies that would more quickly attenuate and reduce noise. A survey of Fenestron tail configurations³⁷ revealed that designers traditionally choose between 8 and 13 blades. In order to meet an aspect ratio of at least 5, and reduce the required Fenestron diameter, the Athena uses 10 blades as shown in Figure 5-2. A solidity of 0.56 was selected to ensure the blades do not stall throughout their operating range.

5.2.3 Blade Spacing

Eurocopter has successfully employed phase modulation on the EC-135 Fenestron blades to reduce its noise signature. Equation 5-2 was used to determine blade spacing based on a sinusoidal modulation³⁸ where θ_i is the angular position of the i^{th} unmodulated blade, ϕ_i is the angular position of the i^{th} modulated blade, and b is the modulation parameter. For a 10-bladed fan, m and b are respectively 2 and 6 deg for dynamic balance.³⁹ In order to reduce noise, the Athena also uses this angle modulation.

$$\phi_i = \theta_i + b \sin(m\theta_i)$$

Equation 5-2: Fenestron Blade Spacing

5.2.4 Airfoil Selection and Blade Twist

The efficiency of the Fenestron fan is directly proportional to the lift-to-drag ratio of the fan’s airfoil. The VR-7 airfoil was chosen due to its lower power requirement (Figure 5-3) and good lift-to-drag ratio.

Although useful in reducing power required, blade twist might have an adverse effect on the Fenestron’s reverse thrust characteristics,⁴⁰ and for this reason was not used

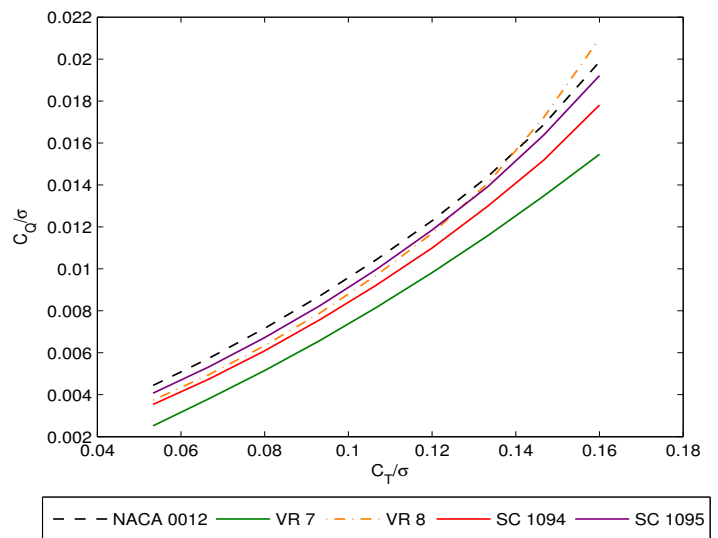


Figure 5-3: Fenestron Airfoil Selection

5.2.5 Number of Stator Vanes

Athena’s Fenestron contains eleven stator vanes to reduce power losses due to the rotation of the fan’s wake. In the interest of noise attenuation, the number of stators was chosen subject to the following criteria:³⁵

- The number of stator blades and rotor blades are unequal and do not have a common factor.
- The product of the stator blade number and the rotor rotational speed does not equal rotor blade natural frequency.
- The stator vanes are placed 1.5 rotor chord lengths downstream of the rotor blades.
- The stator vanes are inclined radially by 5 degrees in the direction opposite to the rotor rotation.³⁹

A patent assigned to Eurocopter France³⁹ proposes that it is “advantageous for the [vanes] to exhibit an aerodynamic profile of the NACA 65 type” with 8% to 12% thickness.

5.2.6 Duct Design

In accordance with the results of wind tunnel tests⁴¹ showing that for high efficiency and high figure-of-merit, the duct’s lip radius should be greater than 7.5% of the fan’s diameter. The duct lip radius was selected to be 8.0% of the fan’s diameter. The diffuser angle is restricted to 10 degrees to abate flow separation at the duct’s outlet.⁴¹ The Fenestron final design parameters are shown in Table 5-2.

Table 5-2: Fenestron Configuration

Tip Speed (ft/s)	575
Diameter (ft)	2.4
Blade Number	10
Blade Airfoil	VR-7
Chord (ft)	0.21
Blade Twist (deg)	0
Solidity	0.56
Direction of Rotation	Bottom-Forward
Blade Spacing	Unequal
Stator Vanes	11
Stator Airfoil	NACA 65 Type
Stator Vane Spacing	Equal

6 PROPULSION AND TRANSMISSION

6.1 Summary of Engine System Design

The Athena propulsion system consists of a turboshaft engine capable of running on either JP8 or biomass synjet fuel, and is optimized through the use of a distributed FADEC system. The turboshaft engine is composed of a single stage axial compressor, a two stage lean-lean Lean Premixed Prevaporized (LPP) combustor, and two free composite turbines. Engine control is accomplished by an advanced distributed FADEC system based on the Open Control Platform (OCP) that ties it to the flight management system to ensure that the engine is optimized in conjunction with the rest of the aircraft. The FADEC also allows for the dual

fuel capability of the aircraft. Although JP-8 is a more readily available fuel, biomass Synjet has lower lifecycle emissions. The transmission is based on the simple split-torque Hanson Transmission,¹⁷ with a Variable Speed Module (VSM) located between the engine and transmission. Specific technology selections are summarized in Table 6-2 along with references for their specific sections in this chapter.

Table 6-1: Athena Engine Specifications

Engine Type	Turboshaft with centrifugal compressor; two stage, lean-lean, Lean Premixed Prevaporized Combustor; and two free composite turbines					
Power Category	Hp	kW	SFC (lb/hp/hr)	SFC (kg/kW/hr)	EI NOx	1.532
Max Continuous Power (100% RPM)	376	280	0.4489	0.2730	EI CO	0.989
Take Off Power (5 min) (100% RPM)	467	348	0.4462	0.2710	EI UHC	1.799
Cruise Category	Hp	kW	Burn Rate (lb/hr)	Burn Rate (lb/hr)	SN	29.7
Max Range (92% RPM)	235	175	116.3	52.75	EI CO2	3157
Max Endurance (92% RPM)	169	126	94.88	43.04		

Table 6-2: Summary of Engine Technologies

Component	New Technology	Advantage	Report Section
Fuel	Synjet &/or JP-8/JetA	↓ CO ₂ , SN, SO _x , ↑ flexibility	6.8
Combustor	Two Stage, Lean-Lean, Lean Premixed Prevaporized Combustor	↓ NOx, CO, UHC	6.9
Turbine	Composite Blades, Cooling	↑ T ₄ , ↓ SFC, ↑ Power/Weight	6.11
Transmission	Variable Speed Module, Hanson	Variable speed rotor, Light Transmission	6.15
FADEC	Open Control Platform SMARTFADEC	Flex Fuel, Optimization, Upgradable	7.2

6.2 Requirements and Approach

The challenge of this propulsion system design lies in developing a small gas turbine engine that maintains its reliability and performance characteristics, while reducing its emissions and fuel consumption—major factors in the pollution chain. The Athena engine design concentrates on efficiency and environmental impact, throughout the life of each part. Figure 6-1 shows the general design process used in this project to translate requirements listed in the RFP, FARs, and military specifications into an efficient propulsion system. The final design presented here represents numerous tradeoffs and offers the most robust propulsion system for air transportation needs in 2020 and beyond.

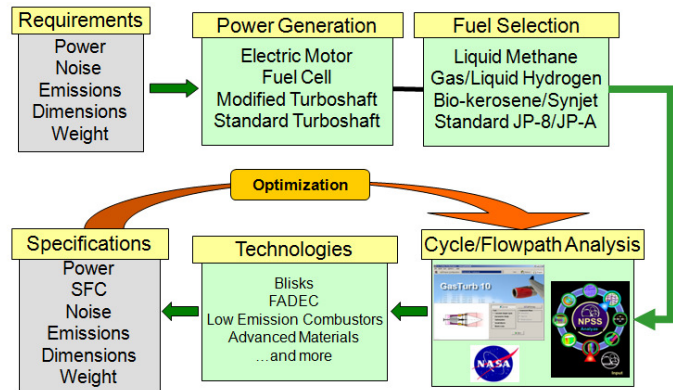


Figure 6-1: Engine Design and Sizing Process

6.3 Power System Selection

Many concepts for power generation were researched including; fuel cells, electric motors, turboshaft engines, diesel engines, and hybrid systems. Weight, volume, efficiency, total life cycle emissions, cost, and other considerations were metrics for comparison in conjunction with a range of fuels. Table 6-3 shows the engine types that were considered and their advantages and disadvantages.

Table 6-3: Engine Types Considered Summary.

Type	Concept	Advantages	Disadvantages
Piston/ Diesel	Engine that uses pistons to turn a crank shaft	Low fuel consumption. Established Technology. Low Complexity. Variable Speed. Low R+D Costs	Power to weight < 1, large vibrations. Large size. Low upper limit to power generated.
Electrical	Electric motor used to spin shaft	Low/No Fuel consumption or emissions. Low noise. Variable speed.	Power to weight <1. Needs Large and heavy batteries. Power station needed at heliport.
Hybrid	Turbine engine with electric boost motor for hover	Turbine engine operates “on design” longer, may lower fuel consumption and emissions.	Power to weight <1. Additional need for heavy batteries. Additional Transmission Components needed.
Hydrogen	Similar to a turbine with Hydrogen Fuel	Low/No emissions.	Lack of fuel stations. Pressurized storage of fuel on aircraft. Unproven technology. Lower crash worthiness.
Turbine	Compressor and two free turbines	Power to weight >1. Established Technology. Lower R+D Costs	Higher emissions. “Off-design” for large parts of mission in cruise flight.

These engine types were compared using a TOPSIS analysis as seen in Figure 6-2. The TOPSIS analysis compared the different propulsion concepts in different missions where the relative weights of design variables (noise, fuel consumption, availability, etc) were changed according to that mission. In this plot, the engines with points closer to the center were more optimal for that mission. The pure electric engine was eliminated before plotting due to its large size and weight of both the engine and batteries. The results of the TOPSIS plot show that the Electric Hybrid proved best for “civilian” type missions, but its complexity, weight, and cost limited it in other applications. The standard turboshaft came out the best in the “military” missions and second best in the “civilian” missions. A further trade study of the electric hybrid and turboshaft engine was undertaken to closely compare these two top engine configurations from the TOPSIS results.

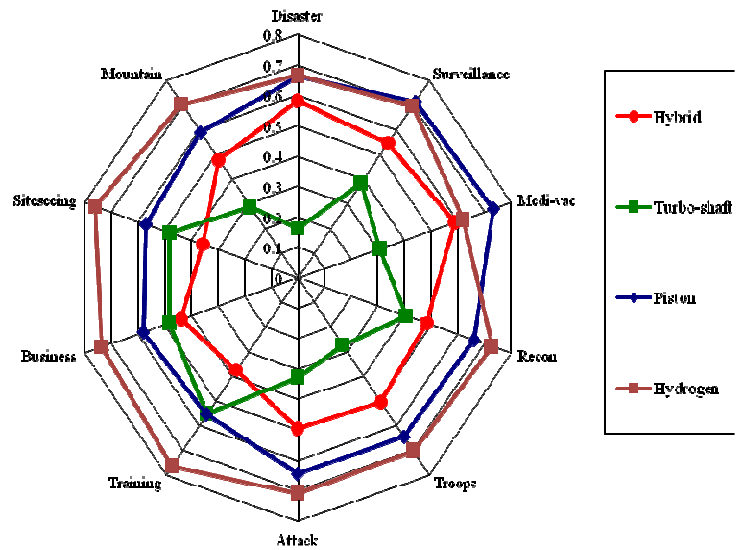


Figure 6-2: TOPSIS Plot Comparing Propulsion Systems

6.4 Electric Hybrid Trade Study

The Electric Hybrid was defined as the combination of a normal turboshaft engine and an electric “boost” motor for additional hover power. For the electric motor, a 70 HP, 50 lb, proof-of-concept motor designed by Astroflight and Sonex Aircraft was selected because it provided a better than the typical 1-1 HP-to-weight ratio. This 70 HP was nearly the difference between Athena’s power required during hover and forward flight, and would enable the turboshaft to be designed closer to cruise conditions and therefore minimize SFC.

The initial design of the hybrid included the motor, batteries, wiring, and additional transmission components required to combine the outputs of the two motors. The motor was the Sonex Aircraft proof-of-concept motor which ensured production capability by 2016. Lithium polymer (LiPo) batteries were chosen because they possess high discharge rates, and are more stable than Lithium ion batteries, while still having a high power density. A transmission trade study was performed which selected a paracyclic continuously variable transmission⁴² to mix the outputs of the two power plants.

The power required for each variant was computed using CIRADS for out of ground effect hover and 120 knot forward flight (5,000 MSL) in both a standard and a hot day atmosphere. The added weight from the additional transmission and electric motor components were taken into consideration in the CIRADS analysis. The required horsepower values for each propulsion system combination were then used for engine sizing. In both cases, the high hot hover requirement sized the engines; however, in the hybrid case, the electric motor accounted for 70 HP, resulting in a smaller turboshaft engine. GasTurb was used to determine the engine parameters in each case. Outputs from GasTurb were used in an Excel spreadsheet to compute emissions for the Two Stage, Lean-Lean, Lean Premixed Prevaporized (LPP) combustor (see section 6.7 for combustor design and selection). The results were computed for a 15 minute hover followed by a 2.5 hr flight at 120 kts for a 2.75 hr total flight (300 NM) and are shown in Table 6-4.

The results showed that the hybrid engine only saved 4.20 lbs of JP8 (0.63 gal) ISA and only 30.91 lbs of JP8 (4.61 gal) on a hot day. There was also minimal change in the emissions index. The error in the emissions index for the hot day resulted because the engine burned rich at a hover in

Table 6-4: Hybrid vs Turboshaft Trade Study Results.

	ISA		HOT	
	Turboshaft	Hybrid	Turboshaft	Hybrid
Fuel Used (lbs)	421.83	417.63	405.32	374.41
NOx (g)	292.19	290.33	276.77	256.18
CO (g)	188.78	187.54	215.25	195.56
UHC (g)	342.41	334.50	219.83	204.36
Emissions Index (EI)	0.1608	0.1623	Error due to Rich Burn	Error due to Rich Burn
Fuel Consumption Index (FCI)	0.9206	0.9296	0.9081	0.9123

both cases on the hot day in order to produce the power for hover. The Excel program that was designed to predict emissions from the LPP combustor assumed lean or stoichiometric condition. However, even without this data, it is evident that the hybrid did not offer enough savings in fuel or emissions to offset the increased system cost, its research and development cost, or the increased maintenance and complexity of the hybrid. A standard turboshaft engine was therefore selected for the Athena Helicopter.

6.5 Parametric Cycle Analysis

During initial design the engine was considered to be a “rubber” engine, whose size and performance characteristics were scalable to meet the mission requirements. The “on-design” point, which represents the most taxing condition for power generation, was the 15 minute hover out of ground effect (HOGE) at an altitude of 5,000 feet with ISA+20°C. The engine was modeled as a simple two-spool turboshaft, allowing for a separate “free” or “power” turbine. This free power turbine design provided increased operational flexibility by allowing separate optimization of both the compressor and the power turbine shaft RPM, improving the overall efficiency of the engine and reducing fuel consumption. The “on-design” point was then evaluated using GasTurb 10, an engine cycle analysis

program. Each component was treated as a “black box,” with non-ideal Brayton Cycle conditions captured via polytropic component efficiencies and pressure losses.⁴³

Table 6-5 provides a summary of the efficiencies as a function of their appropriate level of technology. Level 4 values were used to reflect the entry-into-service date of 2020.

Table 6-5: Component Efficiency Assumptions for Tech. Level⁴⁴

Component	Figure of Merit	Type	Level of Technology			
			1 (1945-1965)	2 (1965-1985)	3 (1985-2005)	4 (2005-2025)
Diffuser	$\pi_{d(max)}$	Nacelle	0.90	0.95	0.98	0.995
		Internal	0.88	0.93	0.96	0.97
Compressor	η_{pc}		0.80	0.84	0.88	0.90
Burner	π_b		0.90	0.92	0.94	0.96
	η_{pb}		0.88	0.94	0.99	1.00
Turbine	η_{pt}	Uncooled	0.80	0.85	0.89	0.91
		Cooled		0.83	0.87	0.89
Maximum T_{04}		(°R)	2000	2500	3200	3600

Parametric studies were conducted to initially size the engine, focusing on ideal pressure ratios and turbine

inlet temperatures to maximize engine efficiency while preventing component over-design. This analysis helped define the relationships between several critical inputs and outputs, such as power and SFC. Plots from the parametric cycle analysis, shown in Figure 6-3, show that increasing both burner exit temperature and compressor pressure ratios yield large efficiency benefits, up to the pressure ratio of 9:1. Increasing compressor pressure ratio above this value requires greater component cost and complexity for a diminishing increase in SFC or specific power benefit.

Having identified turboshaft trends for changing compressor pressure ratio and burner exit temperature, a scaled engine model was constructed. A value for mass flow rate was selected based on preliminary mission analysis “power required.” GasTurb does not distinguish between axial and centrifugal compressors, by carefully choosing the pressure ratio and efficiency input values this discrepancy was adequately resolved.

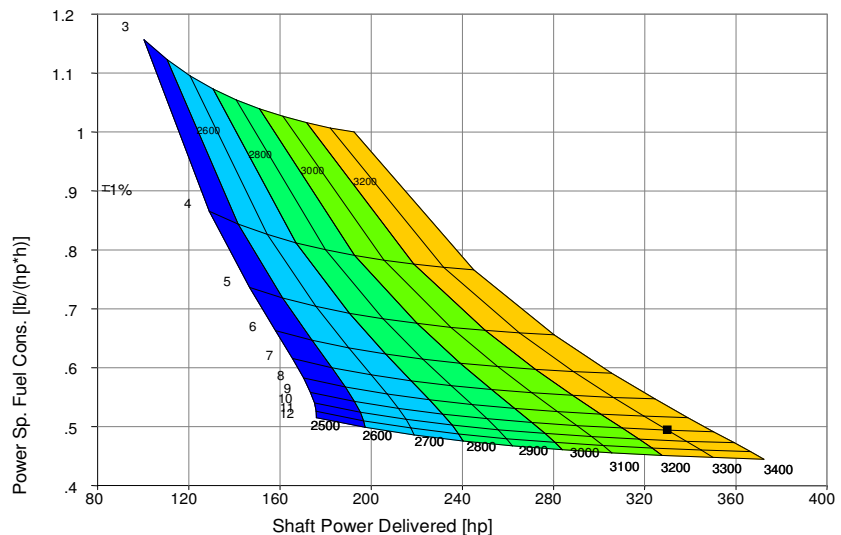


Figure 6-3: Parametric Cycle Analysis in GasTurb 10

6.6 Performance Cycle Analysis

While the “rubber engine” was scalable to meet the various mission requirements, even the performance of a rubber engine designed for one mission will perform less than optimally given a different mission. If power required for hover is very different from forward flight, the engine cruise will be at partial power and will cause a rise in fuel consumption for the long-duration forward flight mission segment. The engine must be able to perform well—in this case, achieve close to an SFC of 0.5 lb/hp*hr—for all long-duration segments of the missions, while performing moderately well for the shorter, more intensive segments in order to be competitive. Figure 6-4 summarizes these tradeoffs; it shows the changes in SFC, shaft power, and NOx severity index with changing Mach number and altitude for the sized rubber engine.

Iterations between CIRADS and GasTurb—and later NPSS—defined the range, ceiling, and other performance parameters of the Athena with this rubber engine. Although GasTurb application was useful for calculating the engine performance estimates necessary for initial design, a more accurate analysis required a higher fidelity engine simulation. Therefore the “rubber” engine was modeled using the NASA Numerical Propulsion System Simulation (NPSS).

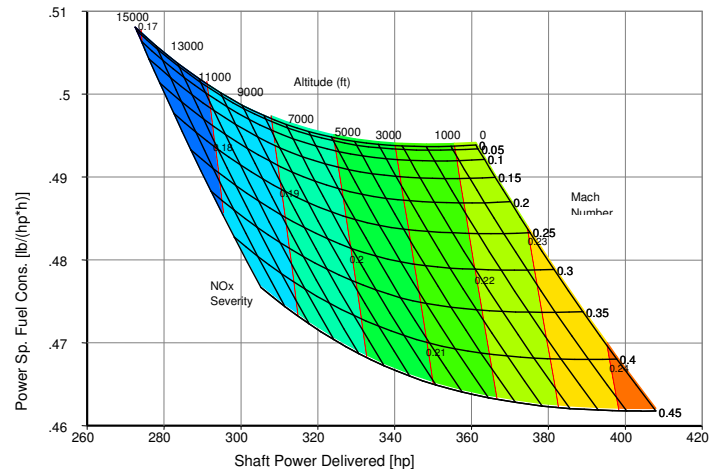


Figure 6-4: Off Design Performance Analysis

NPSS is a computer code for calculating on-/off-design, steady-state/transient engine performance. It’s object-oriented syntax accommodates nearly any gas turbine engine configuration. Figure 6-5 depicts a top-level summary of the Athena’s turboshaft engine modeled in the NPSS environment where each engine component was represented as an object in the NPSS code. These objects were specified to ensure the analysis took into account the actual geometry of the centrifugal compressor (“Comp.” block) and specific fuel properties and chemical composition (“Fuel In” block). The elements were linked together using the appropriate type of connection (fluid, fuel, or shaft linkages).

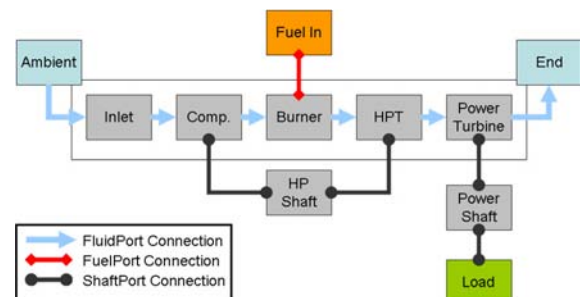


Figure 6-5: Athena Engine Modeled Using NPSS

GasTurb engine simulations with synjet fuel and standard JP-8 validated the Excel emissions estimation spreadsheet, and therefore the previous trade studies. Based on the maximum continuous power (MCP) setting for the sea-level standard condition of 376 HP from NPSS, it was necessary to establish a value for the 5-minute maximum takeoff power requirement as stipulated in Federal Aviation Regulation (FAR) Part 27. Equation 6-1 was used to estimate this short duration power where HP_{NR} refers to normal rated power (replaced by MCP) and t is the time in minutes.³ Figure 6-6 and Figure 6-7 depict the overall engine performance, at MCP and 5-minute takeoff power throughout its full operational envelope and at varying atmospheric conditions. As expected, emissions estimations with GasTurb 10 predicted higher pollutant counts at hotter engine conditions with standard jet fuel. Similar trends were seen with the synjet blends, though the magnitude of pollution decreased tremendously.

$$HP_{SD} = HP_{NR} (1 + 0.252 e^{-0.0173t})$$

Equation 6-1: 5-Minute Takeoff Power

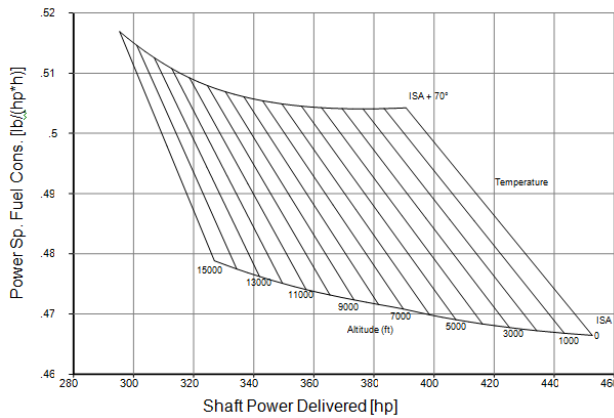


Figure 6-6: Athena Engine Performance Plot- MCP

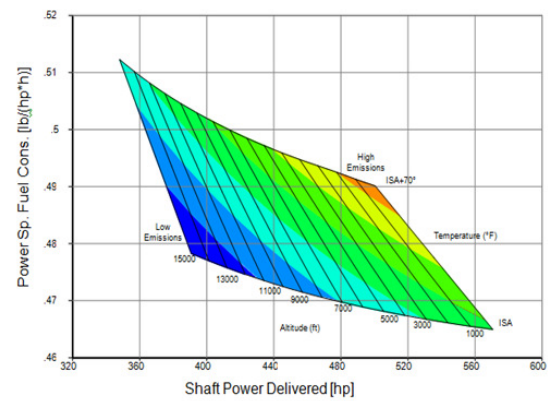


Figure 6-7: Athena Engine Performance Plot 5-Minute TO Power with Emissions Trends

6.7 Compressor

Increased compressor pressure ratios result in increased power and reduced fuel consumption for a fixed engine weight. However, compressor efficiency and engine efficiency is also a function of engine size. The manufacturing tolerances of compressor blades are critical in influencing the compressor's overall efficiency due to tip loss factors and secondary flows. Tip clearances on rotating components do not scale photographically like the rest of the engine.⁴⁵ Material thickness requirements become another limiting condition, because as component sizes get smaller, the associated materials must maintain a minimum thickness level. However, recent advancements in stall prevention technology have allowed increasing compression through each stage of a centrifugal compressor. Current technology permits

pressure ratios of 7:1, and future advancements should enable ratios of 9:1 or 10:1⁴⁶ without large increases in complexity or cost. Previously discussed parametric studies showed large increases in efficiency through increasing pressure ratios up to 9:1 (Figure 6-3). For this reason, the Athena engine was designed with a pressure ratio of 9:1.

Centrifugal compressors achieve higher pressure ratios per stage than heavier, larger axial compressors which require more materials and maintenance to support. Though centrifugal compressor stages are limited in their compression range, the Athena requires a relatively low pressure ratio. The optimal pressure ratio of 9:1, as well as the desire for a robust and simple solution, supports the centrifugal compressor as the most efficient choice for the Athena engine.

In order to determine the geometric and performance characteristics of the compressor, an Excel spreadsheet was developed to calculate velocity triangles and produce off-design compressor maps. Calculations in the Excel sheet mirror the calculations and techniques described in an *Introduction to Turbomachine*.⁴⁶ This technique used an iterative process of solving the entrance velocity triangle by guessing

$$\sigma = 1 - \frac{\sqrt{\cos(\beta_{b2})}}{Z^{0.7}}$$

Equation 6-2: Wiesner

the inlet Mach number at the tip, M_{1t} , and then continuously calculating a new value for M_{1t} until the two converged. The exit velocity triangle was calculated using the same iterative process for the exit Mach number, M_{3t} . The Wiesner correlation was also used to estimate the exit slip factor, σ , defined as the ratio of exit swirl velocity to the rotor speed, as shown in Equation 6-2 where $\beta_{2b} = 0$ for high speed impellers and Z is defined as the number of blades.⁴⁴ A modern polytropic efficiency of 90% was assumed to account for improvements in compressor technology and increased losses due to the relatively small size of this engine.

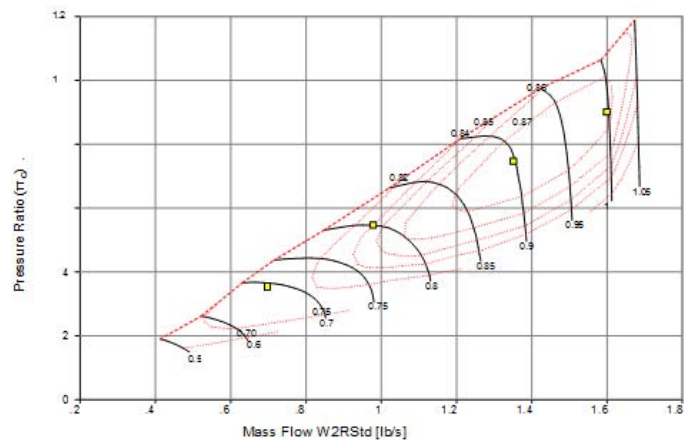


Figure 6-8: Centrifugal Compressor Performance Map

Figure 6-8 shows the component map used for the centrifugal compressor, which depicts efficiency and pressure ratios as a function of corrected flow and corrected speed.

In the Athena engine, flow must be carefully guided from the diffuser into the combustor, because the LPP combustor does not handle unsteady flow well. Stall and surge must be prevented not only to retain the compression abilities of the engine and prevent destabilizing vibrations, but also to prevent flashback in the combustor. For these reasons a diffuser with low solidity vanes was selected for the Athena engine.

In an effective engine compressor weight, cost, and vibrations must be minimized. The materials and manufacturing processes used to create the compressor must also be weighed considering environmental impacts to produce an environmentally friendly design. Implementing advanced technologies to raise air velocity and prevent flow unsteadiness, stall, and surge have resulted in a modern, efficient compressor design for the Athena

6.8 Fuels

6.8.1 Fuels Selection

The range of viable rotorcraft fuels is limited by infrastructure, fuel storage requirements, and safety concerns. Hydrogen, methane, propane, butane, JP8 (and other heavy hydrocarbons), bio-fuels, coal derivatives, and blends (synjet, biofuel/petroleum, coal/petroleum, etc.) were considered for this design, though safety concerns immediately eliminated some toxic fuels such as methanol. An initial trade study was completed comparing these fuels. In this study, the “joule,” or energy required, was fixed and the necessary fuel weight and volume were compared. Table 6-6 shows the fuel types

$$E.CO_2 = \frac{\text{mass } CO_2 \text{ emissions}}{\text{mass fuel}} \left(\frac{kg}{kg} \right)$$

Equation 6-3: Emissions Index of CO₂

Table 6-6: Fuel Comparison by Energy Density

Fuel	Phase	Density kg/m ³ *cryogenic	Energy density by mass MJ/kg (e _m)	Energy density by volume MJ/liter (e _v)	Mass fuel/ Mass JP8 for same energy	Volume fuel / Volume JP8 (liq.) for same energy
Hydrogen	Liquid (1bar, -252C)	70.91*	122.7	8.7	0.35	3.93
Methane	Liquid (1bar, -161C)	422.62*	50.016	21.2	0.86	1.61
Propane	Liquid	507.7	46.357	23.5	0.92	1.45
JP8	Liquid	~800	42.791	34.2	1	1
Hydrogen	Vapor (STP)	0.09	122.7	0.011	0.35	3,096
Methane	Vapor (STP)	0.717	50.016	0.036	0.86	950
Propane	Vapor (STP)	1.8	46.357	0.083	0.92	412

considered and their energy density by mass (e_m) and volume (e_v) as compared to JP-8. This study showed that hydrogen had the highest energy density by mass (e_m), however, it had the lowest by volume (e_v) which means it would require the largest storage tank. Conversely, JP8 had the lowest energy density by mass but the highest by volume.

From the study in Table 6-6, methane, propane and JP-8 were found to be the best options for fuel due to their high energy density by volume. Therefore, a further trade study was taken to analysis the best fuel for the Athena. For this trade study, the emissions were also considered. Since methane, propane, and JP-8 are all heavy hydrocarbons, the emissions would be similar in a given engine for NO_x, SO_x, CO, and UHC. The main emission difference would come from CO₂ due to the different chemical

makeup of the fuel. The CO₂ emissions of a fuel can be expressed by Equation 6-3. The emission per unit energy can then be expressed as in Equation 6-4.

Another factor that must be addressed is the availability of the fuel. JP-8 is a very common fuel and is available at most airports. Propane is easily available to the general public but is not generally present at airport fuel stations. Given these two additional factors, the criteria for choosing a fuel (FC) is defined in Equation 6-5.

$$E.CO_{2,e} \left(\frac{\epsilon}{MJ} \right) = \frac{E.CO_2 / 1000}{\epsilon_m}$$

Equation 6-4: Emissions per Unit Energy of CO₂

$$FC = f \left(\frac{e_m JP8}{e_m}, \frac{e_v JP8}{e_v}, \frac{E.CO_{2,e}}{E.CO_{2,e} JP8}, \frac{C_e}{C_e JP8} \right) + f(\text{fuel storage, delivery, availability})$$

Equation 6-5: Emissions Index of CO₂

Table 6-7 shows the results of this trade study. JP-8 was selected as the fuel for the Athena because it offers the best compromise between energy density, emissions, and availability.

Table 6-7: Fuels with Energy Density, Emissions, and Availability Relative to JP8

Fuel	$e_m JP8 / e_m$	$e_v JP8 / e_v$	$E.CO_{2,e} JP8 / E.CO_{2,e}$	Availability
Methane	0.86	1.61	0.75	Low
Propane	0.923	1.45	0.88	Medium
JP8	1.0	1.0	1.0	High

6.8.2 Overall Life Cycle Emissions: Coal Derivative Fuels and Biomass Fuels

After deciding to use JP8 as fuel, a through literature review was conducted to find ways to reduce emissions from the JP8. Of the emissions considered, CO₂ and particulate emissions are more a function of fuel composition than of combustor design. Therefore, a “drop-in replacement” for JP8 was researched that would have similar properties of JP8 and reduce these emissions. As part of the Assured Fuel Initiative, sponsored by the Department of Defense, the US government is funding research into synthesizing jet fuel from alternate sources. One of the most promising is the Fischer-Tropsch (F-

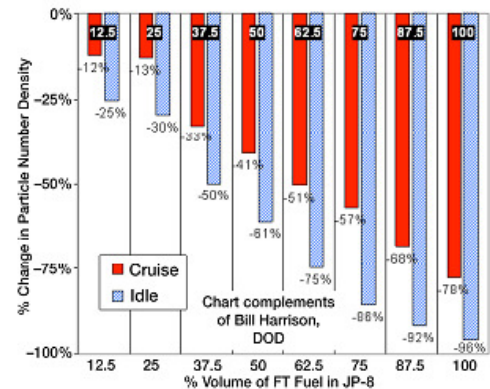


Figure 6-9: Particulate Emissions from F-T Blends with JP8⁴⁷

T) process. In general, the greater the concentration of F-T fuels as compared to JP-8, the lower the particulate emissions due to the lower amount of aromatic carbons (Figure 6-9). Lifecycle CO₂ emissions, however, vary widely depending on the materials used to synthesize the jet fuel (Figure 6-10 compares various synjet fuels with JP8 for lifecycle emissions). The Athena’s flexible fuel system allows use of both JP8 and Biomass Synjet. The F-T Biomass fuel still produces similar amounts of CO₂ when burned, but the CO₂ produced during its creation is considerably less than JP8 (Figure 6-10 and section 6.10).

There is currently a large effort funded by the Department of Energy and other groups to develop new enzymes to break down the initial biomass feedstocks more quickly, as the present process is rather inefficient and expensive. In 10 years the process should be streamlined enough to provide a competitive price and life cycle efficiency. The flexible nature of this Athena’s combustor will allow the helicopter operator to decide whether to use biojet or JP-8 fuel.

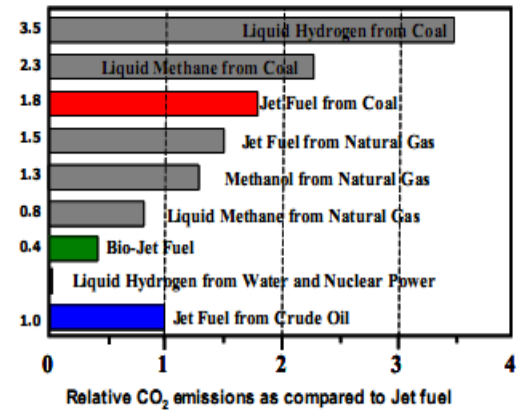


Figure 6-10: Lifecycle Synjet CO₂ Emissions⁴⁸

6.9 Combustor

The objective of the combustor design is to burn fuel with the typical 99% combustion efficiency, minimize pollutants (CO, UHC, and especially NO_x), minimize aerodynamic losses, and minimize cost. In addition, the combustor should perform equally well over a wide range of operating conditions, and allow for fuel flexibility.

6.9.1 Pollutant Formation in Turbine Engine Combustors

The pollutant emissions from aero-engines mostly consist of NO_x, CO, UHC particulates, CO₂, and SO_x. The formation of pollutants in turbine engine combustors is a function of combustion temperature, the time that the combustion products spend at high temperature and the sulfur content of the fuel (for SO_x emissions specifically). All but SO_x, SN, and CO₂ emissions (CO₂ and SN emissions were considered during fuel selection) will be considered in the Athena combustor design because SO_x, SN, and CO₂ are primarily a function of fuel type and not combustor design.

Table 6-8 explains that the main method of reducing NO_x is to decrease combustor temperature and residence time. Unfortunately, this actually increases CO and UHC emissions since these increase with lower combustor temperatures and residence time. This creates a trade-off between minimizing

Table 6-8: Pollutant Formation Methods

Pollutant	Cause	Formation methods that cause an increase in pollutant	Pollutant Problems
Nitrous Oxide species (NO _x)	Product of combustion in nitrogen containing fuels	High Temperatures, Long residence times in combustion chamber, Rich pockets caused from incomplete mixing, droplet burning	Smog, Acid Rain, some species are greenhouse gases
Carbon monoxide (CO)	Incomplete Combustion	Low Temperatures, Short residence times in combustion chamber, Lean pockets caused from incomplete mixing; CO ₂ disassociation at extremely high temperatures.	Greenhouse gas, harmful in large quantities
Unburned Hydrocarbons (UHC)	Incomplete Combustion	Low Temperatures, Short residence times in combustion chamber, Lean pockets caused from incomplete mixing	Leads to health problems
Particulate emissions smoke number (SN)	Carbon build up in fuel rich regions of the flame	Rich pockets of fuel, high pressures, low hydrogen content in fuel, high aromatic carbon content in fuel.	Smog, particles less than 20nm shown to cause health problems.
Sulfur Oxide species (SO _x)	Product of combustion with sulfur containing fuels	Quick formation in combustion of sulfur containing fuels	Acid rain, harmful if breathed.
Carbon Dioxide (CO ₂)	Product of combustion of hydrocarbons	Product of combustion of hydrocarbons	Greenhouse gas

CO/UHCs and NO_x. As with NO_x emissions, CO and UHC emissions can also occur due to incomplete mixing of the fuel vapor and air. When this occurs, the leaner pockets burn at a lower temperature and increase CO and UHC emissions while rich pockets burn at a higher temperature and increase NO_x.

6.9.2 Ultra-low NO_x Combustors

Based on the previous section, a general approach to reduce pollutant emissions is; to ensure complete droplet evaporation, improve mixing, reduce residence time at high temperatures, and find a trade-off for minimizing CO/UHC and NO_x emissions. These concepts are applied in various ways to the ultra-low NO_x combustors. The three types of low emission combustors considered for the Athena were the Rich-burn/Quick-Quench/Lean-burn (RQL) combustor, the Lean Direct Injection (LDI) combustor, and the Lean Premixed Prevaporized (LPP) combustor.

A trade study showed that the two stage, lean-lean, Lean Premixed Prevaporized (LPP) combustor was most beneficial to the Athena. The design principles and advantages and disadvantages of the various combustor types are shown in Table 6-9.

Table 6-9: Summary of Combustor Trade Study Results

Combustor	Principle Operating Method	Disadvantages
Rich-burn/Quick-Quench/Lean-burn (RQL)	Two stage combustor with first stage burning rich with low oxygen to prevent NO _x formation. Air is then added quickly in second stage to complete reaction and rapidly reduce equivalence ratio to lean with little heat loss completing reaction with little NO _x formation.	Can lead to increase NO _x emissions if mixing not sufficiently rapid or if unintended recirculation zone in either stage form increasing residence time.
Lean Direct Injection (LDI)	Similar to conventional combustor but instead of a single swirler and injector, uses multiple miniature swirler and injectors. Increases mixing and reduces recirculation zone to many small zones facilitating mixing and reducing residence time.	NO _x reduction smallest compared to other methods. Reduces engine power by shutting down some injectors—can lead to coking of injectors.
Lean Premixed Prevaporized (LPP)	Similar to conventional combustor but mixes air and fuel prior to injection into combustor creating a near uniform mix thereby eliminating pockets of high and low temperature. <u>Results in lowest NO_x formation of the above combustors.</u>	Susceptible to thermo-acoustic instabilities, autoignition, and flashback.
Two stage Lean-Lean LPP (LL)	<u>Similar to the LPP concept above but uses a two stage combustion region.</u> Primary and secondary stages both supplied premixed/prevaporized fuel/air. The second stage produces a stable flameless combustion zone that increases the overall equivalence ratio without increasing NO _x .	<u>Similar to LPP but much less susceptible to thermo-acoustic instabilities.</u> Still susceptible to autoignition and flashback.

6.9.3 The Athena Combustor: A Two Stage LPP Combustor

The design of the Athena combustor follows the reverse flow annular combustor design. Figure 6-11 shows the Athena reverse flow combustor with the components and airflow paths labeled. The compressor exhaust passes across the liner first, turns and passes through the combustion chamber in the opposite direction and then turns once more toward the turbine inlet. The purpose of this configuration is to reduce the length of the combustor. In 3-D, the combustor cross section is revolved around the axis of the turbine to create an ‘annular’ combustor. The annular combustor is the lightest combustor configuration when compared to ‘can’ or ‘can-annular’ combustors.

To reduce emissions, the reverse flow design was modified into a Lean-Lean, Two Stage, LPP combustor (LL), developed by Hayashi et. al.⁴⁹ as a variant of the LPP approach to ultra-low NO_x combustors. It is also similar to current combustors with axial fuel staging. This combustor configuration gives “high combustion efficiency...while maintaining single digit NO_x emissions over a wide range of overall equivalence ratios.⁴⁹” Moreover, the two stage configuration serves to greatly reduce the combustion instabilities that can be prevalent in single stage LPP combustors.

Figure 6-11 shows a schematic of the LL Athena Combustor. The combustion process is split into two stages: primary and secondary. The primary and secondary injectors both supply lean premixed prevaporized fuel/air mixtures. Injection of the secondary mixture into the hot products of the primary mixture produces a stable, ‘flameless’ combustion zone. The secondary combustion zone increases the *overall* combustor equivalence ratio without increasing NO_x emissions. Experimental results even indicate that NO_x levels can actually decrease after secondary combustion, possibly due to a chemical pathway for NO_x destruction by the secondary fuel.⁵⁰

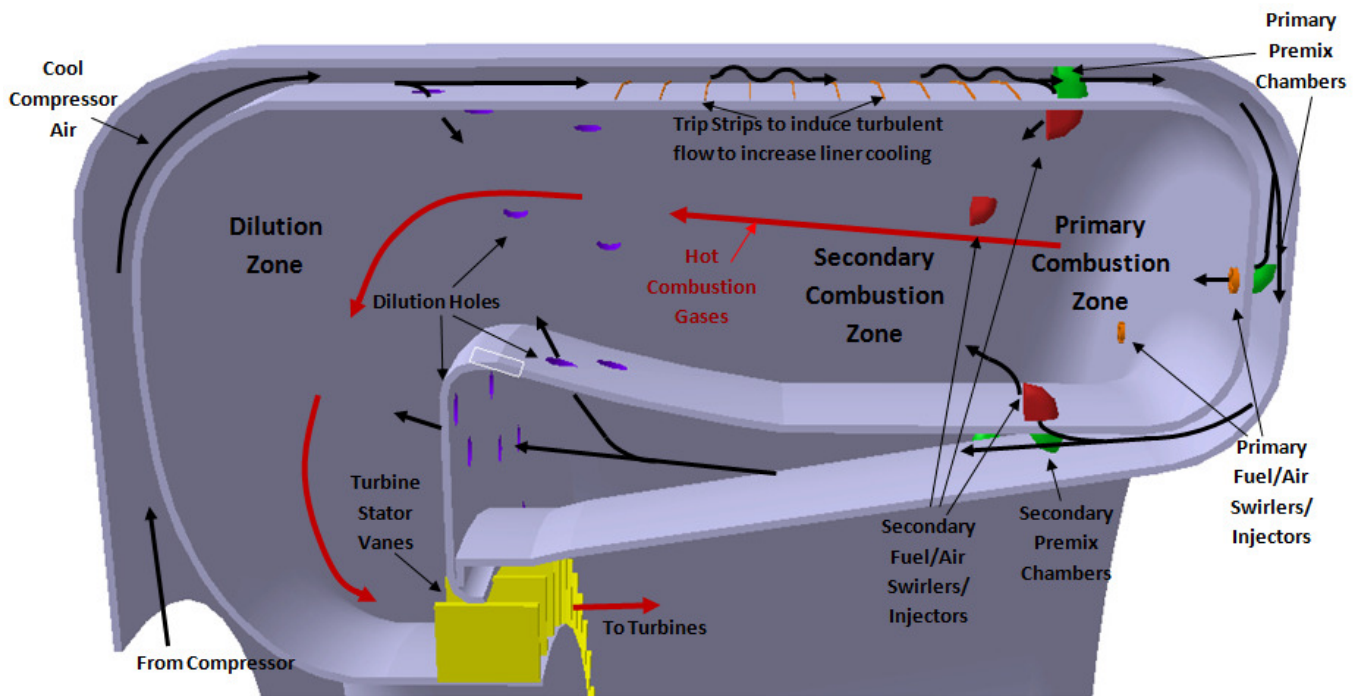


Figure 6-11: Athena Reverse flow, Two Stage Lean-Lean LPP Combustor (LL)

6.9.4 Emissions from Two Stage LPP Combustors

The low NO_x emissions for the two stage, lean-lean, LPP combustor were measured and compiled by Hayashi and are shown in Figure 6-12 and Figure 6-13. Analysis of these figures shows that the Athena combustor must operate with an overall equivalence ratio of 0.45 to 0.65 to minimize NO_x, UHC, and CO emissions. In order to predict the emissions of the Athena, an Excel program was written to extrapolate emissions based off these graphs. The program used the various engine operating parameters predicted by tools such as Gasturb 10 and NPSS, extrapolated the emissions at 15% O₂ from the Hayashi and Aida data, and then converted them to the Athena's exhaust oxygen content.

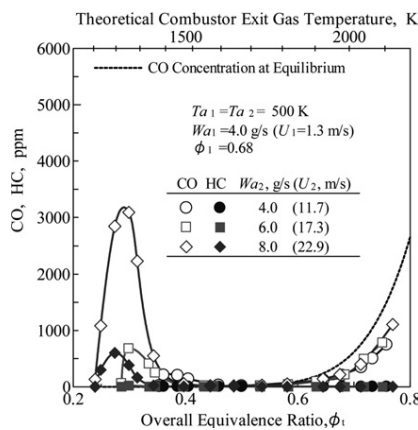


Figure 6-12: CO and UHC Emissions From a Two Stage LPP Combustor Over Various Overall Equivalency Ratios.⁵⁰

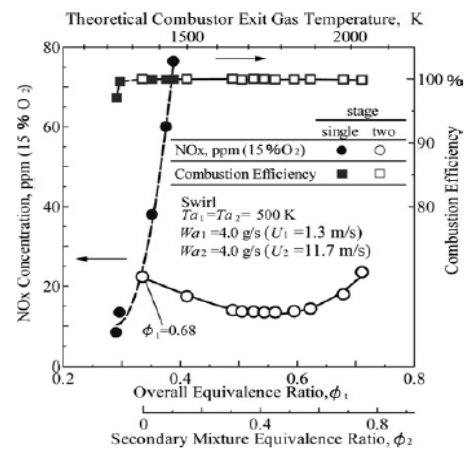


Figure 6-13: NO_x Emissions From a Two Stage Combustor Over Various Equivalency Ratios.⁵⁰

6.9.5 Designing the Two Stage LPP Combustor – overcoming LLP disadvantages

Though often used in large scale ground turbine engine designs, LPP engines have several potential problems which have precluded their use on aircraft. These main problems are autoignition, flashback, and thermo-acoustic instabilities. These problems are explained and presented with the Athena's solutions to overcoming them in Table 6-10.

Table 6-10: Summary of LPP Combustor Issues and Athena's Solution

Problem	Explanation	Athena's Solution
Autoignition	When mixing fuel and hot compressor exhaust gases before the combustion chamber, the fuel can spontaneously ignite	FADEC controller adjusts mass flow of the fuel/air mixture so that the residence time of the fuel is less than the ignition delay time. Premix chamber designed with smooth walls and no potential flame holders.
Flashback	Flame from the combustor travels back into the pre-mixer and causes the fuel to ignite prematurely	FADEC controller will adjust mass flow rate of the fuel/air mixture to remain above 20 m/s. Experimental results show this prevents flashback. Walls of pre-mix chamber sloped to accelerate the flow.
Thermo-Acoustic Instabilities	Caused by interactions in acoustic waves, fluid dynamics, and heat release oscillations. Results in resonance condition where pressure waves damage engine components and cause flame instabilities	Two stage variant of LPP shown by Hayashi to have very low occurrence to instabilities. Active closed loop feedback controller developed by Riley et al. opens and closes bleed air valves to dampen oscillations that do occur.

To prevent flashback and auto ignition, special care needs to be taken on the design of the premixer and combustion chamber. Flashback is where the flame from the combustor travels back into the premixer and causes the fuel to ignite prematurely. Autoignition is when the fuel mixing with the hot gases from the compressor ignite spontaneously in the premix chamber before reaching the combustor. Each of these issues causes damage to the engine and occurs most at high power settings.

Autoignition is prevented by designing the length of the premixer short enough that the residence time of the fuel-air mixture moving through the premixer is less than the ignition delay of the fuel.⁵¹ This is a compromise that results in less complete mixing than a premixer designed to ensure complete evaporation, but it allows the engine to operate at high power settings. The premixer must also be designed so that the walls are smooth with nothing that can hold combustion in its wake, and that no recirculation can take place inside, ensuring that the fuel exits before its ignition delay.⁵¹ Ignition delay times vary with fuels. The Athena will be designed to accommodate both JP-8 and its synjet-biofuel replacement. Although these fuels are extremely similar, the ignition delay times vary slightly and the FADEC controller will be used to accelerate the air-fuel mixture in the premix chamber, based on the fuel type, to ensure that the mixture enters the combustion chamber prior to the ignition delay.

To prevent flashback, the boundary layer inside the premixer must be minimized to prevent the flame creeping back along this slower moving air. Since turbulent flow cannot be used because of autoignition, the premixer walls must converge to accelerate the flow and flatten the boundary layer.⁵¹ Experimental studies by Poeschl et al.⁵² have shown that autoignition should not occur if the mass flow rate in the premix chamber is at least 20m/s. The Athena's FADEC will adjust fuel/air flow rates with power setting to ensure that the mass flow is always above this critical value.

The other potential problem with LPP engines is thermal-acoustic instability. This is caused by the interactions of acoustic waves, fluid dynamics, and heat release oscillations. The result is a resonance condition that results in pressure waves that create instability in the flame and can result in damage to engine components. The Athena's engine minimizes this with its two stage variant; the lean-lean, two-stage, LPP engine has shown in experimentation to be more stable by Hayashi et. al.⁴⁹ However, to ensure that this residence condition does not occur, an active controller will be used in the engine. This controller, developed by Riley et.

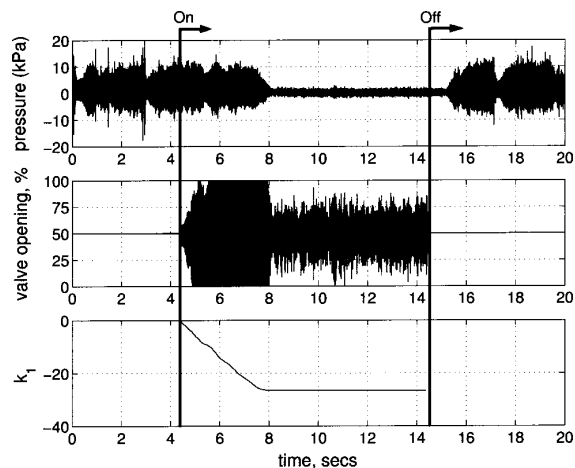


Figure 6-14: Thermo-Acoustic Pressure Fluctuation in Experimental LPP Combustor with STR Controller.⁵³

al.⁵³ senses acoustic waves and uses a closed feedback loop controller to activate an actuator that dampens the waves. The actuator opens and closes valves that cause liner cooling air to enter the combustion chamber and eliminate the instabilities in the flame (Figure 6-14).

6.10 Total Emission Chain

The Athena has been developed to minimize the fuel it consumes and the emissions it produces. However, the life cycle emissions do not only include its operation. To consider the entire pollution chain, the fuel's extraction, refining, transportation, as well as its burning must be calculated. The Athena was developed to use both JP8 and biomass synjet fuel to minimize lifecycle emissions. The two distinct pollution chains used to estimate the lifecycle emissions are summarized below in Figure 6-15.

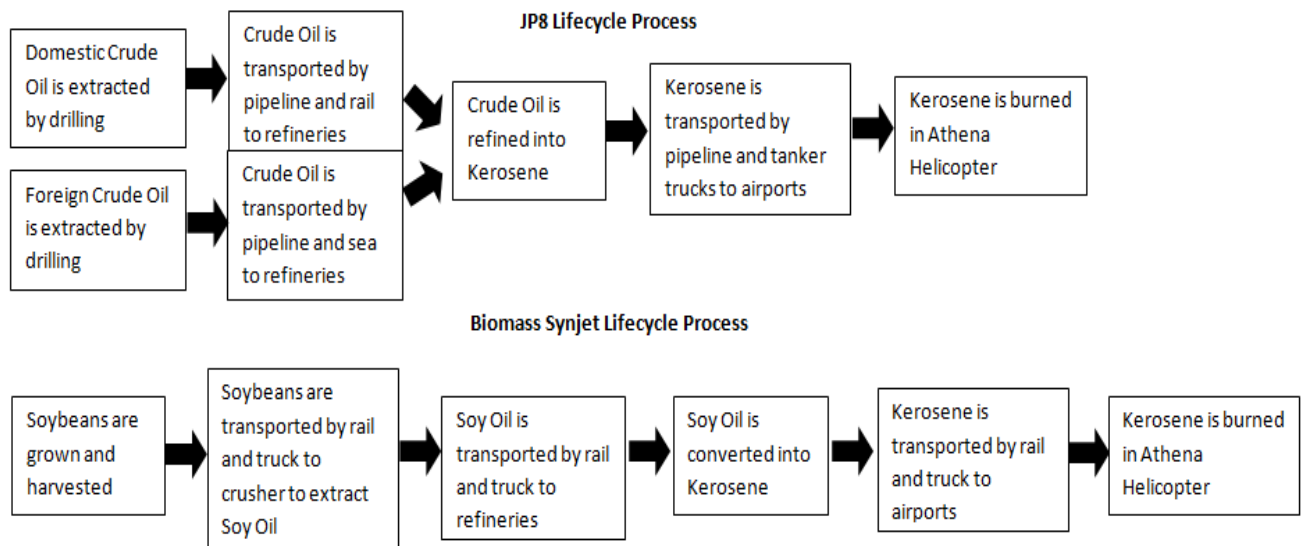


Figure 6-15: Lifecycle Processes for JP8 and Biomass Synjet

The above processes were assumed in the study along with the assumption of using soybean oil for the biodiesel production. Soybeans were selected as the major source of biomass because of their abundance in the U.S., and their ease of use in the production of biomass synjet. In all analysis, inadvertent oil spills and leaks were not taken into account, nor were the emissions from the exploration for oil or the setup of land for agriculture. The Athena's emissions were computed for a 15 minute OGE hover, followed by a 2.5 hour flight at 120 kts (covering 300 NM) both at SSL conditions. Emissions from startup, taxi, and shutdown were assumed negligible.

6.10.1 JP8 Lifecycle Emissions

The JP8 lifecycle emissions were derived primarily from a study by the U.S. Department of Energy that looked at the lifecycle emissions for urban buses running on biodiesel fuel.⁵⁴ This study considered the drilling and transport of both foreign and domestic crude oil and JP8. The transportation of JP8 by Petroleum Administration for Defense District (PADD) is summarized in Table 6-11. The emissions for the refining of JP8 were estimated from the U.S. Energy information Administration⁵⁵ and from an EPA profile of the refining industry.⁵⁶ The results of this study are shown in Table 6-12.

Table 6-11: Foreign and Domestic Crude Oil Transportation by Method and PADD⁵⁴

		Petroleum Administration for Defense District (PADD)									
		I		II		III		IV		V	
Petroleum Source:		Domestic	Foreign	Domestic	Foreign	Domestic	Foreign	Domestic	Foreign	Domestic	Foreign
Breakdown by Source		2.68%	97.32%	56.03%	43.97%	39.37%	60.63%	81.33%	18.67%	90.12%	9.88%
Pipeline	Domestic	13.30%		96.90%		84.40%		86.80%		38.60%	
	Foreign		4.76%		100.00%		23.21%		99.80%		18.10%
Tanker	Domestic	1.73%		0.00%		0.78%		0.00%		59.50%	
	Foreign		90.70%		0.00%		75.70%		0.00%		70.50%
Barge	Domestic	10.70%		0.19%		11.80%		0.00%		0.67%	
	Foreign		4.57%		0.00%		1.12%		0.00%		11.40%
Tanker Car	Domestic	41.20%		0.00%		0.08%		0.65%		0.21%	
	Foreign		0.00%		0.00%		0.00%		0.19%		0.00%
Truck	Domestic	33.10%		2.93%		2.99%		13.10%		0.98%	
	Foreign		0.00%		0.00%		0.00%		0.00%		0.00%
Total		100.00%	100.00%	100.00%	100.00%	100.00%	100.00%	100.00%	100.00%	100.00%	100.00%

Table 6-12: Lifecycle Emissions From JP8

Species	Extraction (g/gal)		Transportation (g/gal)		JP8 Refining (g/gal)	JP8 Transport (g/gal)	Athena Flight (g/gal)			Life Cycle Emissions for 15 min Hover, 2.5 hr Cruise (351.4 gal) - kg
	Domestic	Foreign	Domestic	Foreign			HOGE	Cruise	Weighted Total (15 min HOGE, 2.5 Hr Cruise)	
CO	0.215	0.395	0.037	0.055	3.783	0.128	0.451	0.444	0.445	2.133
CO2	150.030	254.766	57.566	246.516	7.100	58.744	1431.7	1431.746	1431.746	930.688
NOx	0.845	0.560	0.234	0.365	3.434	0.412	0.676	0.690	0.689	2.758
UHC	2.079	3.888	0.456	2.133	3.329	0.116	0.694	0.821	0.809	5.404
SN	0.598	0.526	0.180	0.315	0.502	0.151	13.469	13.469	13.469	6.640

6.10.2 Biomass Synjet Lifecycle Emissions

The biomass selected to estimate the lifecycle emissions of synjet was Soybeans. Soybeans are a major crop of the U.S., whose conversion process is well understood and would require minimal research and development for conversion into Synjet. Soybeans are grown throughout the U.S., however, to limit the study, only the top 14 soybean production states were examined and it was assumed that all soybean production would come exclusively from these states (Figure 6-11). The data for the agriculture, transportation, and soybean crushing came

Table 6-13: Soybean Production by State⁵⁴

State	Production (1,000 bushels)				Fraction of Total
	1993	1994	1995	3 Year Avg.	
Alabama	7,080	9,145	5,400	7,208	0.0038
Arkansas	92,300	115,600	86,700	98,200	0.052
Georgia	8,160	15,500	8,370	10,677	0.0057
Illinois	387,000	429,065	373,450	396,505	0.21
Indiana	223,100	215,260	194,220	210,860	0.11
Iowa	257,300	442,885	398,180	366,122	0.20
Kansas	53,200	73,500	51,250	59,317	0.032
Minnesota	115,000	224,000	232,000	190,333	0.10
Mississippi	42,900	57,035	37,800	45,912	0.024
Missouri	118,800	173,280	130,500	140,860	0.075
Nebraska	90,000	134,420	99,450	107,957	0.058
Ohio	156,180	173,565	153,140	160,962	0.086
South Carolina	7,800	15,660	12,720	12,060	0.0064
South Dakota	38,500	91,200	75,000	68,233	0.036
Total:				1,875,205	1.000

from the 1998 U.S. Department of Energy Study.⁵⁴ The data for the conversion of Soy oil to JP8 was also from this study. Although the study was based on the conversion to diesel and not kerosene, the emissions would be similar. The results of the study are summarized in Table 6-14. The negative emissions for agriculture show that the lifecycle emissions for 1 gallon of synjet actually removes CO₂ from the environment when compared to JP8.

Table 6-14: Lifecycle Emissions From Biomass Synjet

Species	Agriculture (g/gal)	Transport to Crusher (g/gal)	Soybean Crushing (g/gal)	Transport of Soy oil (g/gal)	Conversion of Soy oil (g/gal)	Transport of Synjet (g/gal)	Athena Flight (g/gal)			Life Cycle Emissions for 15 min Hover, 2.5 hr Cruise (351.4 gal) - kg
							HOG E	Cruise	Weighted Total (15 min HOG E, 2.5 Hr Cruise)	
CO	2.909	0.128	0.202	0.244	0.206	0.133	0.451	0.444	0.445	1.800
CO ₂	-5496.203	37.723	667.255	73.203	566.511	60.817	1410.884	1410.884	1410.884	-1130.344
NO _x	4.276	0.355	1.251	1.207	1.362	0.426	0.676	0.690	0.689	4.035
UHC	4.212	0.056	7.464	0.115	2.160	0.120	0.694	0.821	0.809	6.300
SN	0.620	0.051	0.884	0.045	0.009	0.156	1.723	1.723	1.723	1.471

6.11 Turbine

6.11.1 Axial vs. Centrifugal Turbines

Although centrifugal turbines typically offer more compact volumes and higher expansion ratios than axial turbines, their benefits are not as great as those for centrifugal compressors. Normally, fewer centrifugal turbine stages would be needed in a large engine when compared to axial turbines; however, because of the favorable pressure gradient through the turbine, and the small size of the Athena engine, only one axial stage is needed. The mass flow rate is also high enough to prevent large blade tip clearance losses in an axial design. Therefore, the axial turbine was chosen for the Athena due to the reduced frontal area, ease of manufacturing, and greater design flexibility.

6.11.2 Component Design and Materials Selection

Initially, the number of turbine stages was estimated based on efficiency, manufacturing, and reliability concerns. A two-staged, free turbine setup was selected as the best method to allow both engine and rotor speed optimization. This is a common system in rotorcraft, employing a high pressure turbine to convert the thermal energy of the flow leaving the combustor into usable power and a “free turbine” to carry that power to the transmission and ultimately the rotor for thrust generation. Due to recent advances in composites and cooling technology, modern high pressure turbines can withstand much higher temperature flows. Recent trends (Figure 6-16), predict allowable temperatures in excess of 3300°R, though temperatures this high require advanced cooling techniques (Figure 6-17), that increase manufacturing complexity and material costs. Figure 6-3 shows that large decreases in SFC are possible with high turbine temperatures; therefore the most efficient design will be a high temperature combustor.

The Athena's LL combustor has been shown to create combustion temperatures as high as 3300°R, though this temperature is reduced and moderated in the dilution zone to a level that can be handled by the turbine blades. However, in order to maximize the efficiency of the engine, a thorough trade study was conducted, and outlined in the next section, to select blade materials to maximize the exit temperature of the Athena's LL combustor.

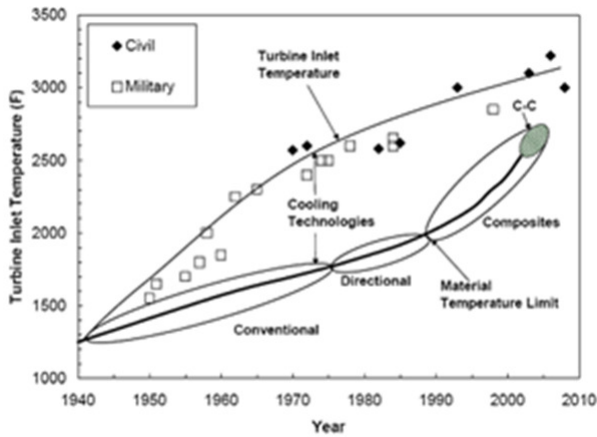


Figure 6-16: Turbine Cooling Technology Projections.⁵⁷

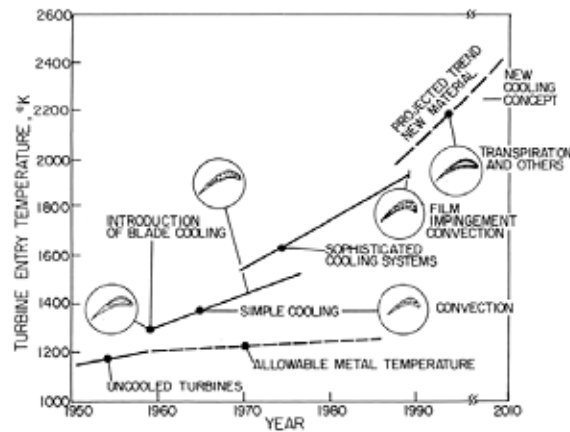


Figure 6-17: Allowable Turbine Temperatures and Cooling Methods.⁵⁸

6.11.3 Turbine Performance and analysis

In addition to composite blade and cooling system design, pressure turbine blade angles must also be optimized. Off-design high pressure and power turbine maps, shown in Figure 6-19 and Figure 6-18 were generated to evaluate turbine performance. The high pressure turbine map, which includes surge margins and other important high pressure turbine characteristics, was converted into a format readable by NPSS and used in the NPSS model to validate the preliminary GasTurb output.

Iterative performance cycle analyses were conducted using these off-design maps, the vehicle

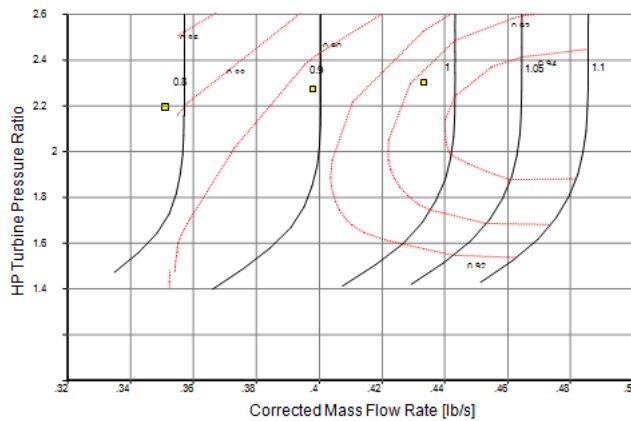


Figure 6-19: High Pressure Turbine Off-Design Performance Map.

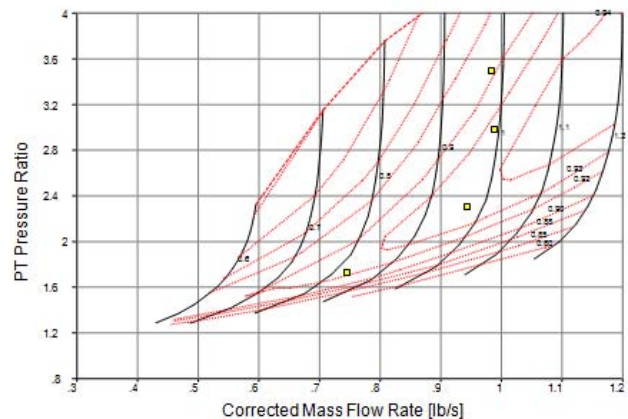


Figure 6-18: Power Turbine Off-Design Performance Map.

sizing and performance codes, and the NPSS model. CIRADS engine models were created based on these maps to more accurately predict fuel and power requirements at various altitudes. The models were refined and updated to reflect the changing engine performance characteristics until a final solution was achieved which effectively satisfied the performance requirements with the lowest SFC.

Using the Turbine Preliminary Analysis Program (TURBN) created by Jack D. Mattingly, further sizing and performance characteristics for both the High Pressure Turbine (HPT) and Power Turbine (PT) were completed. The engine output data from GasTurb 10 and NPSS provided the required input, and the following assumptions were made: two-dimensional flow, constant axial velocity, constant mean radius, adiabatic flow in the rotor and stator, and calorically perfect gas. Polytropic efficiency was 91% for the HPT and 88% for the PT, based on the reference in Figure 6-3 of this report and future projections.

Table 6-15 summarizes the results for the single-stage HPT and PT. The material selection for both turbine disks was based on an analysis of the blade stress factor (AN^2) and the shaft speeds. For the HPT, a shaft speed of 38,000 RPM was selected to achieve a design balance between maximum turbine blade stress and performance at the extremely high operating temperatures.

Table 6-15: Athena Turbine Design Parameters

	HPT	PT	Units
Stage Efficiency η_s	0.91	0.8755	
Stage Pressure Ratio	2.262	3.544	
Inlet Temperature T_4	3300	2731.62	$^{\circ}R$
Hub Radius r_h	3.02	4.13	in
Tip Radius r_t	2.89	3.77	in

A shaft speed of 20,000 RPM was selected for the power turbine because it was the optimum value that allowed the use of less-expensive, more recyclable materials while maintaining a high level of stage efficiency. Figure 6-21 demonstrates the relationship between the blade stress factor “AN” and material specific strength for the high pressure and low pressure turbines at a taper ratio of 1.0. The graph indicates that the required specific strength is approximately 1000 psi/(slugs/ft) for the HPT and 600 psi/(slugs/ft) for the PT. These values were used on the graph in Figure 6-20 to determine the materials required to meet the high temperature demands. This plot shows that the HPT should be constructed from

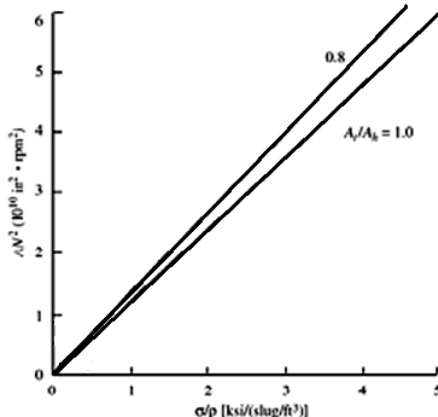


Figure 6-210: Blade Stress vs Specific Strength⁴⁴

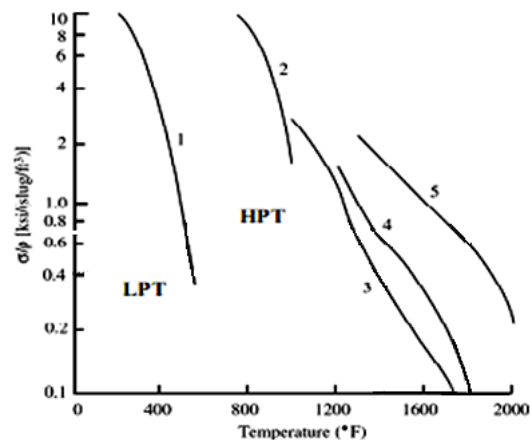


Figure 6-201: Turbine Material Selection Plot.⁴⁴

at least “Material 5,” which refers to a single-crystal or directionally solidified (DS) superalloy, and the PT should be constructed from “Material 4” which refers to a wrought nickel alloy.

6.12 Weight Analysis

CATIA was used to determine the specific volume of each major engine component. These values were then evaluated as a function of their material density to determine an estimated weight breakdown. Table 6-16 summarizes the results of this analysis.

Table 6-16: Athena Engine Component Weight Breakdown

Component	Volume (in³)	Density (lb/in³)	Weight (lb)
Compressor	35.20	0.170	11.5
Combustor	18.60	0.283	5.5
High Pressure Turbine	12.97	0.298	5.8
Low Pressure Turbine	24.06	0.298	8.5
Compressor Shaft	11.88	0.298	3.5
Power Turbine Shaft	7.58	0.276	2.5
Gearbox	220.96	0.283 / 0.098	52.2
Housing	141.99	0.283	40.5
Total Weight			130.0

6.13 Manufacturing

The small sizes of the engine’s rotating components demand the use of state-of-the-art manufacturing techniques to achieve the tight tolerances required for high efficiency. For the centrifugal compressor, a Computer Numerically Controlled (CNC) five-axis milling machine will be used to precisely machine its complex geometry. The tool path programs that define the intricacies of the cutting motions are easily generated using a suite of CAD/CAM software. As future improvements are made in the aerodynamic design of the radial compressor using computational fluid dynamics (CFD) analysis, the five-axis milling machine can immediately update its tool paths to capture the design upgrades without an engineering compromise for manufacturability. This integration between the design and manufacturing steps increases both process and component efficiency.

The turbine section of the engine will utilize directional solidification to produce the high pressure turbine blades with a vacuum chamber casting process. By closely controlling the temperature of the casting process, directional solidification results in a turbine airfoil composed of columnar grains along its spanwise axis. This grain alignment strengthens the blade and effectively eliminates the potential for destructive intergranular crack initiation.⁵⁹ Although more expensive to manufacture, the structural benefits offset the cost by reducing the long term maintenance requirements of the engine’s turbine section. Directionally solidified superalloys exhibit increased ductility and fatigue life which will lengthen the time between overhaul (TBO) for the entire engine. For the low pressure turbine, which experiences lower relative temperatures, an integrally cast turbine wheel and blades will be used to reduce parts count, manufacturing time, and overall complexity.

6.14 Federal Aviation Regulations (FAR) Requirements

A new engine design is subject to the Code of Federal Regulations, Title 14 – Aeronautics and Space, Chapter 1 – Federal Aviation Administration, Subchapter C – Aircraft, Part 27 – Airworthiness Standards: Normal Category Rotorcraft and Part 33 – Airworthiness Standards: Aircraft Engines. Beginning with Part 27, this regulation lists numerous requirements in Subpart E – Powerplant. Table 6-17 highlights those that are applicable at this conceptual level of engine design:

Table 6-17: FAR Part 27 Engine Requirements and Athena’s Solutions

Para.	Title	Summary
27.907	Engine Vibration	Engine and rotor drive system must be free from excessive vibrations -- Transmission mounted with dampers to eliminate excessive vibrations due to the rotor
27.917	Rotor Drive System Design	Engine must automatically disengage from rotor drive system for autorotational capability -- Freewheeling unit installed in engine gearbox
27.1091	Air Induction	Inlets must supply the engine with the required air during all operating conditions and minimize the ingestion of debris -- Screened engine cowling and inlet barrier filters surround the engine inlet
27.1093	Induction System Icing Prevention	Engine must be capable of operating at all power settings without accumulating ice on the inlet detrimental to engine operation -- Engine anti-ice system uses bleed air from the compressor to heat the walls of the engine
27.1141	Powerplant Controls: General	No single point failure in any powerplant control system can cause the loss of a powerplant function necessary for safety -- FADEC engine control has an analog backup mode
27.1191	Firewalls	Engine must be isolated from personnel compartments, structures, controls, and rotor mechanisms by a firewall or shroud -- Engine compartment is isolated

Part 33 is more focused on specific testing and evaluation requirements used during the certification process of a new aircraft engine. Table 6-18 summarizes the applicable requirements from Part 33 for this engine design; testing requirements will be addressed in the certification section of the report.

Table 6-18: FAR Part 33 Engine Requirements and Athena’s Solutions

Para.	Title	Summary
33.7	Engine Ratings and Operating Limits	Established relating to horsepower, RPM, gas temperature, and time for MCP and TOP -- See engine specifications
33.15	Materials	Suitability and durability must be based on experience or testing -- Material selection based on historical experience
33.66	Bleed Air System	If the engine anti-icing can be controlled, a means to indicate its functioning is required -- Pilot display light will illuminate when system is active
33.75	Safety Analysis	No probable engine malfunction or improper operation can result in a fire, engine burst, loads greater than ultimate loads, or loss of engine shut down capability
33.76	Bird Ingestion	Not applicable due to the inlet design on this aircraft

6.15 Transmission Design

6.15.1 Hanson Transmission Design

A Hanson split-torque transmission was selected for the Athena's drive system. Based on the engine horse power, the need to save weight, energy, and fuel, and reduce emissions, it was determined that a planetary transmission would not suffice. The split-torque Hanson transmission offers the greatest savings in weight and complexity. Based on the design from "A Designer Friendly Handbook of Helicopter Rotor Hubs", the Hanson Transmission requires only four gears to produce the necessary reduction in RPM.¹⁷ Figure 6-22 depicts the simplified gear configuration and Figure 6-23 shows an actual Hanson Transmission.

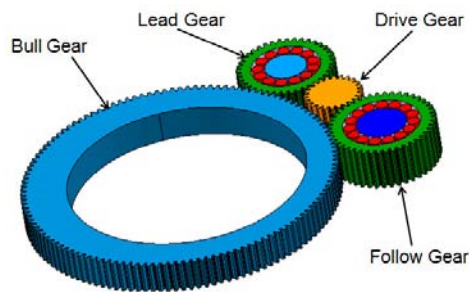


Figure 6-22: Athena's Hanson Transmission



Figure 6-23: Actual Hanson Transmission¹⁷

The Hanson transmission is unique in that it couples the bull gear of the transmission directly to the rotating mast. This provides a weight saving by having the hub bearing also serve as the gear bearing. The short length, large diameter rotating mast attaches directly to this bull gear. The non-rotating mast is located inside the rotating mast and is attached to the base of the transmission housing. Together, the rotating and non-rotating mast offer structural redundancy to transfer rotor loads into the airframe structure. This savings in weight and complexity directly translates into savings in cost, energy, fuel, and emissions, and an increase in reliability and safety.

The design of the gearbox followed the procedure outlined in Andrew Bellocchino's Design Thesis⁶⁰ and in Robert Norton's Machine Design Textbook.⁶¹ All gears were assumed to be spur gears. Although helical gears may run quieter due to reduced vibrations from the gradual tooth contact,⁶¹ they require thrust bearings⁶⁰ which result in a heavier transmission, more fuel burned, and increased energy consumption and emissions. The gear material selected was VASCO X2M for its high hardness, strength, and relatively low weight as compared to other steel alloys. For sizing, the following design criteria were selected:

- Engine operated at 514 HP, 30,000RPM (10% over 5 min power of 467 HP)
- Engine Nose Gear box 4:1 reduction

- Rotor tip speed: 680 ft/s in High Mode, 630 ft/s in Low Mode.
- Transmission component life: 3,500 flight hours

Using this design criteria, an excel program was written to vary the diameter, number of teeth, and face width of each gear and to measure the contact and bending stress of the teeth vs. the allowable contact and bending stress. A factor of safety of 1.1 was used in the study. The results of the stress study are provided in Table 6-19 and Table 6-20.

Table 6-19: Transmission Gear Stress (TO Power), VSM High (680 ft/s Rotor Tip Speed)

	Drive - Lead		Drive - Follow		Lead - Bull		Follow - Bull		Bevel Gear	
	Drive	Lead	Drive	Follow	Lead	Bull	Follow	Bull	VSM	Transmission
Contact Stress (PSI)	176,639	182,004	184,577	182,721	139,874	138,468	133,364	132,024	186,703	103,864
Allowable Stress (PSI)	190,863	194,636	190,863	195,350	194,636	203,561	195,350	203,561	190,692	199,295
Bending Stress (PSI)	40,210	39,905	39,748	40,325	38,645	41,514	38,502	41,118	19,700	22,816
Allowable Stress (PSI)	42,683	43,226	42,683	43,328	43,226	44,491	43,328	44,491	42,433	43,661

Table 6-20: Transmission Gear Stress (TO Power), VSM Low (630 ft/s Rotor Tip Speed)

	Drive - Lead		Drive - Follow		Lead - Bull		Follow - Bull		Bevel Gear	
	Drive	Lead	Drive	Follow	Lead	Bull	Follow	Bull	VSM	Transmission
Contact Stress (PSI)	180,880	186,374	189,009	187,109	143,232	141,793	136,567	135,194	191,187	106,358
Allowable Stress (PSI)	191,506	195,294	191,506	196,011	195,294	204,255	196,011	204,255	191,332	199,969
Bending Stress (PSI)	42,164	41,845	41,679	42,285	40,523	43,531	40,373	43,117	20,658	23,925
Allowable Stress (PSI)	42,776	43,320	42,776	43,423	43,320	44,589	43,423	44,589	42,525	43,756

As highlighted in Table 6-20, the low speed mode sized the gears. The bevel gear was sized based on contact stress while the rest of the gears were sized based on bending stress. The sized gears are shown in Table 6-21.

Table 6-21: Transmission Gear Dimensions

Main Transmission	Pitch Diameter (in)	Teeth	Diametral Pitch	Face Width (in)	Material
Bevel Gear - VSM	1.8	18	10	6.6	VASCO X2M Steel
Bevel Gear - Transmission	5.7	57	10	6.6	
Drive Gear	3	24	8	2.6	
Lead Gear	5	40	8	2.4	
Follow Gear	5.5	44	8	2.3	
Bull Gear	16	128	8	2	

6.15.2 Variable Speed Module (VSM) Selection and Operation

The Variable Speed Module (VSM) allows the Athena to change its tip speed from 680ft/s (207m/s) to 630ft/s (192m/s). The concept picture is shown in Figure 6-24. This change reduces noise and vibrations at high speed and increased the performance of the Athena. Several designs of variable speed concepts were considered including a torodial continually variable transmission (CVT), a traction

drive, a paracyclic CVT (P-CVT), and a planetary gear system with clutch. The evaluation criteria were based on the size of the system needed to achieve the approximate 8% RPM reduction, the loss inherent in each system, and the complexity. Due to the need to save on weight, lower fuel burn, reduce emissions, and lower the system cost, a planetary gear system with clutch was chosen. The Athena operates at two distinct speeds, high and low. Therefore CVT style systems were determined to be overly complex and costly in R&D and production despite a slightly lower gross weight. A planetary system has the advantage of being a proven technology (the clutch system is based on an automobiles automatic transmission) where gears are always engaged, even while switching speeds, which results in the fastest rotor speed change and provides improved safety.

The initial design revealed that the desired reduction could not be achieved by a single planetary gear system; the reduction was too small and the designed gears could not mesh. Therefore, a dual planetary system was designed with the first set of planetary gears providing a large reduction and a second set increasing the speed such that the net reduction was the required 8%. An important safety feature that was mandated when the system was designed was that the system could only use one clutch assembly. This would not only reduce weight, but would also ensure that there would not be a dramatic reduction in rotor RPM should one clutch fail and the other one engage. By designing the system to use only one clutch the system could only fail in high or low mode, and either mode has enough rotor speed to allow a safe landing of the helicopter. A summary of the input-output structure is shown in Table 6-22 and a schematic is shown in Figure 6-24.

Table 6-22: Variable Speed Module (VSM) Operating Methods

Operation	Tip Speed (ft/s)	Overall Speed Ratio	Clutch Position	Input Member	Output Member
High Mode	680	1 : 1	Lock Planet Carrier to Ring Gear 1 and 2	Sun Gear 1	Sun Gear 2
Low Mode	630	1 : 0.92	Lock Ring Gear 1 and 2 stationary	Sun Gear 1	Sun Gear 2

When operating in high speed mode, the VSM is in “pass-through” mode. The piston actuates the clutch to the right, as shown in Figure 6-24, and causes the clutch plate to press the planetary gear clutch assembly against the outer clutch plate. This locks the two ring gears of gear sets one and two (which are connected to the same outer housing) to the planet arm carrier and connector plate (which connects the planet gears of the two planetary sets). Because no internal rotation can then occur in either set, this causes the entire VSM to rotate at the input speed, the engine output RPM, with no reduction. When in the low speed mode, the piston actuates the clutch left as shown in Figure 6-24. This causes the clutch plate to press against the outer housing holding it stationary. Because this outer housing is also connected to both ring gears, this locks the ring gears in each planetary system stationary. This also releases the planet arm carrier to rotate freely. This results in a speed reduction of 1:0.92 or a rotor tip speed of 630 ft/s (192m/s).

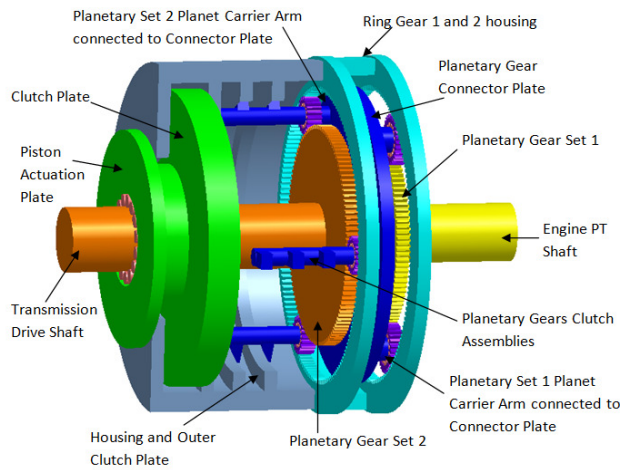


Figure 6-24: Variable Speed Module (VSM) Concept

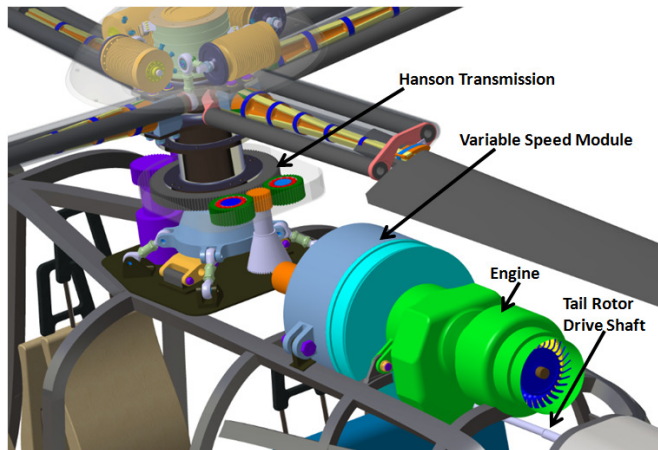


Figure 6-25: Mounted Variable Speed Module (VSM)

6.15.3 Variable Speed Module (VSM) Design

The VSM is a modular item intentionally not built into the transmission. If a customer does not feel the benefits of the noise and power reduction outweigh the added weight, he/she may opt to buy the helicopter without the VSM. In order to determine the smallest configuration, a Matlab program⁶² was written to determine all combinations of the two gear sets resulting in the required reduction with a sun gear and ring gear tooth count ranging from 5 to 600. From these possible solutions, the gear system with the lowest tooth count was selected because it would result in the lowest mass.

The Excel program designed for the Hanson transmission was modified for the planetary system to determine the face width needed to withstand the contact and bending stresses. The pitch diameters of the systems were varied from 6 to 20 to determine the system with the lowest mass. Table 6-23 shows the resulting VSM's gear parameters and Table 6-24 shows the VSM's stresses when operating in low mode which produces the highest stresses. As can be seen from the table, the planetary gears sized the transmission based on contact stress.

Table 6-23: Variable Speed Module (VSM) Gear Design

GearSet	Transmission Part	Teeth	Pitch Dia (in)	Diametral Pitch	Face Width (in)
Set 1	Ring	162	18	9	0.9
	Planet (x3)	27	3	9	0.9
	Sun	108	12	9	0.9
Set 2	Ring	162	18	9	1.0
	Planet (x3)	21	2.33	9	1.0
	Sun	120	13.33	9	1.0

Table 6-24: Variable Speed Module (VSM) Stresses

	Sun-Planet Set 1		Planet-Ring Set 1		Sun-Planet Set 2		Planet-Ring Set 2	
	Sun	Planet	Planet	Ring	Sun	Planet	Planet	Ring
Contact Stress	58,341	165,015	155,577	44,911	48,741	164,776	159,142	40,516
Allowable Stress	173,771	169,314	169,314	175,236	174,176	167,459	167,459	175,236
Bending Stress	6,782	17,752	20,119	8,541	6,266	15,297	18,575	4,907
Allowable Stress	41,071	39,475	39,475	40,375	40,215	39,191	39,191	40,375

7 INTELLIGENT CONTROL SYSTEM ARCHITECTURE

The Athena control system has a distributed, heterogeneous architecture integrated through a middleware component called the Open Control Platform (OCP),⁶³ and illustrated in Figure 7-1. It consists of traditional flight and engine controllers, as well as advanced components for greater autonomy and improved handling qualities. This intelligent, horizontally-distributed control architecture greatly simplifies component modifications and upgrades and overall control system expansion, allowing Athena to exploit state-of-the-art control technologies. Furthermore, the OCP facilitates communication between the flight-related and engine-related portions of the control system, creating a highly-integrated flight-propulsion control system that reduces emissions and fuel consumption.

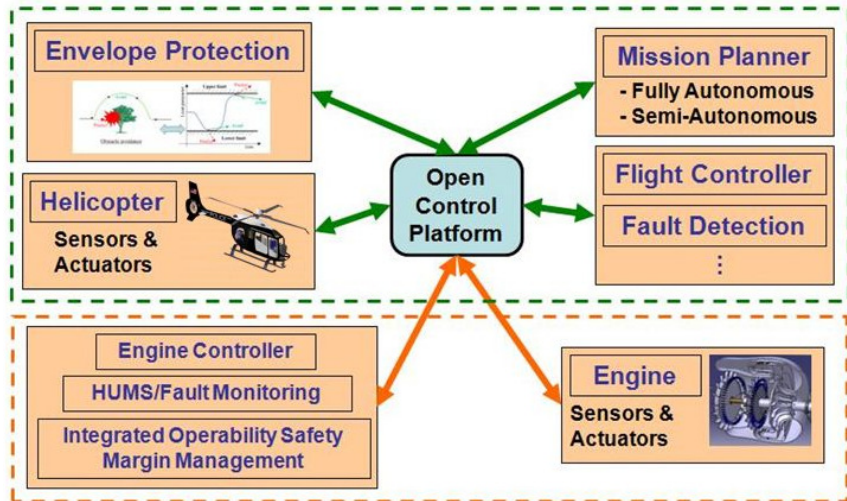


Figure 7-1: Overall Control System Architecture

7.1 Open Control Platform

The Open Control Platform (OCP) is a software infrastructure prototyped by the Georgia Institute of Technology and Boeing. It has already been demonstrated on the GT Max UAV helicopter at Georgia Tech. The OCP is middleware software and serves to integrate various control components by providing a “substrate through which [they] can communicate with each other regardless of whether they are collocated on the same processor...and regardless of whether they are written in different programming languages.” In addition to component integration, the OCP also allows for real-time reconfiguration of the control system,⁶⁴ which is essential for an intelligent, distributed control architecture.

The overall control system architecture for Athena (Figure 7-1) consists of numerous control components communicating with each other through the OCP substrate. Familiar examples of such components include the flight and engine controllers and diagnostic components. Advanced components such as the mission planner and envelope protection system are included to increase the autonomous capabilities of the aircraft, and simplify vehicle operation. Thus, Athena can accommodate pilots with a wide spectrum of helicopter training.

The components can be roughly organized as a flight control system (the top box) and an engine control system (the bottom box). However, because of the distributed architecture, this traditional categorization need not be applied. Instead, the control system can be seen as interactions among a collection of control components (flight controller component, engine diagnostic component, etc.) and sensors and actuators (helicopter and engine). Indeed, this latter description is more accurate since communication between the flight and engine portions of the control system is important to the vehicle's ability to optimize for different missions in terms of parameters such as fuel consumption and noise.

7.1.1 Levels of Autonomy

Athena offers three levels of control autonomy: manual, semi-autonomous, and autonomous operation. These levels are selectable by the pilot and are intended to reduce pilot workload allow the pilot to focus on other aspects of his/her mission and not only on aircraft control.

These levels are:

- *Manual operation* corresponds to the traditional method of controlling the vehicle via collective, cyclic, and pedal inputs.
- *Semi-autonomous operation* simplifies the interaction between the pilot and the vehicle. In this mode, Athena is controlled via velocity commands (speed and direction, both laterally and vertically) from the pilot in the form of button pushes or a control stick.
- *Fully-autonomous operation* grants the pilot the most simplicity and the greatest level of versatility. The pilot can specify anything from a single destination, to a set of waypoints, to a full continuous trajectory. Moreover, the Athena mission planner module allows for the optimization of a custom-weighted set of parameters such as minimum time to target or minimum fuel consumption.

The distributed and reconfigurable control architecture that the OCP supports allows the pilot to change and tailor the desired level of autonomy to the mission at hand. The fully and semi-autonomous modes have already been implemented at Georgia Tech on the GT Max helicopter UAV, and would require minimal R&D, allowing it to easily meet the 2020 operational requirement.

7.2 FADEC Engine Control System

A Full Authority Digital Engine Control (FADEC) unit provides engine control during engine operation. Athena's fly-by-wire design allows seamless FADEC integration with the flight control system. A FADEC provides capabilities which include:⁶⁵

- Reduced use of hydromechanics
- Automatic engine start
- Over speed protection
- Temperature limiting
- Surge detection/avoidance
- Flameout detection
- Fault monitoring
- Torque Spike Elimination
- Max Torque Rate Attenuator

7.2.1 Distributed FADEC

Athena utilizes an advanced distributed-architecture FADEC which is an improvement to current centralized control architectures because it reduces system interdependencies within the FADEC. A distributed digital engine control system retains the capabilities of present-day FADEC but has the added benefits of modularity, expandability, and obsolescence mitigation. Components in the Athena FADEC system can be modified or upgraded without redesigning other components. This allows for the expansion of FADEC capabilities as control technologies advance and eliminates the need to replace an entire FADEC unit, a costly endeavor. The projected timeline for the deployment of Athena matches well with the proposed roadmap from centralized to distributed FADEC architecture.⁶⁶

Figure 7-2 illustrates the Athena FADEC system, which achieves its distributed architecture through use of the Open Control Platform (OCP). The components of the FADEC system (engine controller, fault monitoring unit) are separate entities communicating with each other through the OCP. In fact, the same OCP facilitates communications among flight control

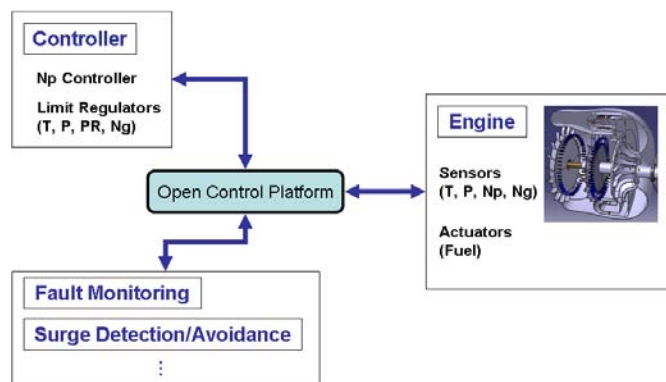


Figure 7-2: Distributed FADEC Architecture Using the OCP

components, thereby achieving a high level of integration between the flight and propulsion control systems which enable Athena’s performance to be optimized for each individual mission.

7.2.2 Engine Controller Architecture

The engine controller architecture is shown in Figure 7-3. The controller takes flight controller and engine sensor signals as inputs and converts them to a desired power turbine RPM. The power turbine RPM controller calculates a corresponding fuel flow rate of change. However, to prevent exceeding engine safety parameters, three limit regulators also calculate flow change values, and the minimum value is selected. The signal is then passed through an acceleration schedule that limits the maximum flow change value to prevent compressor stall. At

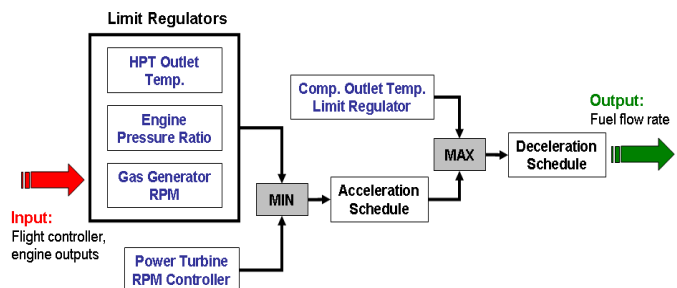


Figure 7-3: Engine Controller Architecture.

this point, a fourth limit regulator on compressor outlet temperature is introduced, and the maximum flow change value is taken to prevent flameout in the combustor. The flow change value is then sent through a deceleration scheduler and integrated to calculate the actual fuel flow command sent to the fuel actuator.

7.2.3 Flight/Propulsion Control System

Communications between the various components of the Athena control system are illustrated by the block diagram in Figure 7-4. Depending on the level of autonomy desired, the pilot can input commands directly to the flight control system using traditional means (collective, cyclic, and anti-torque control), or indirectly using the simplified controls offered by the mission planner.

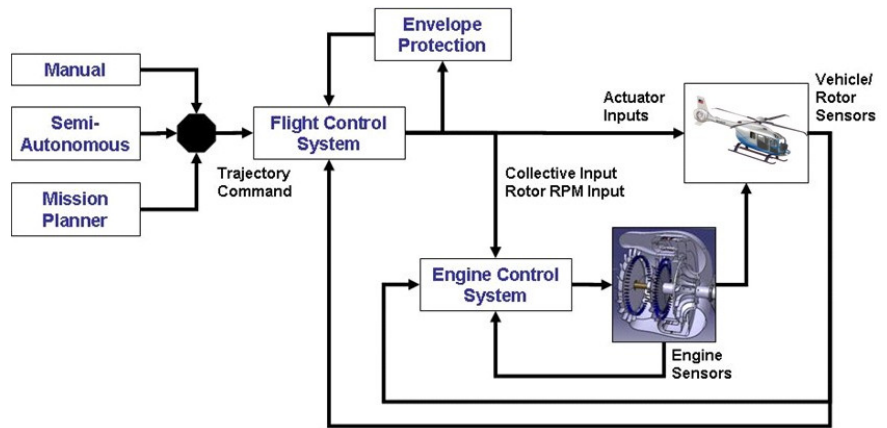


Figure 7-4: Block Diagram of Flight/Propulsion Control

The inputs are constantly monitored, and corrected if necessary, by the envelope protection system to ensure vehicle safety limits are not violated. The flight and engine control systems calculate the actuator commands sent to the vehicle, rotor system, and engine. The sensors listed in Table 7-1 provide feedback information to the control systems. Multiple redundancies in

Table 7-1: Sensor Suite

Parameter	Sensor
Pitch/Roll/Yaw rates	Rate gyroscopes
Pitch/Roll attitudes	Attitude gyroscopes
X, Y, Z accelerations	Accelerometers
Altitude	Barometric altimeter
Height from ground	Radar altimeter
Navigation	Global Positioning System
Obstacle Avoidance	Short-range radar
Vehicle Reconfiguration/Health	IBC actuator failure detection, Exhaust temperature sensor (engine health)
Miscellaneous	Infra-red, Night-vision, Strain gauges (structural limit envelope protection)

the rotor blade control electrical actuators ensure safe and reliable operation of the IBC system. Moreover, the combination of IBC and the OCP allows the control system to efficiently address actuator failures. The overall Athena control system is implemented on two redundant flight control computers.

Figure 7-5 shows the more detailed interactions between the control system and the Athena. The system is based on the model reference adaptive control method.⁶³ This approach was selected because the usage of autonomous and semi-autonomous modes requires precise tracking of trajectory commands. Although the derivation of this architecture assumes full state feedback, output feedback formulations are possible as well.⁶³ Hence, the system is applicable to Athena even though the complexities of certain

technologies such as IBC would prevent full knowledge of all the states of a dynamic model of the helicopter.

In the control system diagram, the dynamic inversion is an approximation of the dynamics of the vehicle. The reference model is used to dictate the desired response characteristics, i.e., ADS 33D requirements. The linear compensator stabilizes the feedback-linearized dynamics and the neural network is used to compensate for model errors in the dynamic inversion. The estimate hedge allows the adaptive control to operate at the actuator limits.

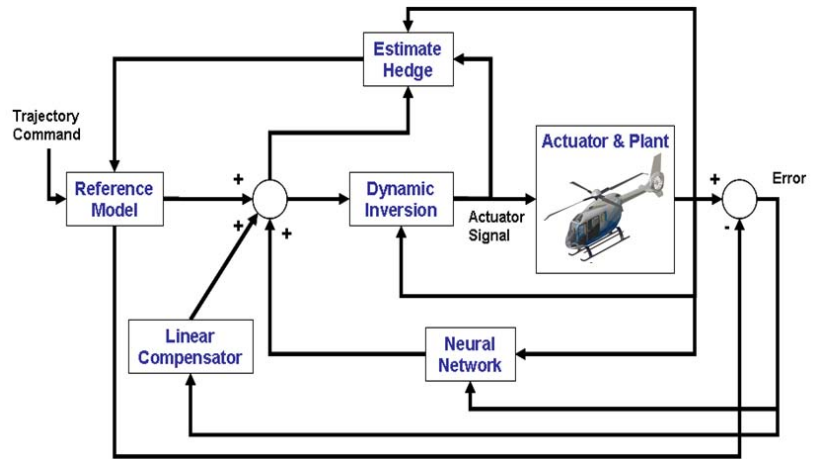


Figure 7-5: Flight Control System.

7.3 Mission Planner

The mission planner is a receding-horizon optimization component. In optimal control theory, the aim is to calculate a time-trace of control commands for a given dynamical system that optimizes (minimize or maximize) a predefined cost parameter over a finite or infinite time interval. For a receding-horizon optimizer, this time interval is fixed and finite in length but constantly recedes from the present time. Figure 7-6 gives a notional illustration of receding-horizon optimization.

For instance, suppose at some point during a mission, fuel actuator commands are calculated to minimize fuel consumption (the cost parameter) for the next 10 minutes. This control command is used only at the present controller time step; at the next time step, the calculations are performed again to optimize over the next 10 minutes.

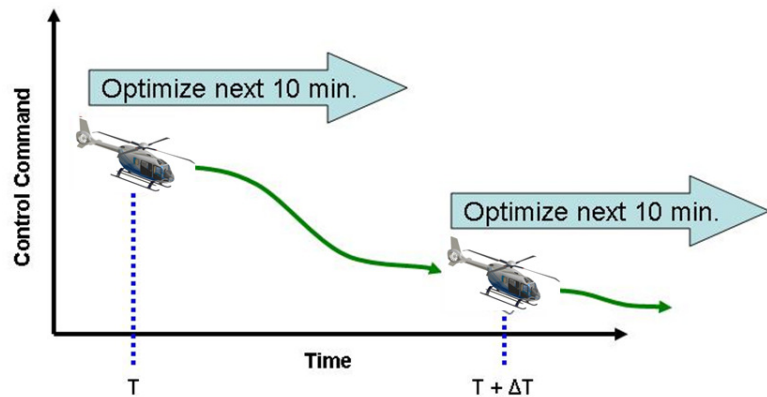


Figure 7-6: Notional Illustration of Receding-Horizon Optimization

Receding-horizon optimization is less computationally intensive than full-horizon optimization, allowing for generation of solutions in real-time. Moreover, since the certainty of flight conditions

decrease as the optimization time interval becomes large, utilizing a receding horizon becomes a natural choice since it makes the best use of computational power available onboard the vehicle. In addition, there is versatility to tailor the optimization process to specific flight phases by varying the length of the receding horizon, i.e. the horizon may be short for takeoff/descent phases but automatically lengthened during forward flight/hover.

Research has been conducted using receding-horizon optimization to generate trajectories that incorporate features such as terrain, visibility, and threats.⁶⁷ The Athena mission planner component generalizes this optimization procedure to incorporate the following features:

- Minimum fuel consumption
- Minimum noise
- Follow prescribed trajectory
- Follow target
- Minimum time to target

These parameters are then weighted and summed into a single cost parameter to be optimized. The weights are dependent on the type of mission, the phase of the mission, and user inputs. For instance, police responding to an emergency situation may select a target and choose minimum time to target as the predominant parameter to be optimized. On the other hand, during a hover phases, the minimum fuel consumption optimizer might be used. Using optimal control theory, the mission planner calculates the control commands, such as rotor RPM and individual blade pitch settings, that will optimize the cost parameter over a chosen time horizon. The mission planner communicates with the flight and propulsion controllers through the OCP to reconfigure and optimize them for the immediate mission phase.

7.3.1 Envelope Protection

Carefree handling is the ability of the pilot to operate the vehicle without concern for exceeding aircraft safety limitations. The nature of these limitations may be aerodynamic, structural, or control-related. While the ability to fly the vehicle in this carefree fashion is a convenient feature for pilots operating Athena in manual mode, it is a necessity for both semi- and fully-autonomous operation since human interaction with the flight control system is indirectly routed through an intermediary mission planner component. The control system must be sufficiently intelligent to detect and avoid possible limit violations without intervention from an experienced human pilot. The envelope protection system allows for this ability. However, the Athena controls also include a manual override switch on the collective so the pilot can bypass the envelope protection and allow the helicopter to exceed a limit in an emergency if required.

The Athena envelope protection system is based on the principles of obstacle avoidance. The system utilizes adaptive neural networks to accurately capture the input-output relationships between control commands and the limit parameters concerned. At each controller time step, the neural network is used to predict the immediate trajectories of the limit parameters. If a violation is predicted, the obstacle avoidance algorithms are used to generate a desired trajectory of the limit parameter concerned which smoothly avoids the threshold (see Figure 7-7). The input-output relationship between the controls and the parameters are then inverted to generate the control commands necessary for the limit parameter to follow this trajectory.⁶⁸

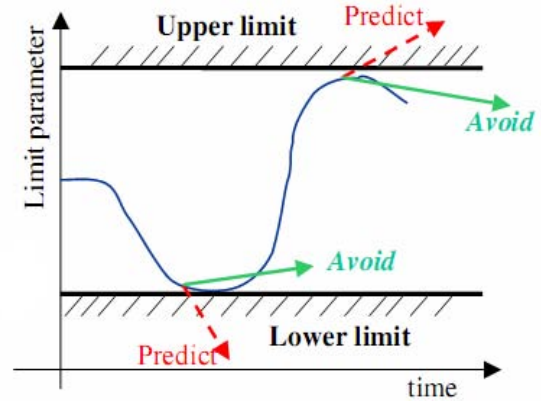


Figure 7-7: Illustration of Envelope Protection

7.3.2 Control Reconfiguration & Safety

The individual blade control and open control platform technologies represent a powerful combination for not only energy and noise minimization but also vehicle safety. The ability to control each rotor blade independently increases the number of options available to the control system for recovering from actuator failures. Some examples of IBC actuator failure scenarios are illustrated in Figure 7-8.

In the development of the Athena control system, numerical simulations must be performed to determine the best control inputs at the functioning actuators in response to different failure scenarios. Such simulations have already been completed for a six-bladed rotor with 50% cyclic amplitude loss at one of the blades.¹⁹ The optimization routine has shown that by appropriately varying the pitch in the remaining blades, the vehicle experiences nearly negligible perturbations in terms of translational and rotational accelerations despite actuator failure (Figure 7-9).

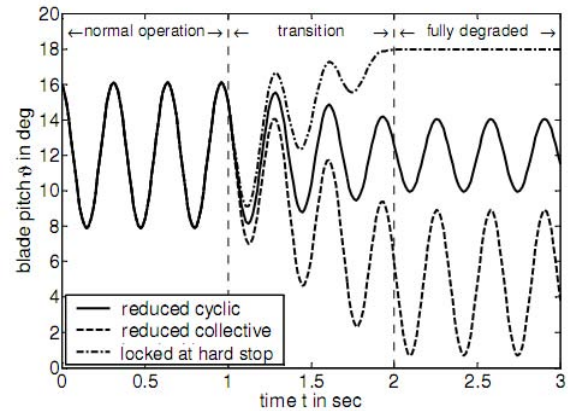


Figure 7-8: Examples of IBC Actuator Failure/Degradation Scenarios¹⁹

These types of simulations and optimizations will be extended during Athena’s control system development. It was found that the acceleration responses are exacerbated with increasing time delays between the original and reconfigured control settings. Thus, the optimal control response to different types of failures must be pre-determined and stored within the fault detection component of the control system. The OCP will then facilitate switching control schemes (from the mission planner, for example, during failure-free operation) if a failure is detected. The ease in control reconfiguration supported by the OCP minimizes the associated time delay.

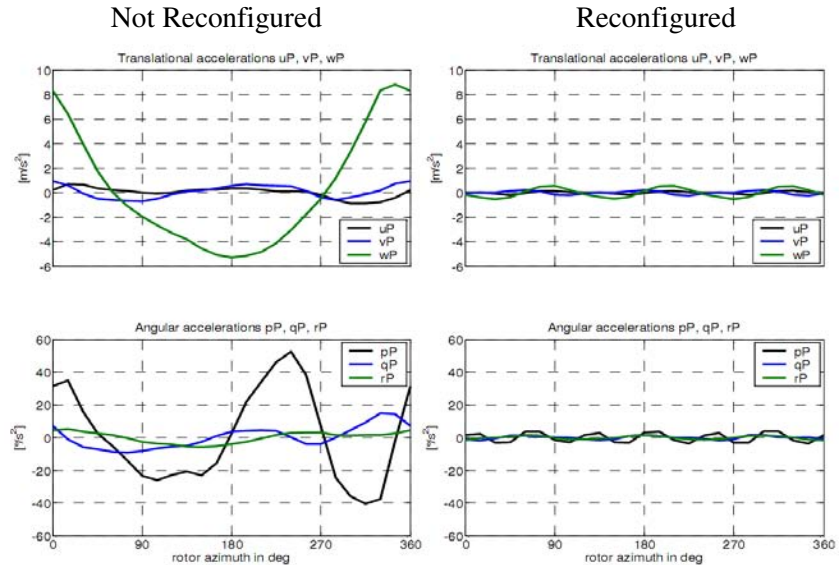


Figure 7-9: Translational and Angular Vehicle Accelerations After Failure at One Rotor Blade Actuator Without and With Control Reconfiguration¹⁹

7.4 Example Mission & GUST Modeling

7.4.1 Example: Police Surveillance Mission

The benefits of the different levels of autonomy are best illustrated through example. Here, a police surveillance mission with an IBC actuator failure event in a noise-sensitive, urban environment is considered. The phases of the mission are described in Figure 7-10. The mission is then carried out as follows:

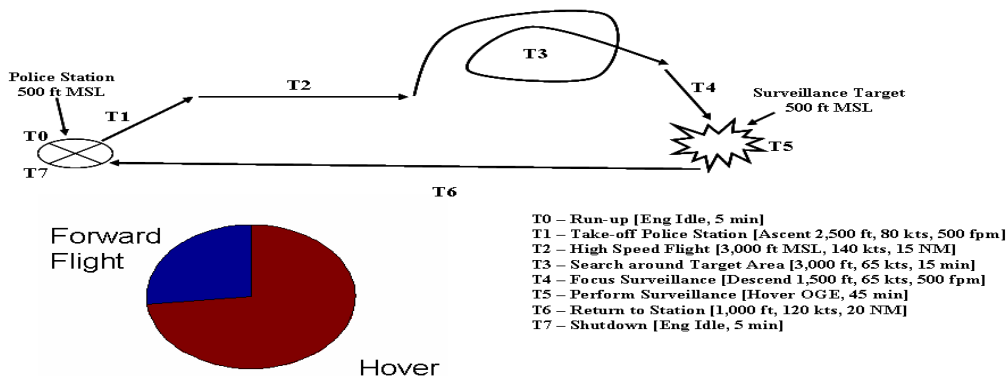


Figure 7-10: Police Surveillance Mission Profile

- *Takeoff and ascent* are performed in semi-autonomous mode for convenience.
- *High-speed dash to target* is then carried out autonomously by setting a target using the Athena control panel. The mission planner is instructed to generate the appropriate control commands to reach the target in minimum time without regard for noise-sensitive areas.
- *Search and descent* maneuvers are done in semi-autonomous mode. This allows more attention to be focused on performing the mission, rather than only flying the vehicle.
- Full autonomy is used while surveying the area during *hover* with the mission planner minimizing fuel consumption, and allowing the pilot to focus on the ground area being surveyed and not on aircraft control.
- Once the mission is completed, *Athena returns to station* under fully autonomous operation to minimize the noise impact on the urban environment. The mission planner decreases main rotor RPM and generates trajectories which avoid pre-designated, noise-sensitive areas.
- *Malfunction of a rotor blade actuator* occurs. The control system detects failure and the OCP reconfigures control of the vehicle from mission planner to fault detection/recovery component. Athena returns to station successfully by individually controlling remaining blades to compensate for the failed actuator.

7.4.2 GUST Modeling

In order to simulate the fully autonomous operation of the vehicle, Athena was modeled using the Georgia Tech UAV Simulation Tool (GUST). GUST is a model of the GTMax, the UAV helicopter used by the Georgia Institute of Technology to demonstrate OCP technologies⁶⁹. The Athena geometric, mass, and inertia parameters were uploaded into the GUST program to properly model the vehicle.

GUST was used to demonstrate the dash and return segments of the police surveillance mission. Figure 7-11 shows a map of the urban environment with a police target and a pre-designated noise-sensitive zone. The flight trajectories generated by the mission planner are shown with arrows. The trajectory to the target is a straight line directly through the noise-sensitive zone since noise concerns were disregarded. However, the return path avoids the noise-sensitive area.

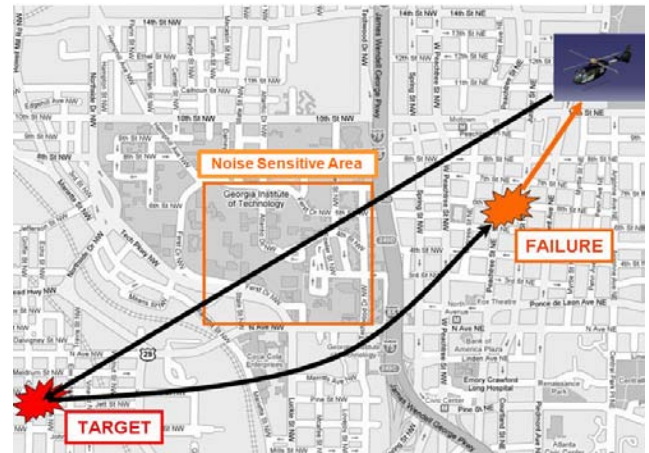


Figure 7-11: Flight Trajectory for Police Surveillance in a Noise-Sensitive Environment

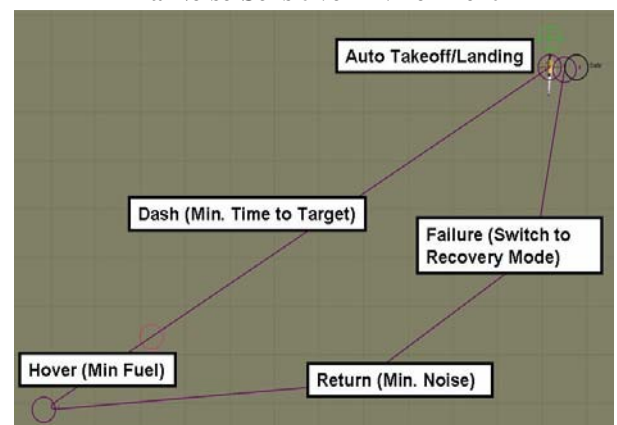


Figure 7-12: Trajectory Simulation in GUST

The mark in the return path designates the aforementioned actuator failure. The remainder of the path represents Athena operating under fault recovery mode.

The trajectory of the vehicle under the autonomous control of the mission planner is simulated in GUST and shown in Figure 7-12. The labels designate the mission phase and corresponding, primary optimization objective.

7.5 Cockpit Display and Interface System

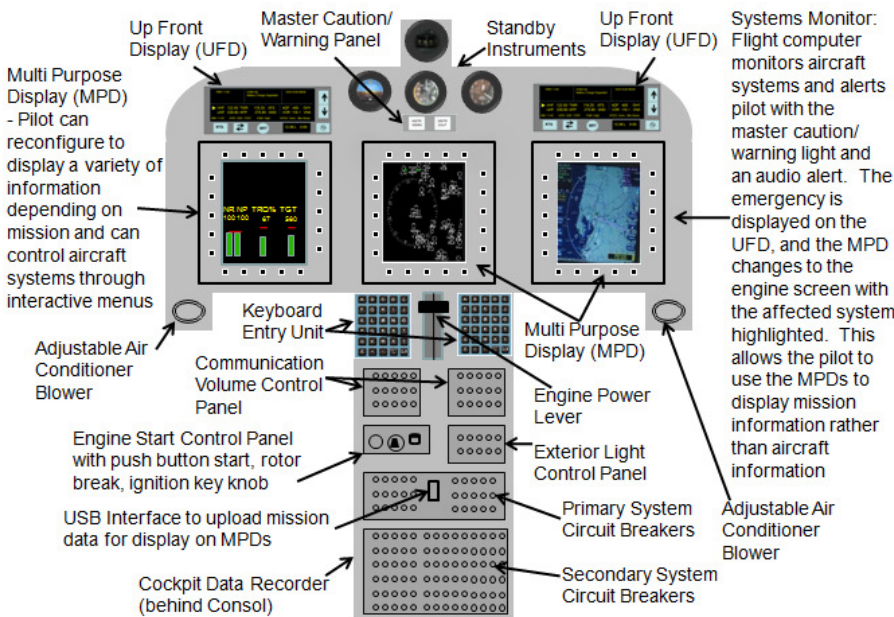


Figure 7-13: Athena Console Layout

Athena’s cockpit display and interface system is based on current full “glass” cockpits such as Boeing’s AH-64D Longbow. The center piece of the Athena’s cockpit console displays are the 7x9 in. (18x23cm) Multipurpose Display Systems (MPD). The screens on the MPDs can be changed by the pilot to show a variety of

information from digitized flight instruments, to aircraft systems, to navigation moving maps and digitized approaches, to communication systems’ statuses. The MPDs are surrounded by Variable Action Buttons (VABs) whose function changes depending on the current information displayed. These VABs allow the pilot to manipulate data and aircraft systems in conjunction with a letter and number keypad located on the center console. Combining the system interface in the displays greatly reduces the number of conventional switches and dials allowing for a smaller console that increases visibility, reduces cost, and provides flexibility for later system upgrades. A diagram of the Athena’s console is shown in Figure 7-13, and the MPD display screen architecture is highlighted in Table 7-2.

Table 7-2: Multipurpose Display (MPD) Architecture

MPD Screen	Flight Screen	Engine Screen	Performance Screen	Navigation Screen	Communication Screen
Information displayed on screen	<ul style="list-style-type: none"> - True Airspeed - Ground Speed - Heading with Fly-to cueing - MSL and AGL altitude - Vertical Speed Indicator - Horizon Ladder - Acceleration Cue - Velocity Cue - Trim Ball and Standard Rate Turn Indicator - Next Waypoint distance and time to intercept - Current Autonomy mode and optimization mode - Current VSM setting 	<ul style="list-style-type: none"> - Engine Torque - Rotor RPM - Engine Temperature - Power Turbine Speed - Free Turbine Speed - Fuel Remaining - Engine Oil Pressure - Fuel Flow Rate - Fuel Type Onboard - *Aircraft will auto-page to this page during a warning or caution advisory and display appropriate emergency procedure* 	<ul style="list-style-type: none"> - Calculated Max hover power available (IGE and OGE) - Current Pressure Altitude - Current Temperature - Calculated Gross Weight and CG - Calculated Max Range Airspeed, Torque, and Fuel Flow - Calculated Max Endurance Airspeed, Torque, and Fuel Flow - Calculated VNE 	<ul style="list-style-type: none"> - Preprogrammed points from aeronautical charts uploaded with data stick - Airports - Radio Navigation Aids - Airspace Markers - Instrument Approach Courses - No-fly and noise sensitive areas - Preprogrammed Mission uploaded with data stick - Route with waypoints - Points of Interest - Boundaries 	<ul style="list-style-type: none"> - Current VHF and UHF Radio Selection with identifier - Current Transponder selection and mode - Current ADF/VOR settings, and Morse Code identifier
Options available on screen through push button actions on the VABs	<ul style="list-style-type: none"> - Heads up display on/off selection - Mission Planner Optimization Mode (MPOM) <ul style="list-style-type: none"> - Full Manual Control - Semi-autonomous - Full-autonomous - Mission Planner Optimization Level (MPOL) <ul style="list-style-type: none"> - Minimum Fuel - Minimum Noise - Trajectory Follow - Target Follow - Minimum Time to Target 	<ul style="list-style-type: none"> - Variable Speed Module (VSM) mode: High/Low - Engine Anti-ice on/off Selection - Cockpit and Cabin Temperature Control - Automated Fuel Flow Check - Stability and Control Augmentation Channels on/off control 	<ul style="list-style-type: none"> - Pilot Weight Entry - Passenger and Cargo Weight Entry - Planning Performance Section for manual entry of pressure altitude, temperature and gross weight 	<ul style="list-style-type: none"> - Current Route Selection - Next Waypoint Selection - Preprogrammed Point database for selecting a fly-to point. - Show page selections for hiding/showing certain information - Map Scale selections - Pan option to freeze screen and pan away from current location - Point entry to enter coordinates of new point in flight 	<ul style="list-style-type: none"> - Preprogrammed list of frequencies and identifiers for airports and agencies loaded via data stick - Transponder setting and mode - ADF/VOR on/off and list preprogrammed settings loaded via data stick - Emergency Selection to tune all radios and transponder to emergency settings

The Athena also features a retractable Heads-Up Display (HUD) that shows critical flight information on a transparent screen in the pilot’s field of view. This greatly reduces pilot workload by allowing the pilot to scan critical flight information while keeping his/her vision outside the helicopter. This also frees up the MPDs to display other information needed for the flight or mission. The HUD is shown in Figure 7-14.

In addition to the HUD, critical information is also displayed on the Up Front Display (UFD). This panel is located below the HUD and above the MPD. It displays all warning, caution, and advisory messages, the current UHF and VHF radio data, the current ADF and VOR data, fuel data, and autonomous mode data. The panel also allows for quick changing between the VHF and UHF radio as well as frequency swapping without having to access the communications page on an MPD. A picture and explanation of the UFD is shown in Figure 7-15.

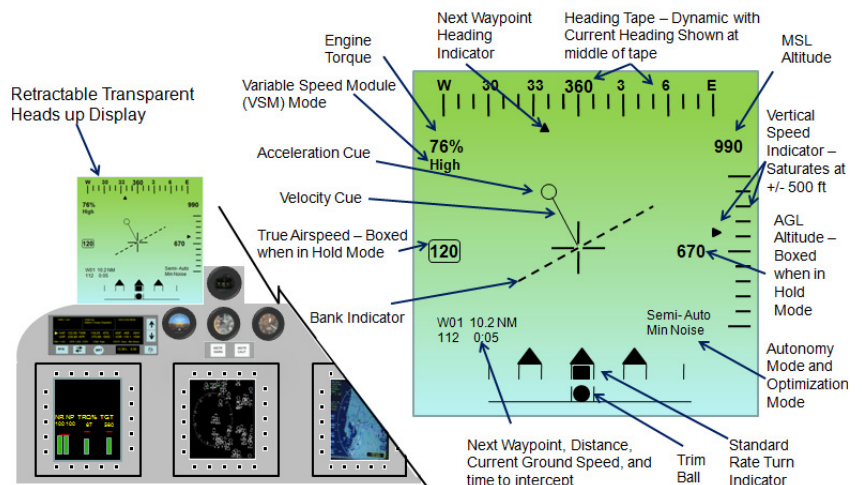


Figure 7-14: Athena Retractable Heads-Up Display (HUD)

A final method that Athena uses to reduce pilot workload and increase safety is a Health Usage and Monitoring System (HUMS) that monitors all aircraft systems and alerts the pilot of any deviation. This allows the MPDs to display mission information and frees the pilot to concentrate on tasks other than monitoring aircraft systems. In the event of an emergency, the master caution or warning is illuminated and accompanied by an audible voice alert. The emergency is displayed in the UFD and the aircraft will switch the MPD to display engine information with the affected system highlighted. It will also display the appropriate emergency procedure on the center MPD.

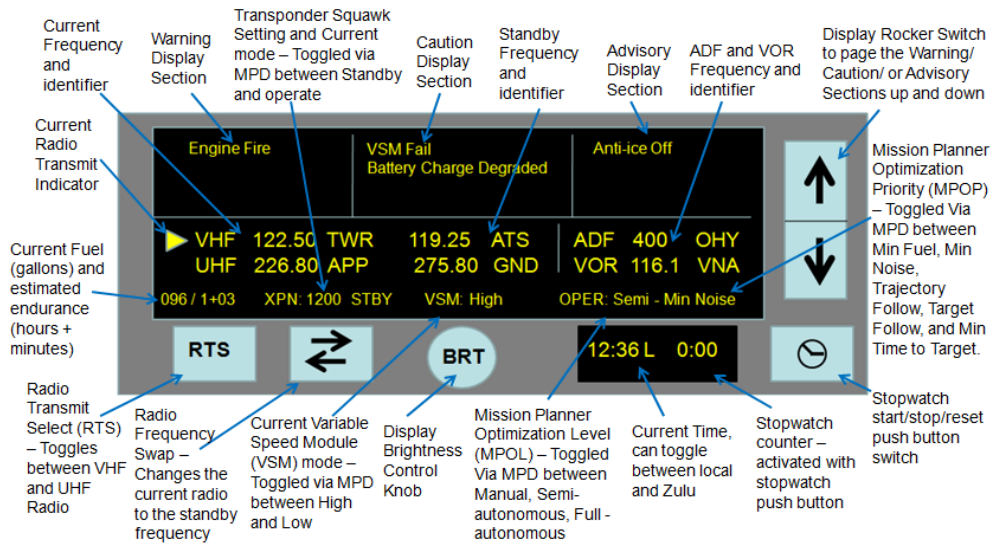


Figure 7-15: Athena Up Front Display (UFD)

7.5.1 Cyclic, Collective, Pedal System

The Athena's control system is similar in design to those of a conventional helicopter. The cyclic and collective have switches and controls for critical systems so the pilot can manipulate aircraft systems without having to take his/her hands off the controls. Because of the aircraft's fly-by-wire design, the controls also include a force feedback system, through the use of springs, to simulate the control loads of normal mechanical rigging. In addition, to reduce pilot work load, the Athena has a force trim feature on the cyclic and pedals. This system holds the controls in a specific pilot-selected position, though the use of magnetic breaks, until the pilot actions the force trim release switch to reposition the controls to another attitude. The collective is held in place with a 1g spring and an adjustable friction lock. This reduces pilot fatigue and provides a limited hands-off capability. Finally, the Athena has a stick shaker installed on the collective to vibrate when the pilot approaches an aircraft limit. This helps to alert the pilot of the approaching condition and informs him/her the aircraft's envelope protection system will soon engage.

8 PERFORMANCE, STABILITY AND HANDLING QUALITIES

8.1 Athena's Performance

Athena meets or exceeds all the performance and weight requirements of the RFP as shown in Table 8-1. Athena's performance charts are shown in Figures 8-1 through 8-7. Figure 8-1 is a plot of power required and maximum rate of climb versus airspeed. Figures 8-2 and 8-3 respectively show specific range and endurance versus airspeed. Those figures show the increase in both specific range and specific endurance at 92% rotor RPM. HOGE altitude versus gross weight is shown in Figure 8-4. Figures 8-5 and 8-6 respectively show the variation of Athena's range and endurance with payload. Figure 8-6 shows the height-velocity diagram, which indicates the combinations of altitudes and velocities that should be avoided for successful autorotation.

Table 8-1: Attained Performance and Weight Specifications

	RFP Requirement	Athena's Capability
Maximum Range	300 NM	390 NM
	556 km	722 km
Payload	1100 lbs	1288 lbs
	499 kg	584.2 kg
Cruise speed	Minimum: 100 kts Target: 120 kts	119 kts

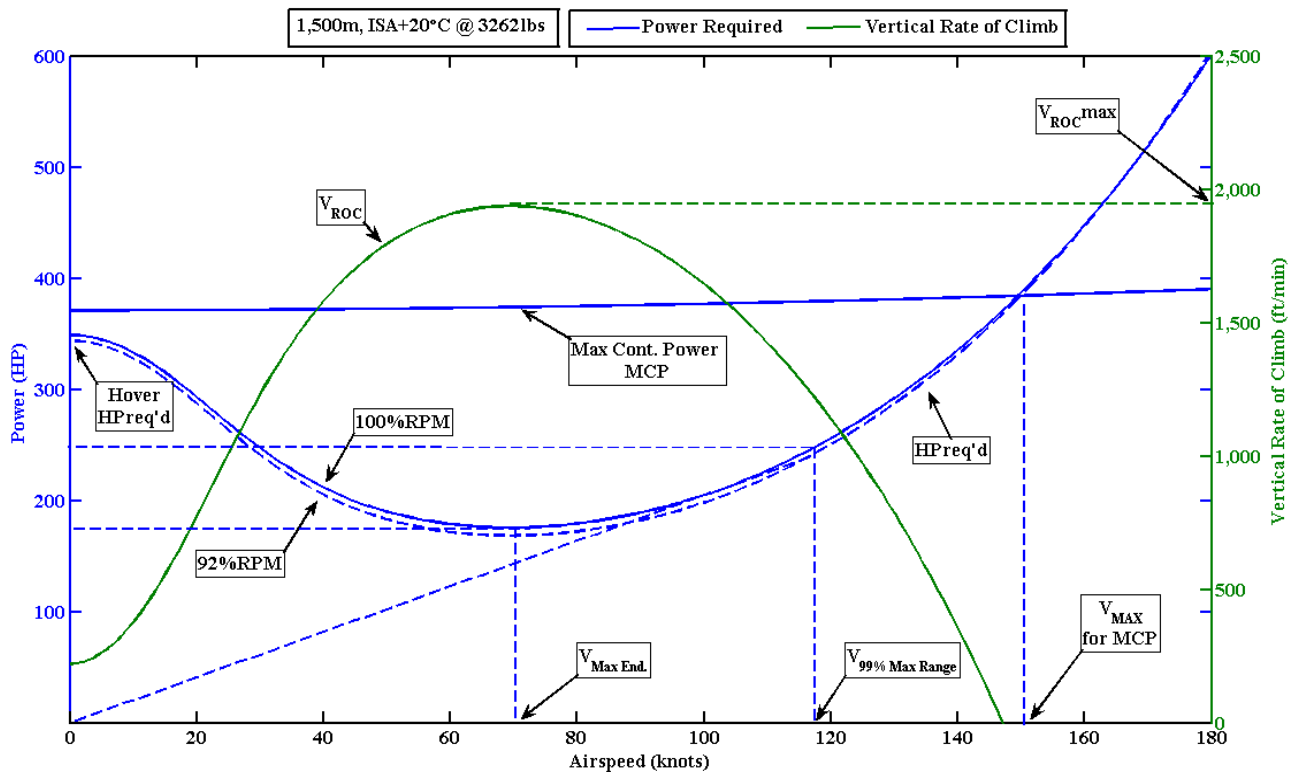


Figure 8-1: Power Required and Rate of Climb vs. Airspeed

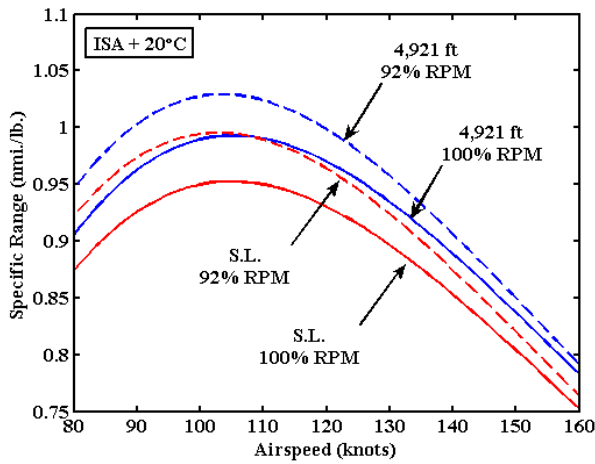


Figure 8-2: Specific Range vs. Airspeed

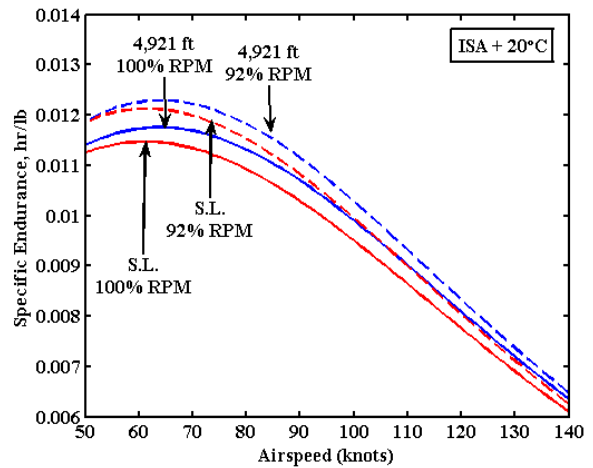


Figure 8-3: Specific Endurance vs. Airspeed

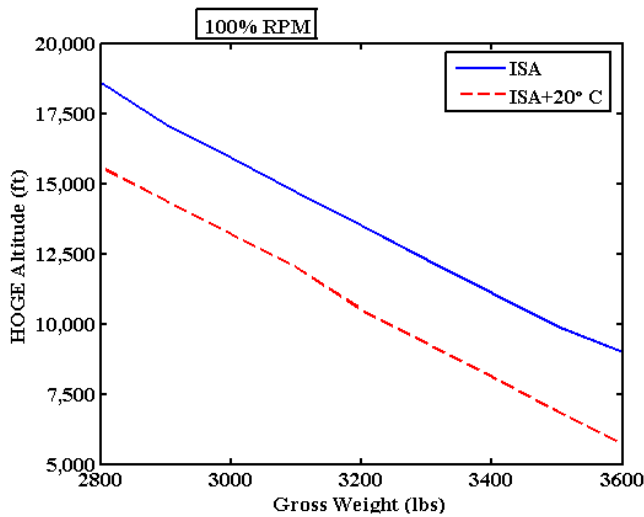


Figure 8-4: HOGE Altitude vs. Weight

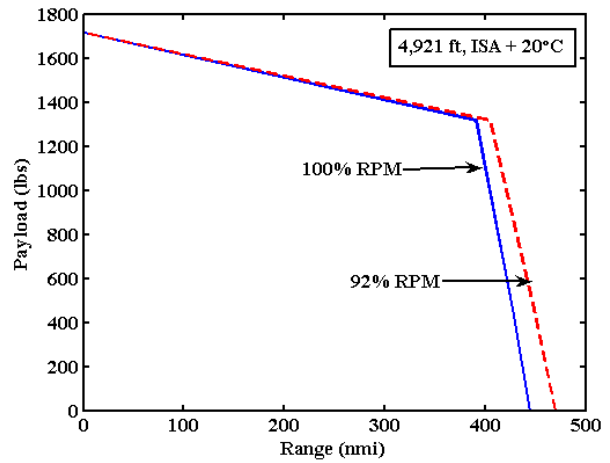


Figure 8-5: Payload vs. Range

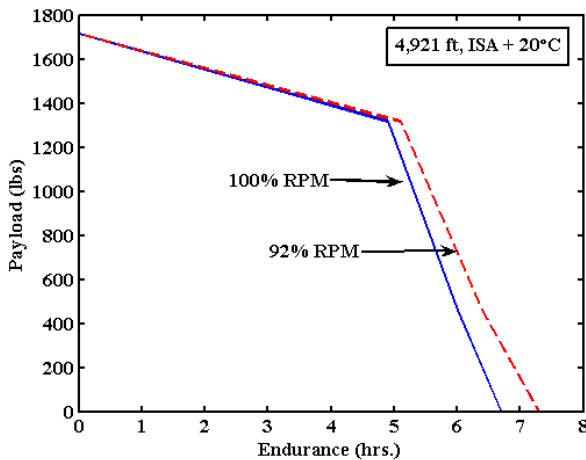


Figure 8-6: Endurance vs. Payload

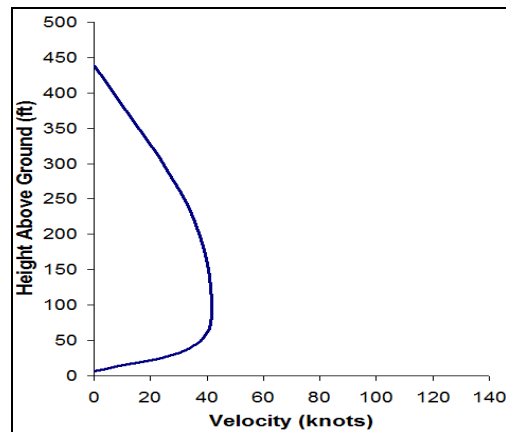


Figure 8-7: Height-Velocity Diagram

8.1.1 Performance Comparison

Figure 8-8 shows the estimated power required curves for the MD 500E and the EC-120B. Table 8-2 summarizes critical performance parameters and compares them with the EC-120 and the MD-500. It is noteworthy that each vehicle’s performance is measured at its maximum gross weight, the EC-120B is the heaviest (3,781 lbs), and that the MD 500E is the lightest (3,000 lbs). However the Athena requires less power and consumes less fuel than either vehicle despite weighing over 250 lbs more than the MD-500E.

Table 8-2: Comparison of Athena Performance with MD 500 and EC 120

4,921 ft ISA+20°C	Athena	EC-120	MD-500
Figure of Merit	0.84	0.78	0.84
Power Loading (lbs / HP)	9.35	8.59	8.8
Rotor L/De (V = 120 kts)	10.5	8.61	9.4
Best Endurance Speed (kts)	67	69	66
99% Best Range Speed (kts)	117	116	114
Range (nmi)	390.8	369.4	266.3
Endurance (hrs.)	4.9	5.2	3.4
Hourly Fuel Consumption (lbs/hr)	165	208	170

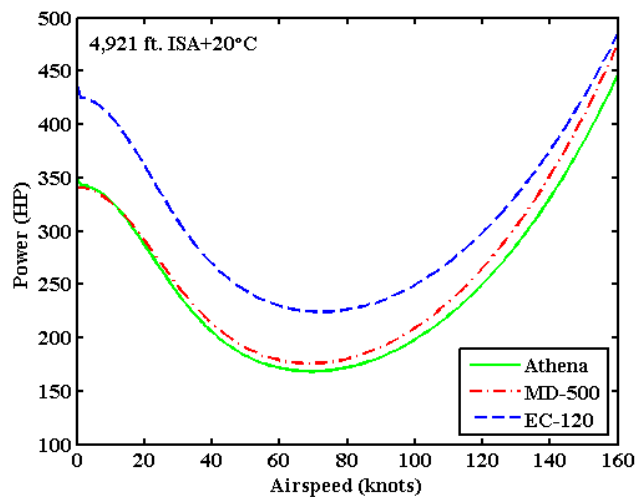


Figure 8-8: Power vs. Airspeed

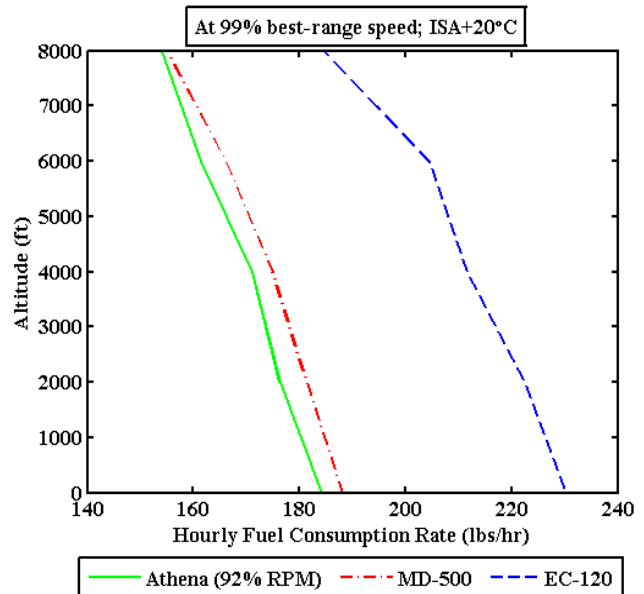


Figure 8-9: Hourly Fuel Consumption vs. Altitude

8.2 FLIGHTLAB Model

The flight dynamics model for the Athena was built and analyzed using FLIGHTLAB.¹⁵ Using the software’s selective fidelity capability, preliminary design studies regarding trim condition, control limits, cg envelope and fuselage loads were estimated through virtual simulations.

FLIGHTLAB is a physics based dynamic modeling simulation environment that combines the capabilities of a time advancing scheme, using first and second order states, and a state space approach. The program uses a blade element model for the main rotor that divides the blades into sections, estimates the loads on each section and then numerically integrates the sections over radial and azimuth stations. Nonlinear aerodynamic properties are introduced as table look-ups while the inflow is modeled using Peters-He three state inflow model (a reduced extension of Generalized Dynamic Wake Theory).⁷⁰ Each empennage is modeled with aerodynamic strips, one for the each component. The fuselage is also modeled similarly. In this analysis, the BO-105 fuselage aerodynamics data⁷¹ was digitized and scaled to match the Athena. The mass and inertial properties for the blade sections and the fuselage were modeled as lumped masses. Geometric properties and variations were handled through transformation matrices. The FLIGHTLAB model is summarized in Figure 8-10.

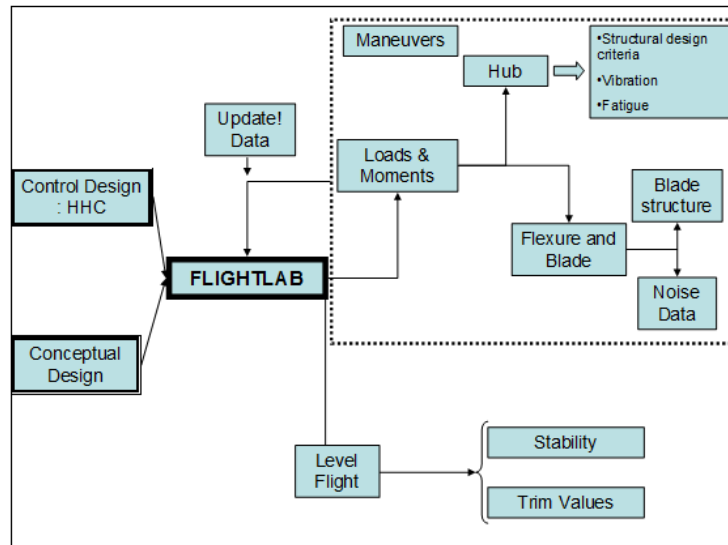


Figure 8-10: FLIGHTLAB Schematic Through Design Process

8.3 FLIGHTLAB Analysis and Results

8.3.1 Trim Variables

Main rotor collective, lateral/longitudinal cyclic and tail rotor collective are plotted below, in addition two pseudo control variables pitch and roll attitude of the vehicle are also shown. These plots show that the main and tail rotors avoid stall conditions for normal flight in a variety of CG locations.

In addition, BO-105 FLIGHTLAB model and Flight Test Data⁷² Are shown in the graphs on the right in order to demonstrate the fidelity of the estimations and validate the FLIGHTLAB data. Trim analysis in forward flight and high-g maneuver analysis were also performed using 5000 ft pressure altitude hot day conditions.

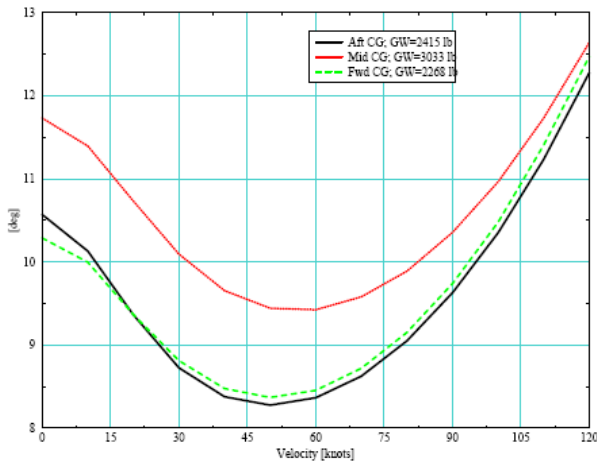


Figure 8-11: Athena MR Collective Position

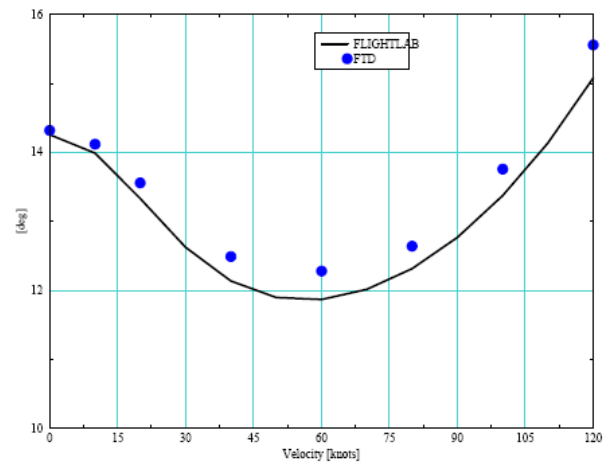


Figure 8-12: BO-105MR Collective Position

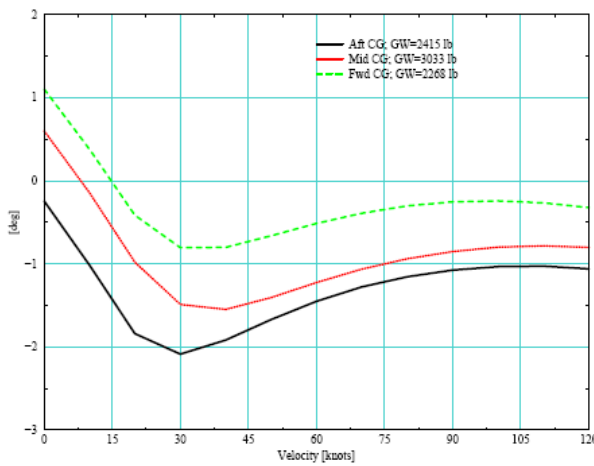


Figure 8-13: Athena MR Lateral Cyclic

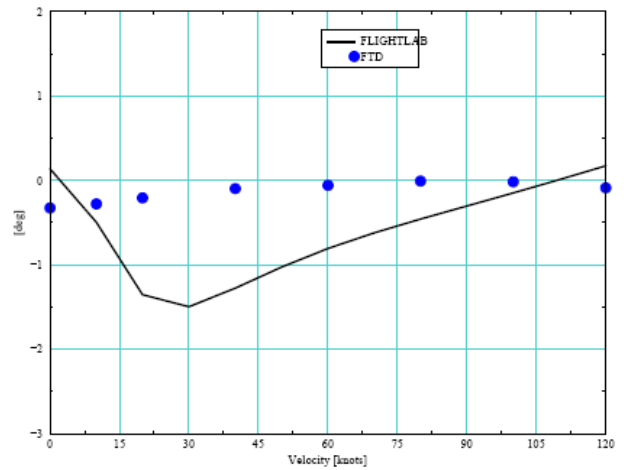


Figure 8-14: BO-105 MR Lateral Cyclic

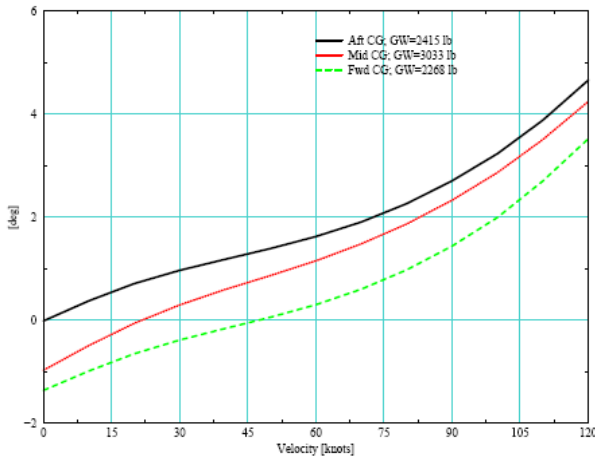


Figure 8-15: Athena MR Longitudinal Cyclic

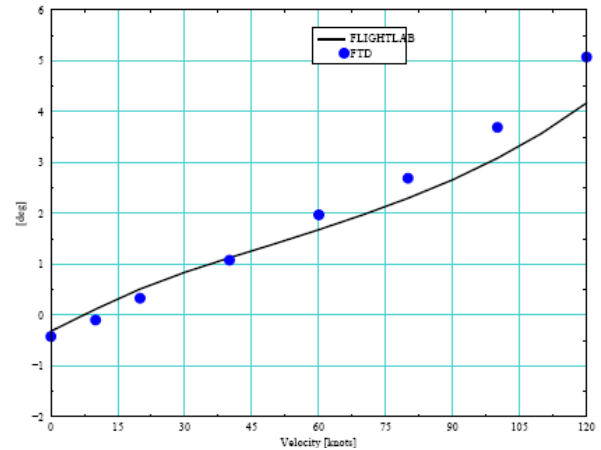


Figure 8-16: BO-105 MR Longitudinal Cyclic

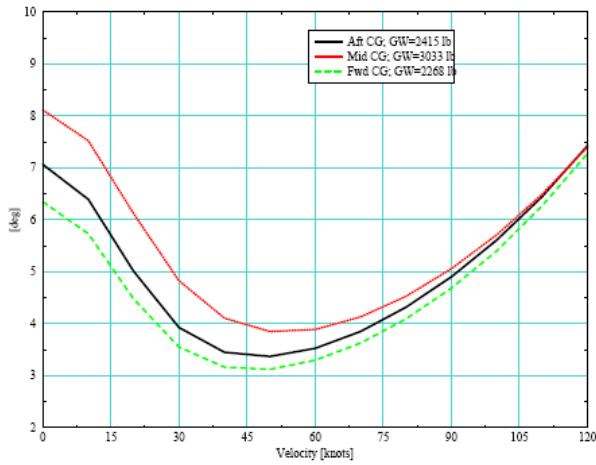


Figure 8-17: TR Collective Position

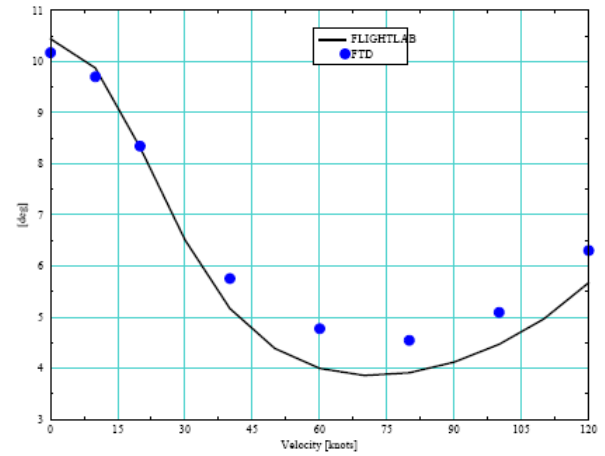


Figure 8-18: BO-105 TR Collective Position

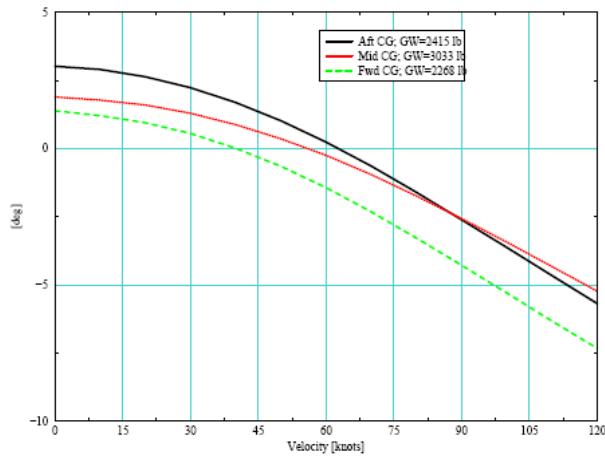


Figure 8-19: Athena Body Pitch Attitude

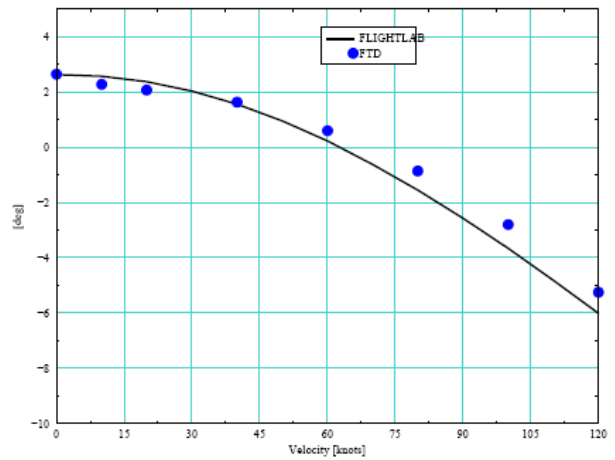


Figure 8-20: BO-105 Body Pitch Attitude

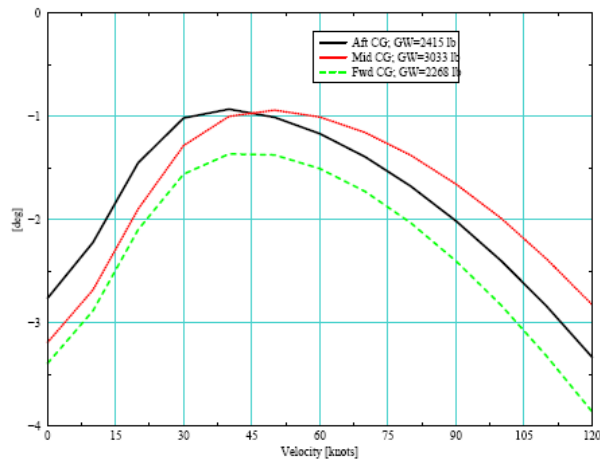


Figure 8-21: Athena Body Roll Attitude

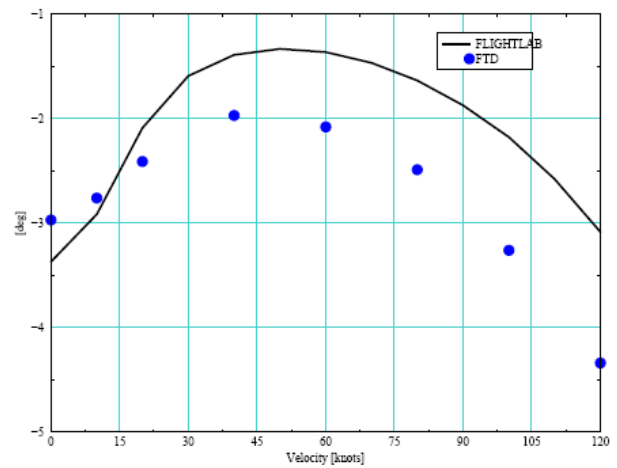


Figure 8-22: BO-105 Body Roll Attitude

8.3.2 High-g Maneuvers

An analysis of high-g maneuvers was completed to show the control limits and limit hub loads. The initial analysis was done on a steady state maneuver to determine the maximum allowable steady g load on the aircraft. The results for level flight at 65 knots are depicted in Figure 8-23. In all cases, it was found that the Athena could not achieve g loads greater than two. The hub loads and moment variation over one cycle are depicted in Figure 8-24. This Figure shows the high vibratory loads at 4/rev frequency. The Athena is capable of transient g loading up to 1140 lbf (3.46g) for the main rotor and 398 lbf for the tail rotor. These forces are for maneuvers such as pull-ups or any other maneuver where the g load is not applied for a significant time.

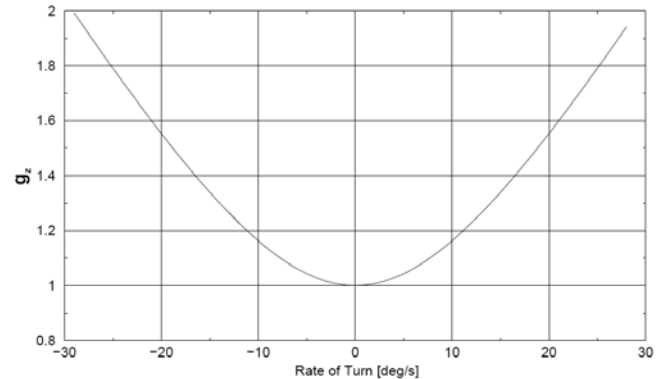


Figure 8-23: Steady Turn Load Factor

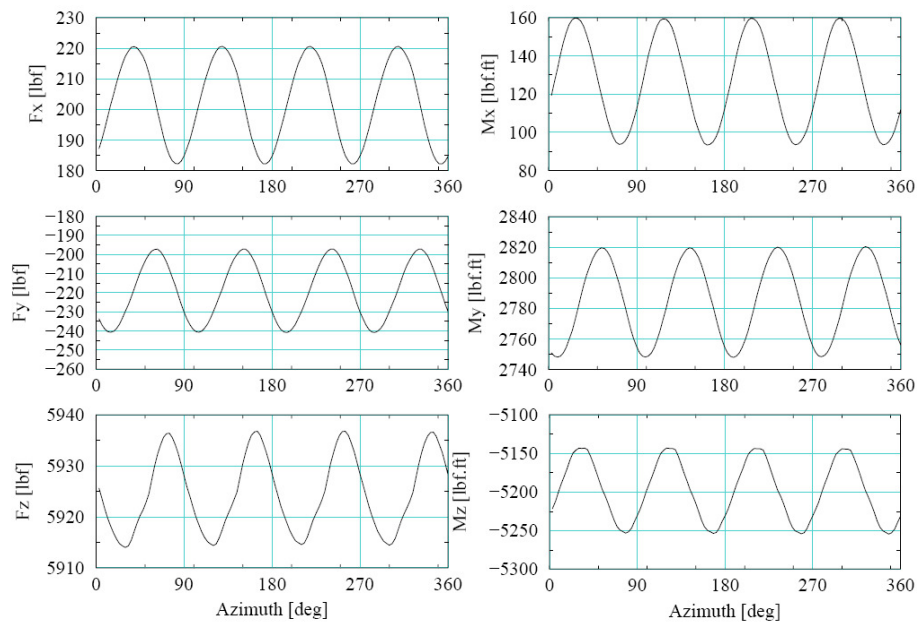


Figure 8-24: Hub Forces and Moments, High-g Maneuver

8.3.3 Flight Loads and Moments

In order to validate the structural strength of the main rotors and hub, large magnitude flight loads were calculated. In this study, the steady flight loads and moments on the main rotor hub were computed and decomposed into a steady average component and a harmonic component. It was found that the steady loads were well below the fatigue limit, however, the large frequency loads had the potential

to cause fatigue damage and force the replacement of blades faster than the proposed time before overhaul (TBO) life. However, the IBC HHC will dampen these vibrations to an acceptable level.

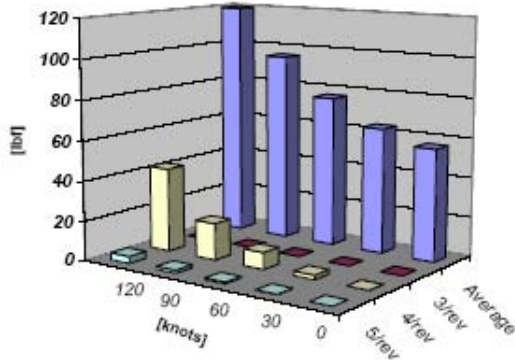


Figure 8-25: MR Hub Horizontal Force

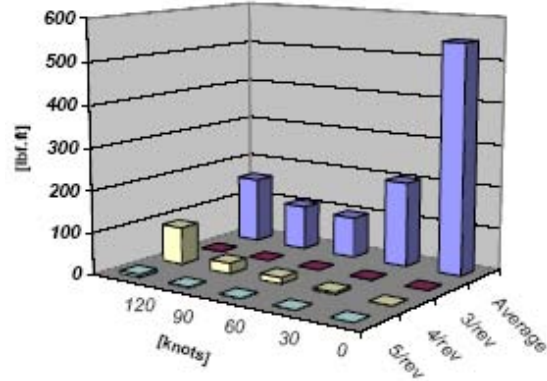


Figure 8-26: MR Hub Rolling Moment

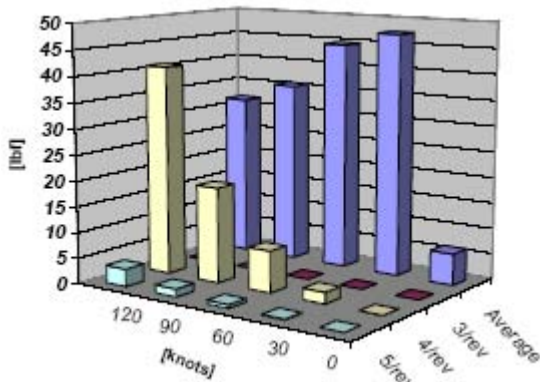


Figure 8-27: MR Hub Side Force

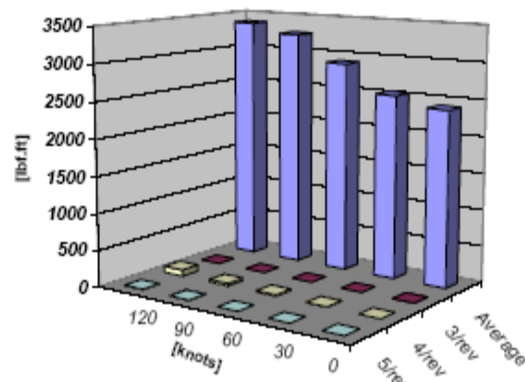


Figure 8-28: MR Hub Pitching Moment

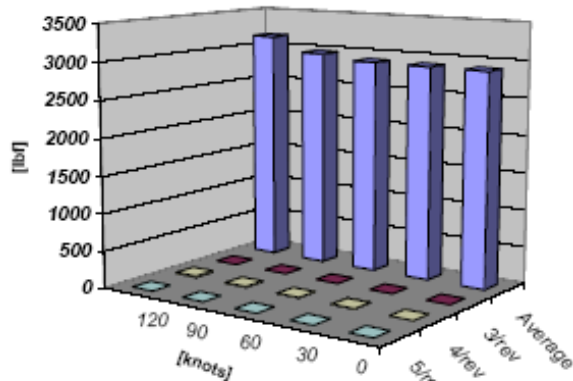


Figure 8-29: MR Hub Normal Force

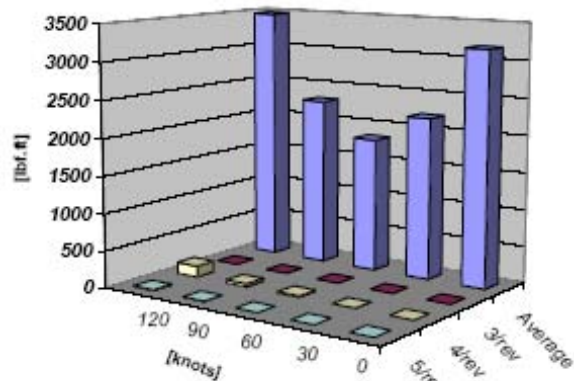


Figure 8-30: MR Hub Torque

8.3.4 Dynamic Stability and Handling Qualities

To determine the Athena's stability, a FLIGHTLAB model was created and linearized about two trim conditions; hover and 100 knots forward flight. It is important to note that this analysis was carried out without any augmentation systems, and therefore shows Athena's pure vehicle dynamics. Results show that even for the baseline case, only a dutch roll mode is observed to be unstable, and would be easily corrected with the Athena's stability augmentation system (SAS).

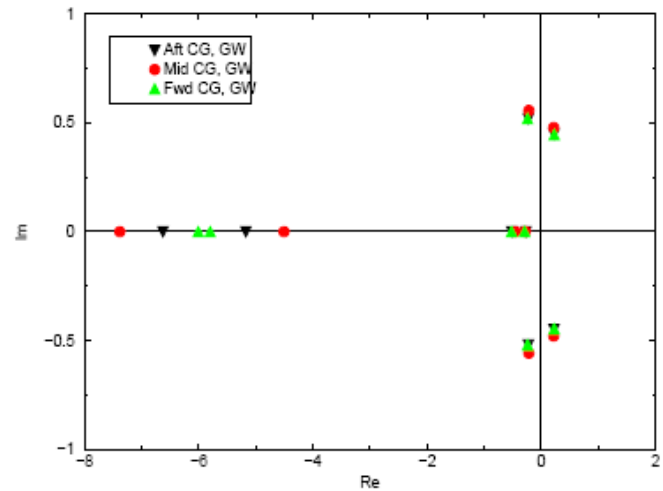


Figure 8-31: Root Locus at a Hover

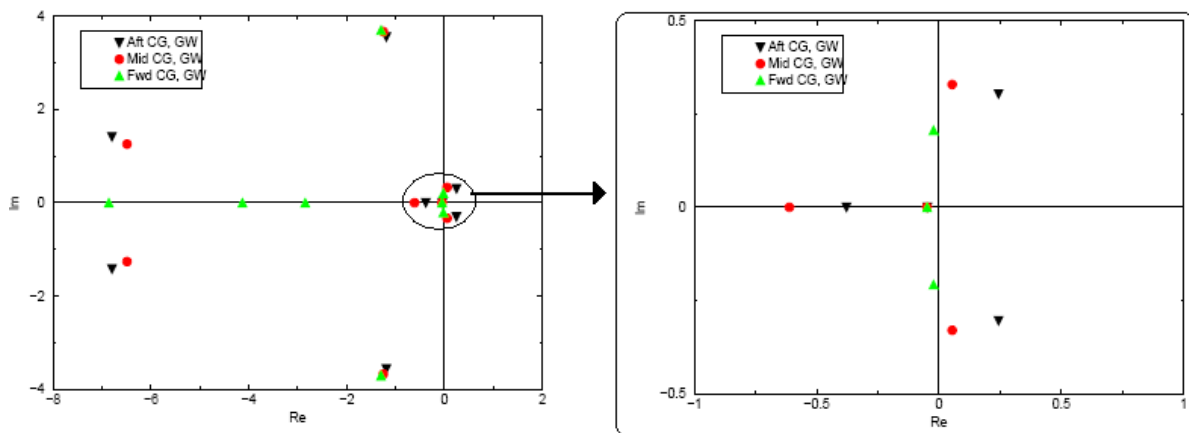


Figure 8-32: Root Locus at 100 knots Forward Flight

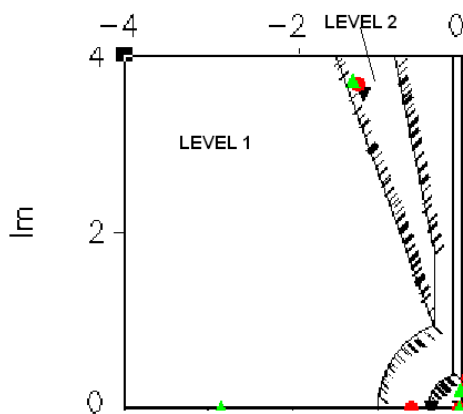


Figure 8-33: Handling Qualities in Forward Flight – Dutch Roll Mode

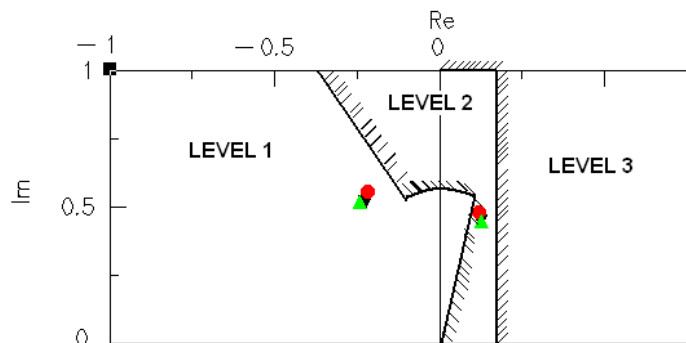


Figure 8-34: Handling Qualities in Hover – Pitch and Roll Oscillations

In the hover case, for the unaugmented helicopter, both pitch and roll oscillations may degrade the handling qualities due to high frequency or unstable roots. This baseline, un augmented, model is compared to the handling qualities requirements in Figure 8-33 and Figure 8-34. The Athena with no SAS is either in Level I or II for all CG arrangements. With the adaptive SAS controller and FMC, the Athena will be able to improve all handling qualities to Level I status.

9 STRUCTURAL DESIGN

Using Dassault Systems’ state-of-the-art CATIA CAD, SIMULIA CAE, and DELMIA CAM software, design modifications were rapidly incorporated based on the results of the multi-disciplinary analysis described in previous sections. The design was populated into ENOVIA PLM software to provide data access for the entire team. A detailed weight and balance analysis was conducted throughout the design modification process. Structural design trade studies were completed to determine the most energy efficient solution over its lifecycle.

9.1 Vehicle Weight and Balance

9.1.1 Weight and Balance Requirements

The weight and center of gravity limits are provided by FAR 27.25 and 27.27 respectively. The Athena’s design maximum weight limit was determined using a component weight build-up. The CG travel range limit was determined by the most forward and aft longitudinal positions at which the desired handling qualities can be achieved.

9.1.2 Weight Analysis

Initial weight estimations were established using weight build-up equations from *Helicopter Performance, Stability, and Control*.³⁶ More detailed component weight analysis was conducted using values from the RFP, CIRADS and CATIA. Table 9-1 provides a summary of the component weight groups. A complete MIL-STD-1374 Weight Statement is included in Appendix A.

Table 9-1: Component Weight Breakdown

Component Group	Weight (lb)	Weight (kg)	Source
ROTOR & HUB	143.2	64.9	CIRADS
ANTI-TORQUE	33.2	15.1	CIRADS
FUSELAGE	273.9	124.2	CIRADS
LANDING GEAR	72.1	32.7	CIRADS
PROPULSION	176.4	80.0	ANALYSIS
DRIVE SYSTEM	132.8	60.2	ANALYSIS
FLIGHT CONTROL	331.3	150.3	CIRADS
NACELLES	10.6	4.8	CIRADS
INSTRUMENTS	15.5	7.0	CIRADS
ELECTRICAL	135.0	61.2	CIRADS
EQUIPMENT	139.6	63.3	CIRADS
VARIATION	12.8	5.8	CIRADS
EMPTY WEIGHT	1476.3	669.6	
CREW	220.5	100.0	RFP
PAYLOAD	1102.3	500.0	RFP
FUEL	389.3	176.6	CIRADS
TOTAL USEFUL LOAD	1712.1	776.6	
CONTINGENCY	73.8	33.5	RFP
GROSS WEIGHT	3262.2	1479.7	

9.1.3 Center of Gravity Analysis

Several tools were implemented to ensure the Athena met FAR 27.27 center of gravity limit requirements. An Excel spreadsheet was developed that allowed component weights and locations to be assigned and then determined the CG location. Using a Matlab script, trim analysis were run for extreme flight conditions, such as high hover out of ground effect, to assure trim could be achieved for each CG location. The process of modifying the layout and running trim analysis was repeated until a desired CG travel range was achieved. Figure 9-1 depicts the calculated longitudinal CG travel for the Athena.

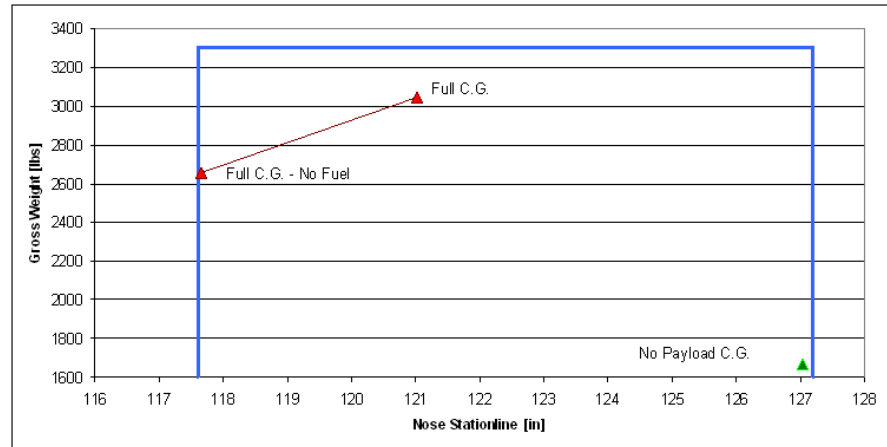


Figure 9-1: Center of Gravity Envelope

The CG results were further verified by a detailed CATIA model. The CATIA model was used to assign component weights from preliminary calculations or material properties. The complete aircraft model allowed for detailed aircraft weight, CG location, and mass moment of inertia calculations and were exported into the FLIGHTLAB model to assure the desired handling qualities were met.

9.2 Structural Design Criteria

The structural design criteria were primarily based on FAR 27 Subpart C and supplemented by ADS-29. The maximum load factor envelope for the Athena was constructed with a load factor ranging from a positive limit of 3.5 to a negative limit of 1.0 in accordance with FAR 27.337. Although these requirements can be reduced to positive 2.0 to negative 0.5 if higher loadings are extremely remote, the Athena uses the higher load factor range due to its multiple users and missions. The design maximum level flight speed, V_H , was 120 knots at maximum load factor based on RFP. The design limit flight speed, V_{DL} , was calculated using a factor of $1.2 V_H$, a typical ratio for utility helicopters. The never-exceed speed, V_{NE} , was assumed to be equal to V_{DL} for preliminary design purposes. The minimum and maximum speed controllability of 35 knots and $1.11 V_{NE}$ was in accordance with FAR 27.337. A conservative fatigue envelope was created using Advisory Circular 20-95 to define reasonable limits for

routine usage. The loads generated at the edge of the fatigue envelope are considered to occur six times per flight hour.

In developing the V-n diagram depicted in Figure 9-2, the following flight maneuvers were also addressed in accordance with FAR 27.337; symmetric pull-up ($n=3.5$), 1-g dive ($n=-1.0$), level flight, takeoff and climb, hover, and rolling pull-up maneuver. The loads for these maneuvers were generated in FLIGHTLAB for use in airframe analysis.

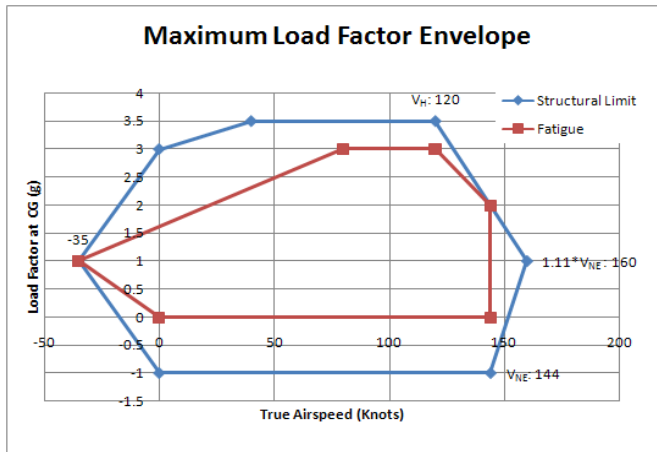


Figure 9-2: Maximum Load Factor Envelope

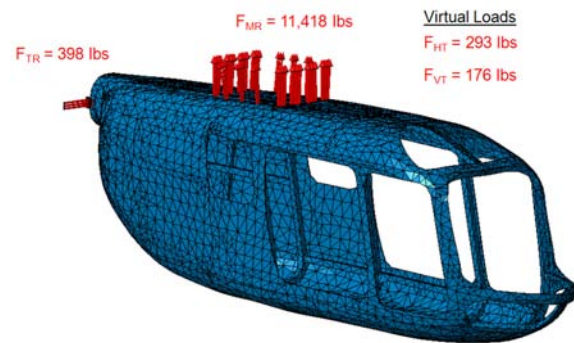


Figure 9-3: 3.5g Loading Conditions

9.3 Fuselage Design

9.3.1 Configuration Selection

An initial trade study was conducted to decide between a full metal, hybrid metal/composite, or full composite fuselage design. This trade study took into account the full life cycle energy consumption. The main advantages of incorporating a metal design are low production cost and ease of disposal through recycling; however, the weight savings, improved reliability, and flexibility of composite materials, along with emerging technological developments in the areas of manufacturing and disposal, supported using an all composite fuselage design.

9.3.2 Composite Structure

Composite material selection for structural parts was based upon the manufacturing and operating requirements. The fuselage is comprised of a Kevlar/epoxy skin and graphite epoxy bulkheads and stringers with a high density Rohacell foam core. A $(45/-45/45/-45/0)_s$ skin layup and $(45/-45/90)_s$ stringer layup ensures that plies in all structural elements are oriented in at least three directions for

laminate stability. Pitch and roll moments as well as lift are transferred into vertical forces in the main bulkheads near the transmission and sheared into the skins. The bulkheads and stringers carry crash loads in the event of a roll over.

The subfloor was designed to provide maximum protection to occupants. The lower fuselage has a frangible carbon/epoxy skin supported by an energy absorbing Rohacell foam core. The stiff supporting subfloor incorporates a lightweight honeycomb sandwich construction that provides further occupant protection.

The tail boom is a filament wound graphite/epoxy fully monocoque structure. The horizontal stabilizer and Fenestron are made of carbon and Kevlar skins with Rohacell support for the duct and vertical fin. The engine support and firewall are constructed from fiberglass with bismaleimide resin due to its favorable high temperature characteristics.

Biocomposite materials, such as flax and hemp, were considered because the materials can be incinerated without harmful residues. The technology readiness levels for these materials will not be mature enough to incorporate into structural components; however, the material can be phased into non-structural members such as interior cabin panels, access panels, and fairings.

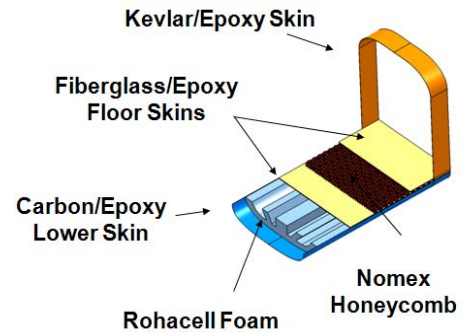


Figure 9-4: Crashworthy Subfloor Design

9.3.3 Fuselage Analysis

Utilizing ABAQUS for CATIA, a finite element model was created for preliminary analysis. Initial static cases were run to determine critical load paths. This analysis was done to simulate a 3.5g maneuver with loads applied from the main rotor, tail rotor, horizontal tail, and vertical tail. The model lends itself to continued static and dynamic testing. Loads placed on the global FEA modal substantiated local fittings and other detailed part analysis.

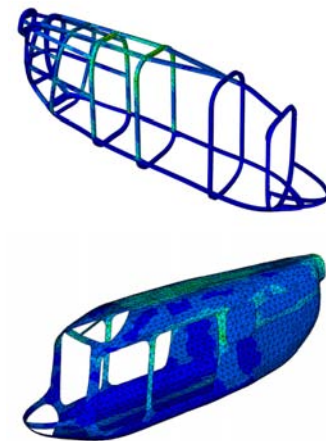


Figure 9-5: Static Fuselage Analysis

9.3.4 Fatigue Monitoring

An efficient maintenance schedule can be prescribed through the flight parameter monitoring system used in the open control architecture. For direct fatigue monitoring, strain gauges will be placed at the critical load locations. An individual aircraft maintenance schedule will be implemented based on

the usage spectrum rather than only by flight hours.. This upfront consideration will reduce the cost of unscheduled repairs.

9.3.5 Manufacturing

A modular design approach was taken in designing the aircraft manufacturing. Composite parts such as the upper fuselage halves, subfloor, and tail boom, will be cured and bonded on final assembly. The rotor head assembly process was modeled in DELMIA CAM. By implementing this tool, energy savings was crated through a reduction in time to market, reduced design changes and retooling, increased communication between product and process engineers,a reduced need for prototypes, and an optimized manufacturing process.

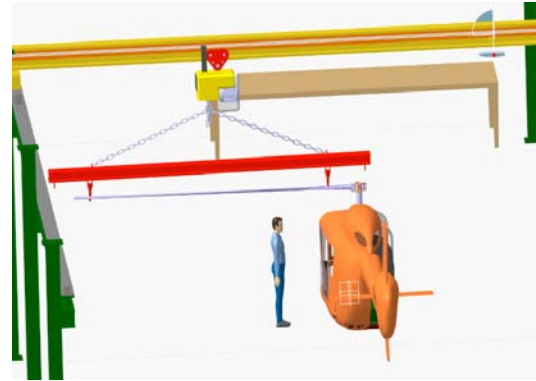


Figure 9-6: DELMIA Assembly

9.4 Landing Gear

9.4.1 Configuration

A comprehensive trade study between skid and retractable and non-retractable wheeled landing gear systems was conducted before selecting the Athena’s configuration. A retractable wheeled landing gear system has the advantage of reducing drag; however, the moderate forward flight speed and performance requirements of the Athena did not to justify the added complexity and weight of a retractable design. The skid landing gear is a simpler, lighter solution that provides energy savings through ease of manufacture and overall reduced power consumption.

9.4.2 Dimensions and Materials

A trade study between structural steel, naval brass, tungsten carbide, aluminum, and composite landing gear was conducted. Structural steel was selected because of its favorable fatigue and energy absorption characteristics. The skid landing gear was designed using hollow circular skid tubes and cross beams. The beams had an outer diameter of 3 in (7.62 cm) and inner diameter of 2.6 in (6.6 cm). The length, width, and height of the landing gear were based upon the structural layout and configuration of the aircraft and desired landing attitude. To reduce drag, lightweight composite fairings were incorporated into the design. The inherent damping of the Hanson ideal rotor also eliminated the need for landing gear dampers.

9.4.3 Limit Drop Test

A finite element analysis was conducted using Abaqus CAE. The skid and cross beams were modeled as beam elements. A yield strength and ultimate tensile strength of 310 MPa and 517 MPa, respectively with a Poisson ratio of 0.33 were assigned to the landing gear. The ground was modeled as a shell with a contact friction coefficient of 0.5. Using four rigid beam connectors, the landing gear was attached to a rigid node with assigned mass and inertial properties from the CATIA model.

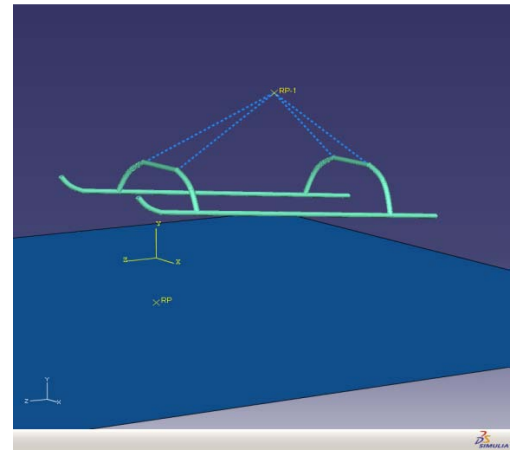


Figure 9-7: Landing Gear Visualization Model

To satisfy the multi-role operation requirements, a landing gear drop test analysis was conducted meeting both civilian FAR 27.725 requirements and US military requirements. Analysis cases were completed for several landing conditions as shown in Table 9-2. All cases were conducted at a drop height of 27 in (0.69m) corresponding to an impact at 12 ft/s (3.675m/s). This is in accordance with the most stringent standards found in Naval Air System document AR-56. Based on the analysis, the landing gear exceeds the federal requirements in all landing gear conditions. The maximum observed stress approach yield without rupture; a desired characteristic of a skid landing gear under limit loads.

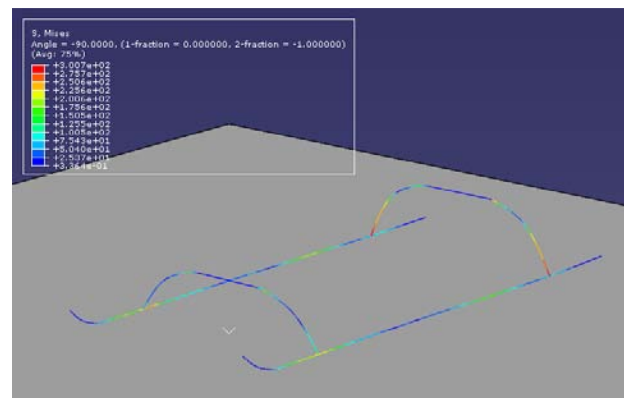


Figure 9-8: Level Reserve Drop Test Analysis

Table 9-2: Drop Test Results

Landing Condition	Maximum Observed Stress	Yield Strength	Ultimate Strength
Level	300 MPa	310 MPa	517 MPa
Nose First	316 MPa	310 MPa	517 MPa
Aft First	314 MPa	310 MPa	517 MPa
Single Skid Rolling	313 MPa	310 MPa	517 MPa

9.5 Cabin Configuration and Layout

The fuselage and cabin configuration were designed concurrently by using CATIA. A baseline model was created, and the design was continuously improved. One of the improvements made was to incorporate an innovative 2-2-1 seating arrangement as shown in Figure 9-10. This allowed for a narrow fuselage body resulting in structural weight savings, reduction in parasite and vertical drag, and increased lateral maneuverability. The fuselage modifications were made with consideration to passenger and crew

comfort. This reduction in frontal area resulted in the equivalent flat plate drag shown in Table 9-3. Drag was also reduced through the design of fairings on the main skid assembly, the rotor blade torque tubes, and the hub fairing over the EMAs as seen in the figures at the beginning of the report.

The cabin shown in Figure 9-9 was designed to accommodate the 5th percentile female to the 95th percentile male. Anthropometric survey data was used to create an ideal cabin. The crew seat design allows for horizontal and vertical adjustment. Pilot's point-of-view images were generated to check for visual cues.

Table 9-3 Athena Equivalent Flat Plate Area

Component	Equivalent Flat Plate Area
Fuselage & Engine Nacelles	1.2 ft ² / 0.37 m ²
Rotor Hub	1.6 ft ² / 0.49 m ²
Landing Gear	0.9 ft ² / 0.27 m ²
Empennage	0.5 ft ² / 0.15 m ²
Miscellaneous	0.8 ft ² / 0.24 m ²
Total	5.0 ft² / 1.52 m²



Figure 9-9: Cabin Layout

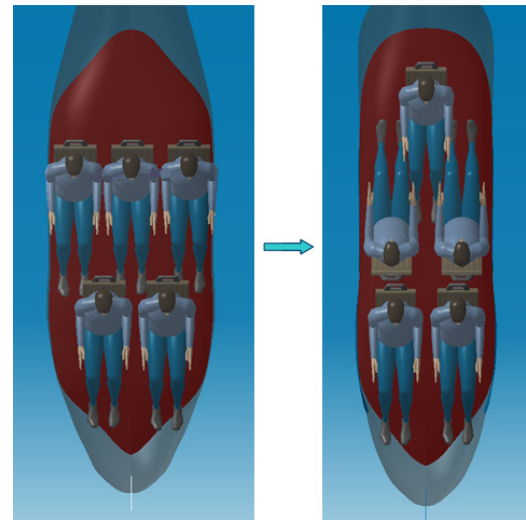


Figure 9-10: Fuselage Configuration Concept

10 COST ANALYSIS

10.1 Overview of Life Cycle Cost

Life Cycle Cost (LCC) considers the total cost of aircraft ownership from cradle to grave; it includes the cost of acquisition, operation, maintenance, conversion, and/or decommission. The goal of a LCC analysis is to determine the most cost effective approach for designing and manufacturing an aircraft. LCC provides a better assessment of the long-term cost



	Advised MD 500E	Estimated using PC Bell Cost Model
Cost	\$ 1,037,003	\$995,118
DOC	\$ 254	262.76

	Advised EC 120	Estimated using PC Bell Cost Model
Cost	\$ 1,350,000	\$1,324,754
DOC	\$ 320	\$ 326.51

Figure 10-1: Validation of PC Bell Cost Model

effectiveness of projects than can be obtained with only first costs decisions. The main industry software used for cost estimation is the PC Bell Cost Model. Prior to using this software for cost estimation, a validation against the EC-120 and the MD-500E^{73 74 75} was performed and shown in Figure 10-1. These aircraft were selected because they are of similar size to the Athena. The results from the software showed a strong correlation and therefore validated the tool. Throughout the analysis, the PC Bell Cost Model predicted the costs in 2001 Dollars. The costs were then converted to 2008 Dollars and Euros based on tabulated inflation rates and the current Dollar to Euro conversion rate.

10.2 Engine Cost Model

Price H, by PRICE systems, was used to generate the cost of the Athena’s engine because Price H is more accurate in predicting engine research & development and production costs. The data in Table 10-1, accounts for 5 prototypes and a total of 250 production units. This unit cost is used as the specified engine cost in the Bell PC Based Cost Model.

Table 10-1: Engine Cost Summary 2008 Dollars / Euros (based on €1=\$1.57)

	Research and Development	Production	Total	Unit Cost
Engine	\$ 27,915,201 / € 17,780,382	\$ 70,573,019 / €44,950,968	\$ 98,488,089 / € 67,731,267	\$ 282,293 / €179,804

10.3 Athena Cost Model

10.3.1 Research, Testing, Development and Evaluation

Total development costs from the Bell PC model include engineering, manufacturing, tooling, logistics, and other costs.⁷⁶ It does not include Engine RTDE, because the engine was priced in section 10-2 and incorporated into the Bell PC model. This resulted in a total RTDE cost for the helicopter of \$ 141,345,619.

Table 10-2: Comparison of Total Development Cost 2008 Dollars / Euros (based on €1=\$1.57)

	Athena	EC 120
Total Development Cost.	\$ 42,857,530 / €27,297,790	\$ 40,356,373 / €25,704,696

10.3.2 Recurring Production Cost

The recurring production cost for the Athena is shown by subsystem cost in Figure 10-2 for 200 vehicles. The engine accounts for nearly 22% of the total production cost followed by the fuselage (14%), drive system (10%), rotor (13%), and flight controls (4%).

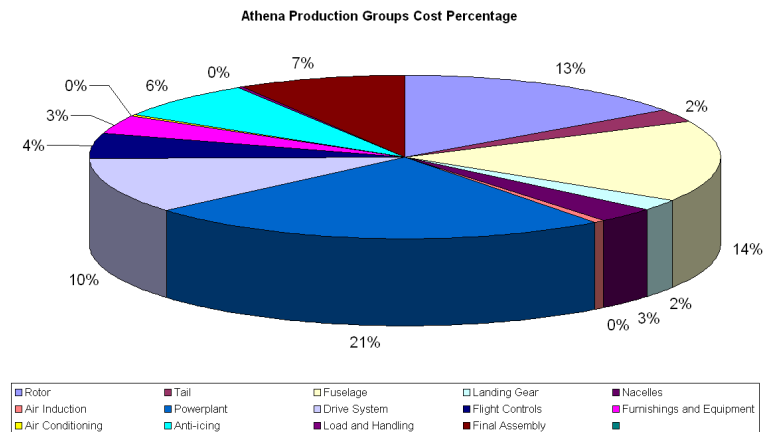


Figure 10-2: Athena Production Cost Breakdown

Table 10-3: Comparison of Athena Vs EC 120 and MD 500 – 2008 Dollars/ Euros (based on €1=\$1.57)

	EC-120	Athena	MD 500
Average Total Cost	\$ 1,326,214.82 € 844,722.82	\$ 1,294,540.66 € 824,548.19	\$ 995,118.44 € 633,833.40
Total First Unit Cost	\$ 2,167,134.25 € 1,380,340.29	\$ 1,979,541.01 € 1,260,854.15	\$ 1,632,237.35 € 1,039,641.62

10.3.3 Direct Operating Cost (DOC)

The direct operation cost is made up of the cost of fuel and airframe/engine labor and maintenance. The PC Bell Operating and Support cost model was used to calculate the Direct Operating Cost (DOC). The PC Bell model assumes values for fuel price and hourly maintenance labor rate based on assumptions for its base year.

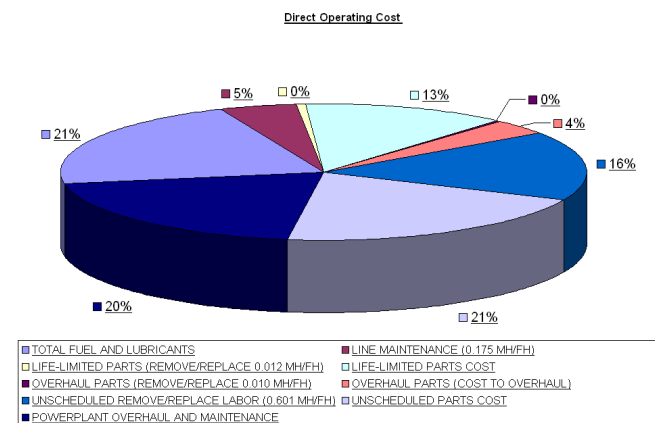


Figure 10-3: Athena Operating Cost Direct Pie Chart

Table 10-4: DOC Comparison of EC 120, MD500 and Athena – 2008 Dollars/Euros (based on €1=\$1.57)

	Operations and Support Cost per Flight Hour
MD 500	\$ 262 / € 166
EC 120	\$ 326 / € 207
Athena	\$ 285.47 / € 181.83

10.4 Economic Uncertainty Analysis

A risk analysis tool, @Risk, published by the Palisade Corporation was used to perform an “economic uncertainty” analysis of the cost results from the Bell PC-Based cost model. In its simplest form, @Risk will determine how likely a certain level of cost outputs can be achieved by providing a range of possible costs associated with its certainty level. Two types of simulations were performed, total development cost risk analysis and recurring production cost risk analysis. The simulations used the total project cost variance to perform a Monte Carlo simulation over 10,000 iterations to determine the probability of achieving the cost predictions. Figure 10-4 shows the probability of achieving the estimated reoccurring cost is 40%. However, the uncertainty analysis gave a 95% probability of the recurring cost being less than \$1,335,204 (\$2008), and the development cost uncertainty results provide a 95% confidence that the total development cost will be less than \$ 44.443 M (\$2008)

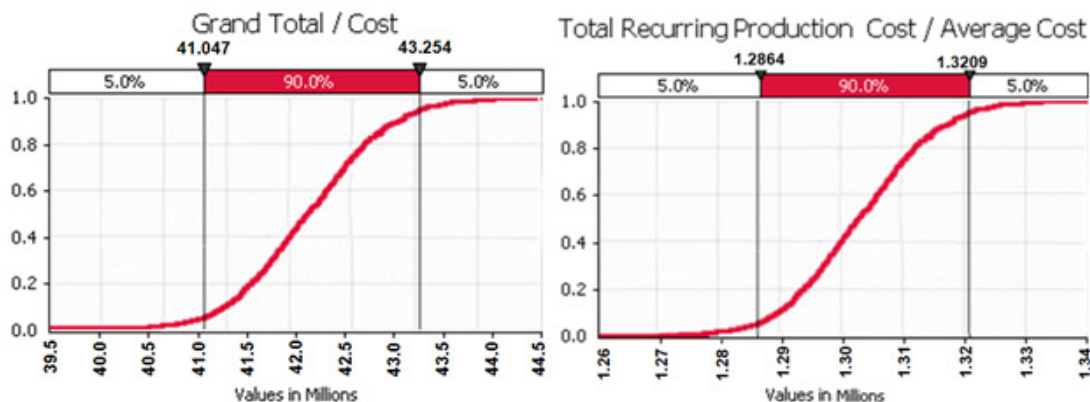


Figure 10-4: @ Risk Output Report (\$2008)

11 SAFETY AND CERTIFICATION

In order to validate the Athena’s preliminary design characteristics, the vehicle’s overall safety rating and certification requirements were evaluated. A safety analysis of the Athena was conducted, and a certification timeline developed to demonstrate compliance with the Federal Aviation Regulations.

11.1 Safety Analysis

The first step to conducting a safety analysis is to develop an understanding of the system being analyzed and the mission set it will be required to accomplish. Although the Athena will perform a variety of missions for multiple users, in this report we will focus on a training scenario. This mission contains a variety of flight regimes and presents an elevated risk due to pilot inexperience. The training mission analyzed will be similar to the one presented in Chapter 2.

11.1.1 Functional Analysis

The purpose of functional analysis is to “transform the functional, performance, interface, and other requirements that were identified through requirements analysis into a coherent description of system functions.”⁷⁷ The training mission profile from Chapter 2 (Figure 2-3) was decomposed into flight segments. These segments were then further decomposed through the use of a functional flow block diagram (FFBD). This analysis tool defines task sequences and relationships – identifying functional interactions within the system. The following figure shows a two-level functional decomposition for the Athena.

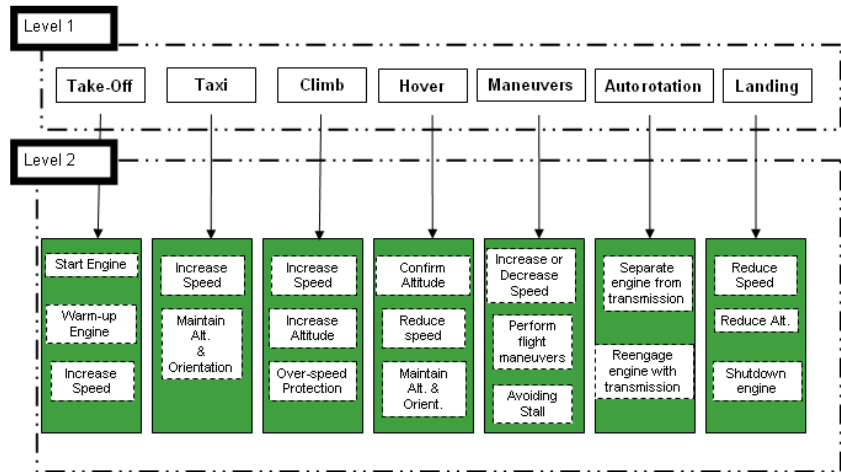


Figure 11-1: Functional Decomposition Block Diagram

11.1.2 Functional Hazard Assessment

The Functional Hazard Assessment (FHA) is a systematic, comprehensive examination of functions to identify failure conditions and organize them according to their importance. It is a qualitative process which demonstrates each possible failure mode of the system and its corresponding effect on the aircraft, crew, and passengers. The objective of the Athena FHA was to consider the potential failure modes associated with the airframe, powerplant, and human interaction functions and to classify the severity of their malfunctioning conditions as catastrophic, severe major, major, minor, or no safety effect.

Table 11-1: Athena’s FHA (Catastrophic)

Failure Category	Failure Event	Flight Phase	FAA Safety Requirement
Airframe Catastrophic Failure	Loss of Flight Control	Take Off	FAILURE RATE LESS THAN 1.0E-10
		Cruise	
	Loss of Tail Rotor	Landing	
		Cruise	
Powerplant Catastrophic Failure	Engine Failure	Take Off	
		Landing	
	Transmission Failure	Take Off	
		Landing	
Human Interaction Catastrophic Failure	Failure to React to Engine Failure	Take Off	
		Landing	

11.1.3 Preliminary System Safety Assessment (PSSA)

A Preliminary System Safety Assessment (PSSA) would be the next step to showing compliance with FAA safety requirements. The inputs for this process are the failure modes identified in the FHA in the previous section. The objective of a PSSA is to quantitatively determine the probabilities of failure for primary aircraft systems according to the failure rates of each subsystem and component. The PSSA will be generated through the use of various quantitative analytic tools, such as Fault Tree Analysis (FTA), Reliability Block Diagrams (RBD), Markov Analysis (MA), and Stochastic Petri Nets (SPN).

11.1.4 Athena Safety Features

The Athena was designed at every stage with safety in mind. Throughout this report, numerous safety features were discussed and several are summarized in Table 11-2. These are not every safety feature, but the major design technologies that increase Athena’s safety.

Table 11-2: Athena Safety Features

System	Safety Design	Safety Effect
Systems Monitor	Flight management system monitors aircraft systems and alerts pilot with a master caution/warning message and an audio cue to any deviation from normal parameters. Emergency procedure displayed on the center Multipurpose Display (MPD)	System emergencies are instantly highlighted with a master warning/caution and the MPD changes to the engine page and highlights the effected system
Reconfigurable Open Control Platform (OCP)	OCP designed to detect fault in rotor blade Electrical Mechanical Actuators (EMAs). If one EMA fails, others are designed to compensate	Aircraft control maintained and vibration levels held constant in the event of an EMA failure.
Three levels of automation	Flight management computer designed with three levels of automation: manual, semi-autonomous, and fully-autonomous. Semi and fully-autonomous modes have the capability to fly a trajectory and approach with minimal interaction	If pilot is disoriented or incapacitated helicopter can navigate and land with minimal pilot interaction
Envelope Protection	OCP designed to detect an approaching aircraft or structural limit and limit the control input as to avoid aircraft damage. Pilot is alerted with a collective stick shaker and has the ability to override the envelope protection system in an emergency	Aircraft can be maneuvered without constant attention on the aircraft systems to ensure they are within limits
Redundant Generator and Large Battery Size	Redundant generators installed in parallel to maintain power to aircraft systems and EMAs in the event of a generator failure. Battery sized to provide 15 minutes of power to the EMAs and critical systems in the event of a dual generator failure.	Aircraft control is maintained in the event of a dual generator failure.
Hanson Hub	Multiple load paths and free of ground and air resonance	Hub is damage tolerant and stable
Fenestron Tail	Enclosed fenestron tail is less likely to be damaged in inadvertent contact with an object. Ground crews less likely to inadvertently walk into trail rotor	Helicopter and ground crew protected in the event of inadvertent contact
Single Clutch Variable Speed Module (VSM)	The VSM is a dual planetary system but is designed with only one clutch. This ensures that the VSM will only fail in the high or low mode and not an unanticipated gear arrangement.	Helicopter can be landed in either high or low mode is the VSM fails or is stuck in one mode.
Crashworthy Subfloor and Landing Gear	Subfloor and landing gear designed to withstand impact and dissipate energy.	Crash energy absorbed by aircraft and not transferred to occupants.
Crashworthy Seats	Seats designed to stroke downwards to absorb energy in crash. Angled to transfer minimum energy to occupant during crash	Crash energy absorbed by seats and not transferred to occupant

11.2 Certification Plan

Figure 11-2 shows the five phases of a typical certification that would go along with Partnership for Safety Plan (PSP). The PSP helps establish the standard operating procedures and expectations of the certification process. Because the Athena is a new design, both Federal Aviation Regulations (FAR) part 27 and part 33 must be satisfied.



Figure 11-2: Five Phases of Certification

11.2.1 Certification schedule

The RFP specifies the Athena must be ready by 2020. A detailed schedule of the rotorcraft certification is provided in Figure 11-3 to ensure the Athena could meet this requirement.

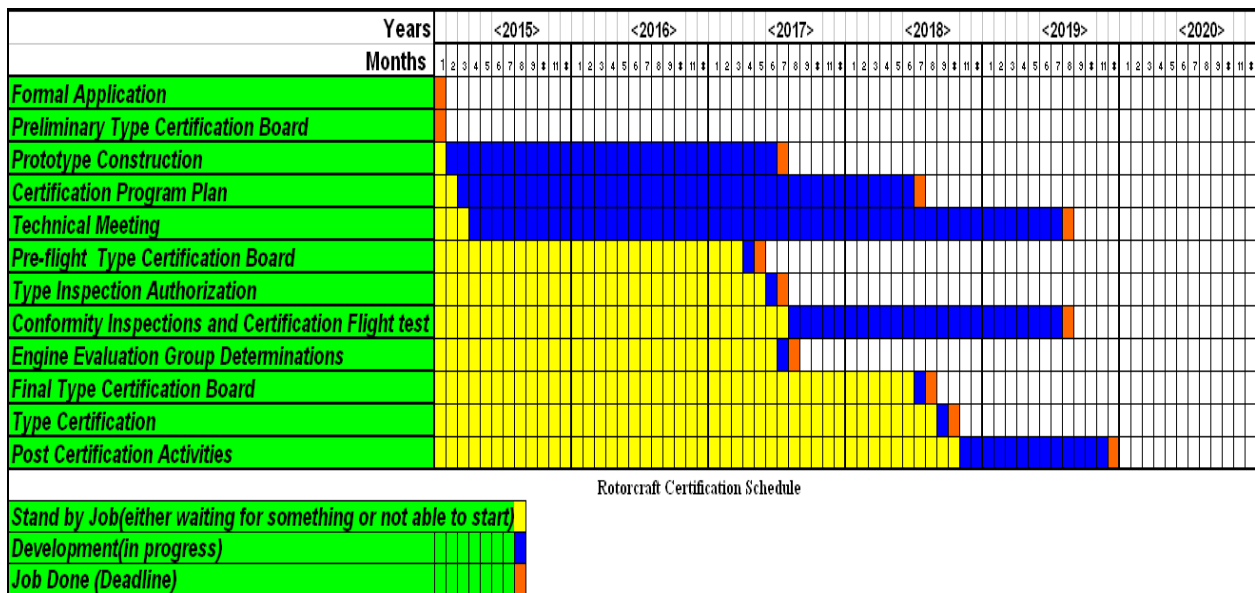


Figure 11-3: Athena Certification Schedule

12 CONCLUSION

The Athena Helicopter is an innovative aircraft that incorporates multiple recent advances in technology to make it intelligent and environmentally friendly. Athena’s robust design allows its use in civilian, para-military, and military applications and will ensure its success in the global marketplace. Its use of new “green” technology reduces environmental impacts, while a strong focus on safety ensures the Athena will be the safest helicopter ever produced. The use of a parallel product and process design methodology will ensure all lifecycle costs are minimized.

The Athena was designed around an Open Control Platform (OCP) that provides an interface for Athena's innovative technologies. This OCP ensures all digital components can communicate with each other and provides obsolescence avoidance by allowing individual components to be upgraded without requiring whole system replacement. The OCP also provides seamless integration for Athena's innovative optimization technologies which reduce emissions, noise, and fuel consumption while increasing vehicle performance.

Athena's Hanson rotor system, in combination with its fly-by-wire control system and electro-mechanical actuators, eliminates the need for a swashplate, lead-lag dampers, and hydraulic pumps. The electro-mechanical actuators provide higher harmonic control (HHC) through individual blade control (IBC) and increase performance while decreasing vibrations and noise. These actuators provide primary flight control and all the benefits of HHC at the lowest system weight and maintenance costs. Other systems designed to provide HHC for performance gains (i.e. morphed rotor or trailing edge flaps) are overly maintenance intensive and require additional hardware to provide collective pitch. The OCP integrates Athena's Flight Mission Planner and Control Systems and optimizes the flight and engine controls to allow a pilot to select optimization parameters including: minimum fuel or noise, target following, or minimum time to a destination. This tight system integration and reconfigurable optimization ability reduces Athena's impact on the environment through minimizing fuel usage and emissions production.

Advanced engine technologies minimize Athena's life cycle emissions and fuel consumption. A new two stage, lean-lean, Lean Premixed Prevaporized (LPP) combustor reduces emissions and ensures stable combustion, while the new compressor and composite turbines maximize engine efficiency and reduce fuel consumption. The distributed FADEC ensures fuel flexibility and allows the engine to be optimized for either JP-8 or biomass synjet fuel. This flexibility allows the Athena to operate in environments where JP-8 is the only available fuel, but also permits a transition to environmentally friendly synjet fuel without modifications or loss of performance. A new Hanson split-torque transmission and a variable speed module allow the Athena to vary its rotor RPM without compromising engine performance and increasing fuel usage. This dual speed design helps Athena minimize vibrations and noise while increasing performance.

Athena's numerous innovative safety features include a crashworthy composite fuselage, a full glass cockpit design, and a flight monitoring system. This focus on safety combined with the advanced technologies outlined in this report makes the Athena one of the most environmentally friendly, safe, and efficient helicopters ever designed. The Athena is a truly a "SMART-COPTER" that exhibits all of the characteristics necessary for success from first unit delivery through its entire lifecycle.

APPENDIX A – GROUP WEIGHT STATEMENT

MIL-STD-1374 GT-ANALYST May 31 2008		Appendix A – MIL-STD-1374 Weight Statement GROUP WEIGHT STATEMENT AIRCRAFT (INCLUDING ROTORCRAFT) ESTIMATED CALCULATED ACTUAL (CROSS OUT THOSE NOT APPLICABLE)				ATHENA Page 1
1	ROTOR GROUP					143.16
2	BLADE MASS					93.33
3	HUB AND HINGE					49.83
4						
5	ANTI-TORQUE GROUP					33.23
6	FAN					23.01
7	HORIZONTAL STABILIZER					6.79
8	VERTICAL STABILIZER					3.43
9						
10	FUSELAGE					273.90
11						
12	LANDING GEAR					72.11
13						
14	PROPULSION GROUP					176.37
15	ENGINE INSTALLATION					124.00
16	PROPULSION SUBSYSTEM					32.10
17	FUEL SYSTEM					20.27
18						
19	DRIVE SYSTEM					132.76
20	HANSON TRANSMISSION					132.76
22						
23	FLIGHT CONTROL GROUP					331.26
24	COCKPIT CONTROL					18.17
25	SYSTEM CONTROL					21.92
26	AVIONICS					264.55
27	HYDROLICS					26.62
28						
29	NACELLES					10.64
30						
31	INSTRUMENTS					15.48
32						
33	ELECTRICAL					134.99
34						
36	FURNISHINGS & EQUIPMENT GROUP					139.60
37	FURNISHINGS AND EQUIPMENT					26.50
38	AIR COND. & ANTI-ICE					25.10
39	SEATS					88.00
40						
41	MANUFACTURING VARIATION					12.80
42						
43	TOTAL WEIGHT EMPTY					1476.30
44	CREW					220.50
45						
46	PAYLOAD GROUP					1102.31
47	PASSENGERS					793.66
48	BAGGAGE					176.37
49	ADDITIONAL FREIGHT					132.28
50						
51	FUEL					389.30
52	UNUSABLE FUEL					
53	AVAILABLE MISSION FUEL					
54						
55	TOTAL USEFUL LOAD					1712.11
57	CONTINGENCY					73.8152
58						
59	GROSS WEIGHT					3262.23

APPENDIX B – RECURRING COST BREAKDOWN

Athena Recurring Cost Breakdown (\$2008)

Athena Total Burdened Cost for Average of 200 Aircraft, 2001\$				
	Total Average Cost by System			
	Labor	Material	Subcontract	Total
Wing	\$0	\$0	\$0	\$0
	\$0	\$0	\$0	\$0
Rotor	\$44,003	\$33,071	\$42,756	\$119,830
Hub	\$13,998	\$5,512	\$20,753	\$40,262
Blade	28,737	25,576	21,787	76,100
Rotor Vibration Suppression	1,268	1,983	217	3,468
Tail	\$10,797	\$3,722	\$3,746	\$18,265
Vertical Stabilizer	\$6,094	\$976	\$782	\$7,852
Horizontal Stabilizer	974	499	0	1,473
Tailrotor	3,729	2,246	2,964	8,939
Fuselage	\$88,537	\$33,896	\$6,055	\$128,488
Basic Structure	\$57,297	\$18,232	\$79	\$75,608
Windows	660	0	2,950	3,611
Crew Doors	4,745	2,389	650	7,784
Passenger Doors	5,029	2,704	54	7,788
Baggage Door	591	137	0	728
Compartment Doors	1,373	865	524	2,762
Floor	5,633	4,648	114	10,395
Tailboom	12,395	2,660	0	15,055
Pylon Support	814	2,260	1,683	4,757
Landing Gear	\$10,499	\$3,151	\$2,889	\$16,531
Landing Gear	\$10,429	\$3,121	\$2,852	\$16,402
Tail Skid	61	30	37	128
Wacelles	\$18,229	\$5,742	\$314	\$24,285
Firewall	\$3,331	\$1,389	\$216	\$4,916
Cowling	13,706	3,394	48	17,148
Engine Mounts	1,192	979	50	2,221
Air Induction	\$968	\$746	\$2,291	\$4,004
Air Inlet	\$540	\$102	\$31	\$673
Inlet Particle Separator	427	644	2,260	3,332
Powerplant	\$1,269	\$22,539	\$287,779	\$311,579
Engine	\$0	\$0	\$272,961	\$272,961
Engine Installation	114	561	0	674
Ejector	0	0	4,582	4,582
Tailpipe	189	0	1,121	1,309
Engine Controls	167	3,285	3,781	7,233
Engine Start System	0	0	1,779	1,779
Engine Wash	0	0	0	0
Lubrication System	315	4,696	733	5,743
Fuel System	476	13,999	2,823	17,297
Drive System	\$33,992	\$22,240	\$38,972	\$87,204
Main Transmission and Mast	\$12,786	\$12,353	\$12,081	\$37,220
Tailrotor Gearbox	4,000	1,108	2,620	7,728

Athena Total Burdened Cost for Average of 200 Aircraft, 2001\$				
Intermediate Gearbox	0	0	0	0
Freewheeling Unit	3,598	2,198	1,797	7,594
	0	0	0	0
Engine Input Shaft	5,515	272	654	6,440
Tailrotor Driveshaft	3,914	3,792	1,001	8,707
Accessory Gearbox	4,179	2,517	12,818	19,514
Flight Controls	\$3,893	\$13,501	\$20,657	\$37,250
Cockpit controls	\$915	\$8,174	\$3,252	\$12,342
Rotating controls - main rotor	965	4,819	2,656	8,440
Rotating controls - tail rotor	1,072	314	702	2,088
Rotor hydraulic actuators	0	0	0	0
Elevator controls	140	194	652	987
Instruments	\$4,255	\$196	\$57,770	\$62,220
Hydraulics	0	0	0	0
Electrical	\$9,594	\$6,209	\$12,984	\$28,797
Avionics	\$3,583	\$344	\$17,110	\$21,037
Furnishings and Equipment	\$7,485	\$7,753	\$14,151	\$29,388
Crew Seats	\$2,455	\$1,232	\$928	\$4,615
Passenger Seats	333	0	11,456	11,789
Fire Extinguishing	236	1,292	619	2,146
Soundproofing	0	0	980	980
Miscellaneous Furnishings	4,461	5,229	168	9,858
Air Conditioning	\$416	\$1,144	\$863	\$2,423
Bleed air, heat, and debg	\$416	\$1,144	\$863	\$2,423
Environmental Control Unit	0	0	0	0
Anti-icing	\$91	\$0	\$57,616	\$57,707
Load and Handling	\$88	\$2,592	\$0	\$2,680
Final Assembly	\$67,473	\$0	\$0	\$67,473
Subtotals	\$384,692	\$157,155	\$565,825	\$1,026,872
Total Average Production Cost				\$1,026,872
Total Average Production Cost 2008\$				\$ 1,294,540.66

-
- ¹ Brentner, K.S., Prediction of Helicopter Rotor Discrete Frequency Noise - A Computer Program Incorporating Realistic Blade Motions and Advanced Acoustic Formation, NASA-TM-87721, 1986.
 - ² Engineering Design Handbook. Helicopter Engineering, Part One. Preliminary Design. AMCP 706-201. Army Materiel Command, Alexandria Virginia. August 1974.
 - ³ Vehicle Synthesis for Advanced VTOL Aircraft. AE 6333: Rotorcraft Design Course Notes. Daniel P. Schrage. www.t-square.gatech.edu. Accessed March 2008.
 - ⁴ Davis, CPT Joseph, Tim Mosig, Dr. Daniel Schrage, Design Methodology for Developing Concept Independent Rotorcraft Analysis and Design Software.
 - ⁵ Performance and Rotor Loads Measurements of the Lynx XZ170 Helicopter with Rectangular Blades. NASA TM 104000. May 1993.
 - ⁶ MD 500E Performance Specifications. www.mdhelicopters.com. Accessed March 2008.
 - ⁷ Lindel, Arthur W. et. al. Variable Diameter Rotor Study. Sikorsky Aircraft Technical Report AFFDL-TR-71-170. January 1972.
 - ⁸ Bowes, Michael A.. Helicopter Noise Reduction Design Trade-off Study. Report No. R-1493. January 1977.
 - ⁹ Giurgiutiu. Victor. Recent Advances in Smart-Material Rotor Control Actuation. Proceedings of the 41st AIAA/ASME/ASCE/AHS/ASC Structures, Structural Dynamics, and Materials Conference. Atlanta, GA. April 2000. Paper No. AIAA 2000-1709.
 - ¹⁰ Sekula, Martin K. Matthew L. Wilbur, William T. Yeager, Jr. Aerodynamic Design Study of an Advanced Active Twist Rotor. U.S. Army Vehicle Technology Directorate. NASA Langley Research Center.
 - ¹¹ Yeo, H., Johnson, W. "Assessment of Comprehensive Analysis Calculation of Airloads on Helicopter Rotors" Journal of Aircraft Vol.42 No 5. September -October 2005.
 - ¹² Gorton, Susan. Berry, John. Hodges, W. and Reis, Deane. "Flow Environment Study Near the Empennage of a 15-percent Scale Helicopter Model." NASA TP-2000-210085.
 - ¹³ S. Xue, B. Docker, and J. Narramore, Z. Han, "Integrated Aero-Acoustic Rotor Simulation and Design Optimization" AIAA-2006-2603.
 - ¹⁴ Sankar, Lakshmi, Collins, Kyle, Bain, Jeremy. "A Pareto Frontier Method for Multi-Disciplinary Optimization of Helicopter Rotors." Presented at the AHS Aeromechanics Specialist's Conference. San Francisco, CA. January 23-25, 2008.
 - ¹⁵ FLIGHTLAB Theory Manual Advanced Rotorcraft Technology, Inc., 2006.
 - ¹⁶ http://216.19.207.5/Rotorcraft/Models/MD520NTechSpecs/520N_Overview.pdf
 - ¹⁷ Hanson, Thomas F., A Designer Friendly Handbook of Helicopter Rotor Hubs, Newhall, CA: by the author, 1998.
 - ¹⁸ <http://www.claverham.com/heat.htm>.
 - ¹⁹ U.T.P., Arnold, D. Fürst, T. Neuheuser, R. Bartels, "Development of an Integrated Electrical Swashplateless Primary and Individual Blade Control System", Cheeseman Award Paper of the 32nd European Rotorcraft Forum, Maastricht, 2006
 - ²⁰ Pavel, M.D., Padfield, G.D., "Defining Consistent ADS-33-Metrics for Agility Enhancement and Structural Loads Alleviation", 58th AHS Forum, 2002.
 - ²¹ Kottapalli, S. et al., "Full-Scale Higher Harmonic Control Research to Reduce Hub Loads and Noise", NASA-TM-112344, 1993.
 - ²² Straub, F.K., Byrns, E.V., "Application of Higher Harmonic Blade Feathering on the OH-6A Helicopter for Vibration Reduction", NASA-CR-4031, 1986.
 - ²³ Jacklin, S.A., et. al., "Reduction of Helicopter BVI Noise, Vibration, and Power Consumption Through Individual Blade Control", AHS 51st Annual Forum, 1995.
 - ²⁴ Jacklin, S.A. et al., "Full-Scale Wind Tunnel Test of an Individual Blade Control System For a UH-60 Helicopter", 58th AHS Forum, 2002.
 - ²⁵ Shaw, J. et al., "Higher Harmonic Control: Wind Tunnel Demonstration of Fully Effective Vibratory Hub Force Suppression", 41st AHS Annual forum, 1985.
 - ²⁶ Straub, F.K. V.R. Anand, TS Birchette, D. Merkley, W.R Cravey, J. Gilling, "Rotating/Nonrotating Interface for Data and Power", 62nd Annual Forum of the American Helicopter Society, Phoenix 2006.
 - ²⁷ Fulton, M.V., "Aeromechanics of the Active Elevon Rotor", 61st AHS Forum, 2005.
 - ²⁸ Bielawa, R., Cheney, M.C., Novak, R.C., "Investigation of a Bearingless Helicopter Rotor Concept Having a Composite Primary Structure", NASA-CR-2637,1977.

-
- ²⁹ Wang, J.M. et. al., "Stability of the Sikorsky S-76 Bearingless Main Rotor", NASA-TM-112345, 49th AHS Forum, 1993.
- ³⁰ Johnson, Wayne, Helicopter Theory, Princeton University Press, Princeton, NJ. 1980.
- ³¹ Hanson, F. Thomas. The Simplicity of Elastic Articulation. Presented at the American Helicopter Society 53rd Annual Forum. Virginia Beach, VA. April-May 1997.
- ³² "Engineering Design Handbook, Helicopter Engineering Part Two: Detail Design" AMCP 706-202 Army Materiel Command, Alexandria, VA.
- ³³ Leishman, Gordon J. Principles of Helicopter Aerodynamics. Cambridge University Press. New York. 2006
- ³⁴ Wiesner, Wayne and G. Kohler, Gary. Tail Rotor Design Guide. Technical Report 73-99, USAAMRDL, January 1974. Contract DAAJ02-73-C-0010 to Boeing Vertol.
- ³⁵ Wallis, R. Allan. Axial Flow Fans and Ducts. John Wiley & Sons, Inc. 1983.
- ³⁶ Prouty, R. Helicopter Performance, Stability, and Control. Krieger Publishing. Malabar, Florida. 1995.
- ³⁷ Jane's All the World's Aircraft 2007-2008. Jackson, Paul. Janes information Group. May 2007.
- ³⁸ Riley, R. G., *Effects of Uneven Blade Spacing on Ducted Tail Rotor Acoustics*, presented at the AHS 52nd Annual Forum, Washington, D. C., 4-6 Jun 1996.
- ³⁹ Andre-Michel L. Dquin, Louis J. Dalsosso, Henri F. Barquet. United States Patent No. 5,498,129. March 1996.
- ⁴⁰ Keys, C., Sheffler, M., Weiner, S., and Heminway, R., "LH Wind Tunnel Testing : Key to Advanced Aerodynamic Design", Proc. 47th American Helicopter Society Annual Forum, May, 1991.
- ⁴¹ Taylor, Robert T NACA TN 4126. Experimental Investigation of the Effects of Some Shroud Design Variables on the Static Thrust Characteristics of a Small-scale Shrouded Propeller Submerged in a Wing.
- ⁴² Lemanski, Alphonse J., Zihni B. Saribay, Michael J. Elmoznino, "Conceptual Design of Pericyclic Non-Traction Continuously Variable Speed Transmissions: Rotorcraft Applications." American Helicopter Society 62nd Annual Forum, Phenix, Az. May 9-11, 2006.
- ⁴³ Suhr, Stephan, Preliminary Turboshaft Engine Design Methodology for Rotorcraft Applications, Georgia Institute of Technology, December 2006.
- ⁴⁴ Mattingly, Jack D., Heiser, William H., and Pratt, Daniel T., Aircraft Engine Design. 2nd ed. Virginia: AIAA, 2002.
- ⁴⁵ Kundu, A.K., S. Crosby, R. Curran, and S. Raghunathan, "Aircraft Component Manufacture Case Studies and Operating Cost Reduction Benefit," AIAA Paper 2003-6829, November 2003.
- ⁴⁶ Japikse, David and Nicholas C. Baines, Introduction to Turbomachinery ,White River Junction, VT: Concepts ETI, 1997.
- ⁴⁷ Corporan, Edwin, et al., "Emissions Characteristics of a Turbine Engine and Reasearch Combustor Buring a Fisher-Tropsch Fuel," Energy & Fuels 2007, 21, 2615-2626.
- ⁴⁸ Daggett, D. and O. Hadaller, "Alternative Fuels and their Potential Impact on Aviation," NASA/TM 2006-214365, Oct. 2006.
- ⁴⁹ Hayashi, Shigeru, Hideshi Yamada, Mitsumasa Makida, "Extending low-NOx Operating Range of a Lean Premixed-prevaporized Gas Turbine Combustor by Reaction of Secondary Mixtures Injected into Primary Stage Burned Gas," proceedings of the Combustion Institute, 2005, pp 2903-2911.
- ⁵⁰ Aida, Naoki, Tomoki Nishijima, Shigeru Hayashi, Hideshi Yamada, Tadashige Kawakami, "Combustion of lean prevaporized fuel-air mixtures mixed with hot burned gas for low-NOx emissions over an extended range of fuel-air ratios," proceedings of the Combustion Institute, 2005, pp 2885-2892.
- ⁵¹ Charest, M.R.J., J.E.D. Gauthier, and X. Huang, "Design of a Lean Premixed Prevaporized Can Combustor," proceedings of GT2006, GT2006-91004, May 2006.
- ⁵² Poeschl, G., Runhkamp, W., and Pfof H., 1994. "Combustion with low pollutant emissions of liquid fuels in gas turbines by premixing and prevaporization." ASME Paper 94-GT-443.
- ⁵³ Riley, A.J. et al., "Advanced Closed-Loop Control on an Atmospheric Gaseous Lean-Premixed Combustor," Journal of Engineering for Gas Turbines and Power, vol. 126, October 2004.
- ⁵⁴ Sheehan, John et al., Life Cycle Inventory of Biodiesel and Petroleum Diesel for Use in an Urban Bus. National Renewable Energy Laboratory, May 1998.
- ⁵⁵ Energy Information Agency, http://www.eia.doe.gov/oil_gas/petroleum/info_glance/petroleum.html.
- ⁵⁶ Profile of the Petroleum Refining Industry, EPA Office of Compliance Sector Notebook Project, U.S. Environmental Protection Agency, 1995.
- ⁵⁷ Dilip R. Ballal and Joseph Zelina, "Progress in Aero Engine Technology (1939-2003)," AIAA Paper 2003-4412 July 2003.
-

-
- ⁵⁸ Bernard L. Koff, "Gas Turbine Technology Evolution – A Designer’s Perspective," AIAA Paper 2003-2722, July 2003.
- ⁵⁹ Langston, Lee S., "Crown Jewels," *Mechanical Engineering Magazine*, 2006.
- ⁶⁰ Bellocchio, Andrew T. "Drive System Design Methodology for a Single Main Rotor Heavy Lift Helicopter." Georgia Institute of Technology, Dec 2005.
- ⁶¹ Norton, Robert L. *Machine Design An Integrated Approach*. Prentice-Hall Inc, 1998.
- ⁶² Bellocchio, Andrew T., MATLAB Program "sizer3.m." MATLAB program modified by authors for use in this report.
- ⁶³ Kannan, Suresh K., "Adaptive Control of Systems in Cascade with Saturation," PhD Dissertation, Georgia Institute of Technology, December 2005.
- ⁶⁴ Wills et al. An Open Platform for Reconfigurable Control. *IEEE Control Systems Magazine*. June 2001.
- ⁶⁵ Bell 430 Product Data. Bell Helicopter Textron, Inc. 2003.
- ⁶⁶ Behbahani, A. et al. Status, Vision, and Challenges of an Intelligent Distributed Engine Control Architecture. AeroTech Congress & Exhibition. Los Angeles, CA. September 2007.
- ⁶⁷ Mettler, Bernard, and Bachelder, Edward. Combining On- and Offline Optimization Techniques for Efficient Autonomous Vehicle’s Trajectory Planning. AIAA Guidance, Navigation, and Control Conference and Exhibit. AIAA-2005-5861. San Francisco, California. Aug 15-18, 2005.
- ⁶⁸ Unnikrishnan, Suraj and Prasad, J.V.R. "Flight evaluation of a Reactionary Envelope Protection Systems for UAVs," AHS 62nd Annual Forum, Phoenix, AZ, May 2006.
- ⁶⁹ Johnson, Eric N. and Schrage, Daniel P. The Georgia Tech Unmanned Aerial Research Vehicle: GTMax. AIAA Guidance, Navigation, and Control Conference and Exhibit. AIAA-2003-5741. Austin, Texas. Aug 11-14, 2003.
- ⁷⁰ He, C., Development and Application of a Generalized Dynamic Wake Theory for Lifting Rotors, Ph.D. thesis, School of Aerospace Engineering, Georgia Institute of Technology, Atlanta, Georgia, 1989.
- ⁷¹ Padfield, G.D., "Helicopter Flight Dynamics: The Theory and Application of Flying Qualities and Simulation Modeling", AIAA Education Series, 1996.
- ⁷² Heffley, R. K.; Jewell, W. F.; Lehman, J. M.; Vanwinkle, R. A., "A compilation and analysis of helicopter handling qualities data. Volume 1 Data compilation", NASA-CR-3144, 1979.
- ⁷³ <http://www.fh1100.com/pdf/compare.pdf>.
- ⁷⁴ http://www.aviastar.org/helicopters_eng/mcdonnel-500.php.
- ⁷⁵ http://nl.newsbank.com/nl-earch/we/Archives?p_product=ST&s_site=dfw&p_multi=ST&p_theme=realcities&p_action=search&p_maxdocs=200&p_topdoc=1&p_text_direct-0=1059027159DB9B50&p_field_direct-0=document_id&p_perpage=10&p_sort=YMD_date:D&s_trackval=GooglePM.
- ⁷⁶ PC Based Mode User’s Guide Rev 3.1.
- ⁷⁷ *Systems Engineering Fundamentals*, Defense Acquisition University, Fort Belvoir, VA, January 2001.